

AD-A089 102

UNITED TECHNOLOGIES RESEARCH CENTER EAST HARTFORD CONN

F/G 11/4

EVALUATION OF AMORPHOUS RIBBON REINFORCED RESIN MATRIX COMPOSIT--ETC(U)

APR 80 J R STRIFE, K M PREWO

F33615-78-C-5063

UNCLASSIFIED

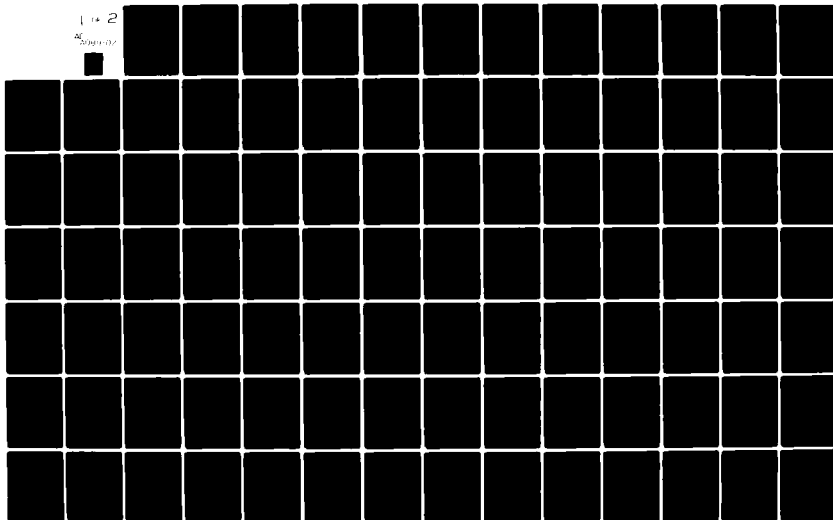
UTRC/R80-914389-18

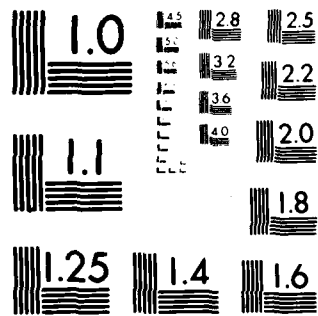
AFWAL-TR-80-4060

NL

1 + 2

20/10/10/





MICROCOPY RESOLUTION TEST CHART  
NATIONAL BUREAU OF STANDARDS-1963-A

AFWAL-TR-80-4080

**LEVEL** *II*

*2*

**AD A089102**

**EVALUATION OF AMORPHOUS RIBBON REINFORCED  
RESIN MATRIX COMPOSITES**

J.R. Strife  
K.M. Prewo

UNITED TECHNOLOGIES RESEARCH CENTER  
EAST HARTFORD, CT 06108

APRIL 30, 1980

DTIC  
ELECTE  
SEP 11 1980  
S D  
E

Final Report July 1978 — April 1980

Approved for Public Release; Distribution Unlimited.

MATERIALS LABORATORY  
AIR FORCE WRIGHT AERONAUTICAL LABORATORIES  
AIR FORCE SYSTEMS COMMAND  
WRIGHT-PATTERSON AIR FORCE BASE, OHIO 45433

FILE COPY

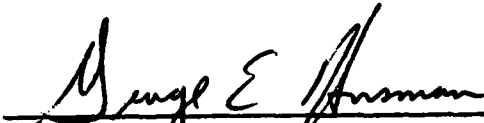
80 9 8 004


# NOTICE

When Government drawings, specifications, or other data are used for any purpose other than in connection with a definitely related Government procurement operation, the United States Government thereby incurs no responsibility nor any obligation whatsoever; and the fact that the government may have formulated, furnished, or in any way supplied the said drawings, specifications, or other data, is not to be regarded by implication or otherwise as in any manner licensing the holder or any other person or corporation, or conveying any rights or permission to manufacture use, or sell any patented invention that may in any way be related thereto.


This report has been reviewed by the Office of Public Affairs (ASD/PA) and is releasable to the National Technical Information Service (NTIS). At NTIS, it will be available to the general public, including foreign nations.

This technical report has been reviewed and is approved for publication.

  
GEORGE E. HUSMAN  
Project Monitor

  
THEODORE J. REINHART, JR., Chief  
Composites, Adhesives & Fibrous Matls Br  
Nonmetallic Materials Division

FOR THE COMMANDER

  
F. D. CHERRY, Chief  
Nonmetallic Materials Division

"If your address has changed, if you wish to be removed from our mailing list, or if the addressee is no longer employed by your organization please notify \_\_\_\_\_ W-PAFB, OH 45433 to help us maintain a current mailing list".

Copies of this report should not be returned unless return is required by security considerations, contractual obligations, or notice on a specific document.

UNCLASSIFIED

SECURITY CLASSIFICATION OF THIS PAGE (When Data Entered)

19 REPORT DOCUMENTATION PAGE		READ INSTRUCTIONS BEFORE COMPLETING FORM	
1. REPORT NUMBER AFWAL/IR-80-4060	2. GOVT ACCESSION NO. AD-A089 102	3. RECIPIENT'S CATALOG NUMBER	
4. TITLE (and Subtitle) EVALUATION OF AMORPHOUS RIBBON REINFORCED RESIN MATRIX COMPOSITES	5. TYPE OF REPORT & PERIOD COVERED Final Report - 31 July 1978 - 30 April 1980		
7. AUTHOR(s) J. R. Strife and K. M. Prew	6. PERFORMING ORG. REPORT NUMBER UTRC/R80-914389-18		
9. PERFORMING ORGANIZATION NAME AND ADDRESS United Technologies Research Center / East Hartford, CT 06108		8. CONTRACT OR GRANT NUMBER(s) 333615-78-C-5063	
11. CONTROLLING OFFICE NAME AND ADDRESS Materials Laboratory Air Force Wright Aeronautical Laboratories Air Force Systems Command Wright-Patterson Air Force Base, Ohio 45433		10. PROGRAM ELEMENT, PROJECT, TASK AREA & WORK UNIT NUMBERS 24190307 1703	
14. MONITORING AGENCY NAME & ADDRESS (if different from Controlling Office) 30 APR 1980		12. REPORT DATE April 30, 1980	
		13. NUMBER OF PAGES 167	
		15. SECURITY CLASS. (of this report) Unclassified	
16. DISTRIBUTION STATEMENT (of this Report) Approved for public release; distribution unlimited.			
17. DISTRIBUTION STATEMENT (of the abstract entered in Block 20, if different from Report)			
18. SUPPLEMENTARY NOTES			
19. KEY WORDS (Continue on reverse side if necessary and identify by block number) Composite, Laminate, Resin Matrix Composite, Amorphous Metal Ribbon, Ribbon Reinforced Composite, Adhesive Films, Tensile Properties, Fatigue, Impact Resistance, Thermal Expansion			
20. ABSTRACT (Continue on reverse side if necessary and identify by block number) Ribbon reinforced composites are attractive as structural materials since relatively isotropic in-plane properties are achieved if the ribbon aspect ratio is sufficiently high. Recent advances in the production of amorphous metal ribbons on a continuous basis have resulted in a ribbon material which exhibits unique properties and is potentially low cost. Commercially available amorphous metal ribbon materials were utilized in this investigation to reinforce resin matrices. Typical ribbon properties were a density of 8.02 gm/cm <sup>3</sup> .			

DD FORM 1 JAN 73 1473

EDITION OF 1 NOV 68 IS OBSOLETE

UNCLASSIFIED

SECURITY CLASSIFICATION OF THIS PAGE (When Data Entered)

JOB

UNCLASSIFIED

SECURITY CLASSIFICATION OF THIS PAGE(When Data Entered)

#20 continued

(0.29 lb/in<sup>3</sup>), tensile strengths in the range of 2550-2900 MPa, (370-420 ksi), a tensile modulus of 165 GPa, (24 Msi), and aspect ratios, w/t, up to 380. The longitudinal properties of the composites developed were in agreement with the simple rule of mixtures. The transverse composite properties were dependent on ribbon aspect ratio and the ribbon stacking pattern. Using high aspect ratio ribbon, a strength ratio,  $\sigma_{22}/\sigma_{11}$ , of 0.76 and modulus ratio,  $E_{22}/E_{11}$  of 1.0 were achieved.

A broad spectrum of composite properties was also investigated using high aspect ratio ribbon and a simple stacking pattern. Typical composite properties at 0.60 ribbon volume fraction were a density of 5.27 gm/cm<sup>3</sup> (0.190 lb/in<sup>3</sup>), a longitudinal tensile strength of 1720 MPa (250 ksi), a transverse tensile strength of 862 MPa (125 ksi), and an isotropic in-plane modulus of 96.5 GPa (14 Msi). These composites were shown to have poor mechanical fatigue resistance, fracture toughness similar to 6061-T6 aluminum alloy, and excellent room temperature transverse creep properties. Exposure to moist environment seriously degraded composite mechanical properties.

The composites developed were compared on a specific property basis to currently utilized quasi-isotropic graphite/epoxy. It was demonstrated that amorphous metal ribbon reinforced resins are competitive with quasi-isotropic graphite/epoxy on a specific strength basis. However, amorphous metal ribbon reinforced resins are not competitive on a specific modulus basis. Due to the relatively invariant nature of the specific modulus of amorphous metal ribbon materials, no improvement is expected in this regard. Thus, it was concluded that these composites would not be in a competitive position for most high performance composite applications, particularly in the aerospace industry. However, the high biaxial composite strength properties, potential low cost, and the unusual soft magnetic properties offered by the ribbons may result in some unique composite applications. used

UNCLASSIFIED

SECURITY CLASSIFICATION OF THIS PAGE(When Data Entered)

## FOREWORD

Presented in this final report is the work accomplished by the United Technologies Research Center under Contract F33615-78-C-5063 for the Materials Laboratory, Air Force Wright Aeronautical Laboratories, Air Force Systems Command, Wright-Patterson Air Force Base, Ohio. Mr. George E. Husman (AFWAL/MLBC) served as the Air Force project engineer.

This study was conducted at the United Technologies Research Center, East Hartford, CT, with Dr. Karl M. Prewé and Dr. James R. Strife serving as co-investigators. The work was performed during the period of 31 July 1978 to 30 April 1980.

Accession For	
NTIS GRA&I	<input checked="checked" type="checkbox"/>
DDC TAB	<input type="checkbox"/>
Unannounced	<input type="checkbox"/>
Justification	
By	
Distribution/	
Availability Codes	
Dist.	Avail and/or special
A	

Evaluation of Amorphous Ribbon Reinforced  
Resin Matrix Composites

TABLE OF CONTENTS

I.	INTRODUCTION . . . . .	1
II.	RESULTS AND DISCUSSION . . . . .	3
A.	Selection of Amorphous Metal Ribbon . . . . .	3
1.	Evaluation of Available Ribbon Materials . . . . .	3
2.	Evaluation of 2826 MB Ribbon Mechanical Properties . . . . .	5
a.	Materials and Tensile Test Procedure . . . . .	5
b.	Tensile Strength of As-Received Ribbon . . . . .	5
c.	Effect of Gage Length on Tensile Strength . . . . .	6
d.	Effect of Elevated Temperature Exposure on Ribbon Tensile Strength . . . . .	6
e.	Variation in Tensile Strength as a Function of Reel Position . . . . .	7
f.	Observations of Tensile Fracture Surfaces . . . . .	8
g.	Determination of Ribbon Elastic Modulus . . . . .	8
B.	Selection of Matrix Materials . . . . .	9
1.	Preliminary Screening of Matrix Candidates . . . . .	9
a.	Materials . . . . .	9
b.	Ribbon/Matrix Bond Strength Determination . . . . .	9
c.	Effect of Ribbon Cleaning Procedures on Ribbon/Matrix Bond Strength . . . . .	10
2.	Evaluation of Adhesive Films . . . . .	13
a.	Materials . . . . .	13
b.	Determination of Ribbon/Matrix Bond Shear Strength . . . . .	14
c.	Determination of Laminate Interlaminar Shear Properties . . . . .	15
d.	Matrix Selection . . . . .	17
C.	Composite Fabrication Procedures . . . . .	17
1.	Fabrication of Prepreg Tape . . . . .	17
a.	Prepreg Bonding by Primer Application . . . . .	18
b.	Prepreg Bonding by Heat Application . . . . .	18
2.	Composite Construction and Hot Pressing Procedure . . . . .	19

REPRODUCTION OF THIS DOCUMENT IS PROHIBITED



## TABLE OF CONTENTS (Cont'd)

D.	The Effect of Composite Construction Parameters on Tensile Properties . . . . .	19
1.	Evaluation of Ribbon Surface Treatment . . . . .	19
2.	The Effect of Ribbon Spacing and Volume Fraction on Composite Properties . . . . .	20
3.	The Effect of Ribbon Stacking Sequence on Composite Transverse Tensile Properties . . . . .	22
a.	Experimental Results . . . . .	22
b.	Comparison of Experimental Results with the Theory of Ribbon Reinforcement . . . . .	24
(1)	Elastic Modulus . . . . .	24
(2)	Tensile Strength . . . . .	25
c.	Composites Design . . . . .	27
4.	Investigation of 0/90 Lay-up Patterns . . . . .	27
E.	Physical and Mechanical Properties of 2826 MB/FM-1000 Composites . . . . .	29
1.	2826 MB Ribbon Tensile Properties . . . . .	29
2.	Thermal Expansion Characteristics . . . . .	30
a.	Ribbon Thermal Expansion Behavior . . . . .	30
b.	Composite Thermal Expansion Behavior . . . . .	31
3.	Composite Mechanical Properties . . . . .	31
a.	Interlaminar Shear Strength . . . . .	31
b.	Tensile Properties . . . . .	32
(1)	Ribbons Oriented at 0° to the Tensile Axis . . . . .	32
(2)	Ribbons Oriented at 90° to the Tensile Axis . . . . .	33
(3)	Ribbons Oriented at 45° to the Tensile Axis . . . . .	35
c.	Effect of Thermal Fatigue on Transverse Tensile Strength . . . . .	36
d.	Effect of Moist Environment on Transverse Tensile Strength . . . . .	37
e.	Compression Properties . . . . .	38
(1)	Compression Testing . . . . .	38
f.	Mechanical Fatigue Properties . . . . .	39
(1)	Longitudinal Ribbon Orientation . . . . .	39
(2)	Transverse Ribbon Orientation . . . . .	40
(3)	Summary . . . . .	40
g.	Assessment of Composite Impact Resistance and Fracture Toughness . . . . .	40
h.	Room Temperature Creep Properties . . . . .	43
III.	ASSESSMENT OF AMORPHOUS RIBBON REINFORCED RESIN MATRIX COMPOSITES . . . . .	44
REFERENCES	. . . . .	46

## LIST OF FIGURES

- Fig. 1  $E_{22}/E_{11}$  vs Ribbon Aspect Ratio Calculated for Three Ribbon to Matrix Modulus Ratios
- Fig. 2 Calculated Transverse Composite Modulus vs Ribbon Aspect Ratio
- Fig. 3  $\sigma_{22}/\sigma_{11}$  vs Ribbon Aspect Ratio Calculated for Several Ribbon/Matrix Bond Strengths
- Fig. 4 Optical Micrographs of Ribbon Cross Sections. Nominal Ribbon Thickness is 0.05 mm (0.002 in)
- Fig. 5 Tensile Properties of As-Received Ribbon
- Fig. 6 Effect of Gage Length on Tensile Strength
- Fig. 7 Effect of Elevated Temperature Exposure on Tensile Strength
- Fig. 8 Scanning Electron Micrographs of Ribbon Edges
- Fig. 9 Comparison of Tensile Properties of As-Received Ribbon
- Fig. 10 Optical Micrographs of Ribbon Cross Sections
- Fig. 11 SEM of Ribbon Surface Contacting the Wheel
- Fig. 12 Scanning Electron Micrographs of Low Strength Ribbon Fracture Surfaces
- Fig. 13 Scanning Electron Micrograph of Low Strength Ribbon Fracture Surface. Arrows Indicate Areas of Plastic Deformation Characteristic of Ductile Fracture
- Fig. 14 Scanning Electron Micrographs of High Strength Ribbon Fracture Surfaces
- Fig. 15 Scanning Electron Micrographs of High Strength Ribbon Fracture Surface Showing Area of Extensive Plastic Deformation
- Fig. 16 Schematic of Single Lap Shear Specimen
- Fig. 17 Cohesive and Adhesive Bond Failure Modes

### LIST OF FIGURES (Cont'd)

- Fig. 18      Curing Behavior of Epoxy-Nylon Adhesive Films
- Fig. 19      Curing Behavior of Epoxy Based Adhesive Films
- Fig. 20      Curing Behavior of AF-163 Adhesive Film
- Fig. 21      Shear Stress vs Crosshead Deflection for 60 Layer Laminates in  
3 Point Bend at Span/Depth = 5.0
- Fig. 22      Low Speed Winder for Fabrication of Composite Tapes
- Fig. 23      2826MB/FM-1000 Tape
- Fig. 24      Schematic Cross Section of Ribbon Layup Pattern Used in  
Composite Fabrication
- Fig. 25      Longitudinal Tensile Fracture Surfaces. 2.5 mm in-ply Ribbon  
Spacing
- Fig. 26      Transverse Tensile Fracture Surfaces. 2.5 mm in-ply Ribbon  
Spacing
- Fig. 27      Transverse Tensile Fracture Surfaces. 2.5 mm in-ply Ribbon  
Spacing. Ribbon Fracture Observed
- Fig. 28      Transverse Composite Cross Section. 2.5 mm in-ply Ribbon  
Spacing. Ribbon Sliding at A
- Fig. 29      Transverse Composite Cross Section. 0.5 mm in-ply Ribbon  
Spacing
- Fig. 30      Transverse Tensile Fracture Surface. 0.5 mm in-ply Ribbon  
Spacing. Ribbon Fracture Observed
- Fig. 31      Ribbon Embedded in Matrix Loaded for Pullout
- Fig. 32      2826MB Ribbon in Widths of 3.18, 6.35, 13.0 mm
- Fig. 33      Schematic Transverse Composite Cross Sections with Expected  
Fracture Plane Indicated
- Fig. 34      Transverse Tensile Failure Showing Ribbon Pullout - Ribbon  
Width is 3.18 mm

### LIST OF FIGURES (Cont'd)

- Fig. 35      Transverse Tensile Specimens Tested at Room Temperature
- Fig. 36      Fracture Surface of Composite Constructed with 0.5w Ribbon Overlap
- Fig. 37      Fracture Surface of Composite Constructed with 0.2w Ribbon Overlap
- Fig. 38      Schematic Transverse Composite Cross Sections with Expected Fracture Mode Utilizing 0.125 in. Wide Ribbon
- Fig. 39      Schematic Transverse Composite Cross Sections with Expected Fracture Mode Utilizing 0.51 in. Wide Ribbon
- Fig. 40      Tensile Properties of 13mm Ribbon - RB776-1PF4545 Spool #1
- Fig. 41      Thermal Expansion of 2826MB Ribbon - Longitudinal Orientation
- Fig. 42      Thermal Expansion of 2826MB Ribbon - Transverse Orientation
- Fig. 43      Thermal Expansion of 2826MB Ribbon - Longitudinal Orientation
- Fig. 44      Thermal Expansion of 2826MB Ribbon - Transverse Orientation
- Fig. 45      Composite Thermal Expansion Behavior - 0° Ribbon Orientation
- Fig. 46      Composite Thermal Expansion Behavior - 45° Ribbon Orientation
- Fig. 47      Composite Thermal Expansion Behavior - 90° Ribbon Orientation
- Fig. 48      Load-Deflection Curves for 2826 MB/FM1000 Composites Tested in 3 Point Bend at S/h = 5
- Fig. 49      Laminates Tested in Three Point Bend at S/h = 5
- Fig. 50      Schematic Transverse Composite Cross Sections with Expected Fracture Plane Indicated
- Fig. 51      Longitudinal Stress-Strain Behavior at Room Temperature
- Fig. 52      Longitudinal Tensile Fractures - Testing at Room Temperature
- Fig. 53      Effect of Test Temperature on Transverse Tensile Properties

# LIST OF FIGURES (Cont'd)

- Fig. 54 Transverse Tensile Fracture - Ribbon Overlap was  $0.5w$
- Fig. 55 Transverse Tensile Fracture - Ribbon Overlap was  $0.3w$
- Fig. 56 Schematic Diagrams of Strain Gage Pair Locations for Transverse Tensile Test
- Fig. 57 Transverse Stress-Strain Behavior at Room Temperature
- Fig. 58 Tensile Fractures at Room Temperature - Ribbons Oriented at  $45^{\circ}$  to the Tensile Axis
- Fig. 59 Effect of Test Temperature on Tensile Properties with Ribbons Oriented at  $45^{\circ}$  to the Tensile Axis
- Fig. 60 Tensile Fractures for  $45^{\circ}$  Ribbon Orientation - Ribbon Overlap was  $0.5w$
- Fig. 61 Tensile Fractures for  $45^{\circ}$  Ribbon Orientation - Ribbon Overlap was  $0.3w$
- Fig. 62 Stress-Strain Behavior at Room Temperature with Ribbons Oriented at  $45^{\circ}$  to the Tensile Axis
- Fig. 63 Thermal Cycle Utilized for Thermal Fatigue Test
- Fig. 64 Transverse Tensile Specimens Exposed to Moist Environment
- Fig. 65 Compression Stress-Strain Curve for  $0^{\circ}$  Ribbon Orientation
- Fig. 66 Compression Stress-Strain Curve for  $90^{\circ}$  Ribbon Orientation
- Fig. 67 Composite Tension-Tension Fatigue Behavior ( $R = 0.1$ )
- Fig. 68 Tension-Tension Fatigue Failures
- Fig. 69 Instrumented Impact Traces
- Fig. 70 Instrumented Impact Traces
- Fig. 71 Impact Specimens - Longitudinal Laminates

### LIST OF FIGURES (Cont'd)

- Fig. 72      Energy Dissipated as a Function of Specimen Geometry
- Fig. 73      Impact Specimens - Transverse Ribbon Orientation
- Fig. 74      Room Temperature Creep Behavior - Transverse Ribbon Orientation
- Fig. 75      Assessment of Composite Transverse Specific Strength
- Fig. 76      Assessment of Composite Transverse Specific Modulus

## LIST OF TABLES

Table 1	Comparison of Unidirectionally Reinforced Resin Matrix Composites
Table 2	Summary of Metal Ribbon Reinforced Resin Matrix Composites Data
Table 3	Commercially Available Amorphous Metal Ribbons (Allied Chemical)
Table 4	Summary of 2826 MB Ribbon Purchased for the Research Program
Table 5	Ribbon Dimensional Parameters
Table 6	Chemical Composition of Ribbon Cross Sections Exhibiting Varying Strength
Table 7	Summary of Bond Shear Strengths for Various Bonding Materials with Solvent Cleaned 2826 MB Ribbon
Table 8	Summary of Bond Shear Strengths for Various Ribbon Surface Treatments and Bonding Materials with 2826 MB Ribbon
Table 9	Summary of Adhesive Films Investigated
Table 10	Results of Lap Shear Testing Using Various Adhesive Films with Alkaline Cleaned 2826 MB Ribbon
Table 11	Curing Characteristics of Adhesive Films Investigated as Determined Using the Audrey Dielectric Analyzer
Table 12	Hot Pressing Procedures Utilized for Preparing Ribbon Reinforced Laminates Using the Indicated Matrix Materials
Table 13	Interlaminar Shear Strength of 60 Layer Laminates Tested in Three Point Bend at Span/Depth = 5
Table 14	Tensile Test Results for 2826 MB/FM-1000 Composites Comparing Solvent Cleaned and Alkaline Cleaned Ribbon
Table 15	Tensile Test Results for 2826 MB/FM-1000 Composites
Table 16	Summary of 2826 MB Ribbon Tensile Strength Data from Reel Locations Associated with Composite Fabrication

### LIST OF TABLES (Cont'd)

Table 17	Comparison of Longitudinal Tensile Properties with Rule of Mixture Calculation
Table 18	Transverse to Longitudinal Property Ratios for 2826 MB/FM-1000 Composites
Table 19	2826 MB Ribbon Parameters and Calculated Critical Transfer Length with FM-1000 Adhesive Film
Table 20	Transverse Tensile Test Results for 2826 MB/FM-1000 Composites
Table 21	Summary of 2826 MB Ribbon Tensile Strength Data from Reel Locations Associated with Composite Fabrication
Table 22	Summary of Calculated Composite Strength and Modulus Ratios
Table 23	Comparison of Experimental and Calculated Transverse Composite Property Ratios
Table 24	Transverse Tensile Properties for 2826 MB/FM-1046 Composites
Table 25	Ratio of Transverse Composite Tensile Strength to Axial Unidirectional Laminate Composite Tensile Strength
Table 26	Average Thermal Expansion Coefficients for 2826 MB Ribbon
Table 27	Composite Thermal Expansion Coefficients as a Function of Ribbon Orientation
Table 28	Interlaminar Shear Properties of 2826 MB/FM-1000 Laminates
Table 29	Composite Tensile Properties with Ribbons Oriented at $0^{\circ}$ to the Tensile Axis
Table 30	Composite Tensile Properties with Ribbons Oriented at $90^{\circ}$ to the Tensile Axis, Ribbon Overlap was 0.5w
Table 31	Composite Tensile Properties with Ribbons Oriented at $90^{\circ}$ to the Tensile Axis, Ribbon Overlap was 0.3w
Table 32	Calculated Transverse to Longitudinal Strength Ratios at $70^{\circ}\text{F}$
Table 33	Composite Tensile Properties with Ribbons Oriented at $45^{\circ}$ to the Tensile Axis, Ribbon Overlap was 0.5w



# LIST OF TABLES (Cont'd)

Table 34	Composite Tensile Properties with Ribbons Oriented at 45° to the Tensile Axis, Ribbon Overlap was 0.3w
Table 35	Transverse Tensile Strength after Thermal Fatigue
Table 36	Transverse Tensile Strength after Exposure to Moisture
Table 37	Results of Compression Testing at Room Temperature
Table 38	Results of Tension-Tension Fatigue Testing at Room Temperature, Ribbons Oriented at 0° to the Tensile Axis
Table 39	Results of Tension-Tension Fatigue Testing at Room Temperature, Ribbons Oriented at 90° to the Tensile Axis
Table 40	Results of Instrumented Impact Testing
Table 41	Effect of Test Span to Depth on Energy per Unit Area Absorbed
Table 42	Calculated $K_{ID}$ Values for Charpy V-Notch Specimens
Table 43	Room Temperature Stress-Rupture Data-Transverse Ribbon Orientation
Table 44	Material Property Summary

## SUMMARY

Commercially available amorphous metal ribbons were assessed from the standpoint of mechanical properties and aspect ratio, and Matglas alloy 2826 MB was selected as the optimum ribbon for reinforcing resin matrices. Several lots of ribbon material were purchased which exhibited uniform cross sections and strengths in the range of 2550-2900 MPa (370-420 ksi). Exposure of the ribbon to temperatures of 200°C (390°F) or greater decreased the ribbon tensile strength. For this reason, a limitation on matrix cure temperature of 177°C (350°F) was dictated. The ribbon elastic modulus was 165 GPa (24 Msi).

Liquid epoxies and epoxy based adhesive films were assessed as possible matrix candidates. The adhesive films exhibited an order of magnitude higher ribbon/matrix bond strength than the liquid resins. Subsequently, a series of epoxy based adhesive films were evaluated. Based on determinations of ribbon/matrix bond strength, laminate interlaminar shear strength, and ease of fabrication, FM-1000, an epoxy-nylon, was selected as the matrix material. It was demonstrated that surface preparation using active chemical formulations offered no significant advantages over solvent cleaning in obtaining high ribbon/matrix bond strengths when using FM-1000.

Composite construction parameters were investigated using ribbon material 3.18, 6.35, and 13 mm (0.125, 0.25, and 0.51 in.) wide having aspect ratios of 93, 155, and 380 respectively. Critical transfer lengths were determined for the ribbon/matrix combinations, and a series of ribbon stacking patterns were defined. It was found that the composite transverse elastic modulus depended primarily on the ribbon aspect ratio. Modulus ratios,  $E_{22}/E_{11}$ , of approximately 0.8, 0.9 and 1.0 were obtained with ribbon aspect ratios of 93, 155, and 380 respectively. The experimental values were in close agreement with those calculated using the Halpin-Tsai equations. The transverse composite tensile strength was primarily a function of the ribbon stacking pattern when the ribbon overlap was maintained greater than the critical transfer length. It was demonstrated that the transverse composite strength was increased by altering the stacking pattern to increase the number of ribbon fractures. Using the 13 mm (0.51 in.) ribbon, a strength ratio,  $\sigma_{22}/\sigma_{11}$ , of 0.76 was achieved. The actual composite transverse tensile strength was 1120 MPa (163 ksi). Comparison with theoretical expressions demonstrated that the transverse strength could be predicted from an assumed composite fracture mode based on a knowledge of the critical transfer length and the lay-up pattern utilized. Upper bound values on transverse composite strength were also calculated using an expression derived from uniaxially aligned short fiber theory.

Based on the results of the construction parameter study, a broad-based assessment of composite physical and mechanical properties was performed for composites constructed with high aspect ratio ribbon in a simple stacking pattern. A 4 kg lot of 2826 MB material was obtained for this study characterized by a width of 13.2 mm (0.52 in.) and an aspect ratio of 305. Tensile tests on ribbon sections removed throughout composite fabrication indicated an average ribbon tensile strength of 2570 MPa (373 ksi). The data determined in the material property assessment are summarized in the following paragraphs.

Determination of the ribbon thermal expansion behavior showed that the onset of crystallization was marked by a decrease in specimen volume and occurred at 400°C. The average ribbon coefficient of thermal expansion over the temperature range of 25-170°C was  $11.2 \times 10^{-6} \text{ }^{\circ}\text{C}^{-1}$ .

The composite thermal expansion behavior was determined over a similar temperature range as a function of ribbon orientation. The in-plane coefficient of thermal expansion was relatively isotropic and averaged  $12.7 \times 10^{-6} \text{ }^{\circ}\text{C}^{-1}$ .

The composite interlaminar shear strength was determined as 47.1 MPa (6830 psi) at 21°C (70°F). A dramatic decrease in interlaminar shear strength to 2.56 MPa (371 psi) was reported at 82°C (180°F). Observations of load-deflection curves and specimen deformation modes indicated that the resin was extensively softened at 82°C (180°F).

The tensile properties of composites were investigated as a function of ribbon orientation, test temperature, and ribbon overlap pattern. Determination of the room temperature elastic properties showed that the longitudinal elastic modulus could be closely approximated by a rule of mixtures calculation. The composite modulus with the ribbons oriented at 45° and 90° to the tensile axis was shown to vary widely. This was related to the positioning of strain gages relative to the surface gaps between ribbons, and indicated that nonuniform deformation occurred along the specimen length when testing in these orientations. Specifically, the gap regions exhibited greater deformation at equivalent loads.

The longitudinal tensile strength could also be approximated by the rule of mixtures, but by assuming a ribbon strength of 2900 MPa (420 ksi). This is considerably greater than the average ribbon tensile strength determined.

The ratio of transverse tensile strength to longitudinal tensile strength was closely predicted from the percentage of ribbons failed in the fractured composite cross sections. The transverse tensile strength was significantly reduced as a function of increased test temperature. At 82°C (180°F), 55% of the room temperature strength was retained for a simple overlap pattern, whereas

only 26% of the room temperature strength was retained for a more complex overlap pattern. The dependence on overlap pattern was related to increased critical overlap requirements as bond strength decreased. This was correlated with increased susceptibility for ribbon pullout in lieu of ribbon fracture during tensile testing.

With ribbons oriented at  $45^\circ$  to the tensile axis, tensile strength at room temperature was strongly affected by ribbon overlap. For a simple overlap pattern, the ratio of  $45^\circ$  tensile strength to the transverse tensile strength was 1.0, while for the more complex pattern, this ratio was 1.31. This difference was related to a change in fracture plane as a function of ribbon overlap. At elevated test temperature, significant reductions in tensile strength were observed. At  $82^\circ\text{C}$  ( $180^\circ\text{F}$ ), 47% of the room temperature tensile strength was retained for the simple overlap pattern, and 32% of the room temperature tensile strength was retained for the complex overlap pattern. These results were correlated with increased susceptibility to ribbon pullout for the simple overlap pattern, while both a change in fracture plane as well as increased pullout susceptibility occurred for the complex overlap pattern.

The transverse tensile strength was unaffected after thermal cycling composites between room temperature and  $82^\circ\text{C}$  ( $180^\circ\text{F}$ ) a total of 500 times. However, exposure to 95% relative humidity at  $60^\circ\text{C}$  ( $140^\circ\text{F}$ ) was shown to decrease composite transverse tensile strength by more than 80%.

The longitudinal and transverse compression strengths were found to be only 60% of the respective composite tensile strengths. This difference was attributed to a buckling failure mode in compression.

The results of tension-tension fatigue testing at room temperature indicated that the fatigue resistance of the composites was low. The  $10^6$  cycle fatigue limit was defined at maximum fatigue stress levels which were less than 20% of the composite static strength. Failure modes were similar to those observed for static tensile testing, although some delamination was evident for the longitudinal ribbon orientation.

Composite impact resistance and fracture toughness were assessed utilizing the instrumented impact test. It was shown that the energy absorbed per net section area was not strongly affected by test geometry as in the case of fiber reinforced composites. A comparison of longitudinally reinforced composites with unreinforced metals tested similarly showed that for standard size notched Charpy specimens ( $b = W = 10 \text{ mm}$ ), the composite impact energy was 10 joules while impact energies of 18 joules and 23 joules are associated with 6061-T6 aluminum alloy and Ti-6Al-4V respectively. Calculation of  $K_{ID}$  values from the load-deflection traces indicated that the fracture toughness of the composite as measured by this parameter was equivalent to that of 6061-T6 aluminum alloy.

Finally, determination of room temperature transverse creep and stress rupture properties showed a creep rate of  $8.0 \times 10^{-6} \text{ hr}^{-1}$  and rupture life in excess of 100 hr at a stress level equal to 90% of the composite ultimate tensile strength.

## I. INTRODUCTION

Ribbon reinforced composites possess a unique set of properties which can offer specific advantages when compared to fiber reinforced composites. The potential for this class of composites has been demonstrated in several investigations utilizing ribbon reinforced metal matrix systems (Refs. 1-8) and ribbon reinforced resin matrix systems (Refs. 9-15). However, the development and practical application of ribbon reinforced composites has progressed very slowly due to the absence of a low cost high performance ribbon material.

The primary structural advantage offered by the use of ribbons as the reinforcing phase in composites is demonstrated in Table 1. The mechanical properties typical of unidirectionally reinforced fiber composites are listed and compared with several ribbon reinforced composites. It may be seen that while fiber reinforced composites exhibit excellent axial properties, the transverse properties are significantly reduced resulting in transverse to longitudinal property ratios less than 0.1. The ribbon reinforced composites offer an order of magnitude improvement in the transverse to longitudinal property ratio. In the case of the E-glass reinforced resins, this improvement is observed while axial properties equivalent to the fiber reinforced composite are maintained. The degree of isotropy of the in-plane mechanical properties of unidirectionally reinforced ribbon composites is controlled by the ribbon width to thickness ratio,  $w/t$ . If this ratio is sufficiently high, virtually isotropic properties are achieved. In contrast, in-plane isotropy in fiber reinforced systems is achieved through multi-directional lay-up patterns such as  $[0, +45, 90]_n$ . Thus, although a similar degree of isotropy may be achieved in a fiber reinforced composite, it is achieved at a significant loss in axial properties.

In spite of the structural advantage offered by the use of ribbons as reinforcement, several factors have impeded their use. The primary problem has been the lack of a low cost process to consistently produce high performance ribbon material. The optimum performance on a specific property basis is offered by the reinforcements listed in Table 1. These materials, however, being ceramics and glasses exhibit the classic "size effect" problem characteristic of brittle materials so that wide ribbons can not be consistently produced having the same strength or strength variation equivalent to the fiber form. For example, the glass ribbons, utilized in the investigation referenced in Table 1 were produced under carefully controlled casting conditions, were chemically etched to remove surface defects, and were handled with extreme care prior to fabrication. The expense and impracticality of such a manufacturing process outweigh the structural advantages achieved.

Because of the size effect problem associated with ceramics and glasses, several investigators turned to the use of metals in ribbon form as the reinforcement in resin matrices. The results from several investigations (Refs. 9,10,12) are presented in Table 2. Excellent transverse to longitudinal property ratios are demonstrated in these data. The cold rolled carbon steel/epoxy system offers an axial strength of 1210 MPa (175 ksi), transverse strength of 724 MPa (105 ksi), and essentially isotropic modulus near 1176 GPa (17 Msi). This composite system was used in the fabrication of 80 mm (3.15 in.) diameter pipe.

The discovery of amorphous metal alloys and their ability to be continuously cast has presented the composite scientist with a unique reinforcement which offers several advantages with respect to other metallic reinforcements. Amorphous metals have specific strengths significantly higher than that offered by cold rolled steel alloys. The cold rolled steels have an upper limit on specific strength of approximately  $31.3 \times 10^3$  m while iron base amorphous metal alloys have exhibited specific strengths of  $49.9 \times 10^3$  m. In spite of their very high strength and amorphous structure, amorphous metal alloys do not exhibit the "size effect" characteristic of ceramics and glasses. In ribbon form, these materials are easily handled and can actually be crimped before failure occurs. Other possible advantages depending on composition are excellent corrosion resistance and unusual magnetic softness. Finally, fabrication of amorphous metal ribbon is in principle a low cost forming process since the shaping process is opposed by shear resistance of a liquid rather than a solid as in drawing or rolling operations. Estimates of the intrinsic cost of producing amorphous metal ribbons are on the order of \$1/kg.

Two investigations concerning the use of amorphous metal ribbons as the reinforcement for resin matrices were previously performed within United Technologies Corporation (Refs. 13,14). The longitudinal and transverse properties obtained are listed in Table 2. Although the transverse to longitudinal modulus ratio was improved with respect to fiber reinforced resins, the transverse to longitudinal strength ratio was not improved. The high strength ratios exhibited by the other metal ribbon reinforced systems listed in Table 2 were not achieved. The reason for these results were twofold. The primary reason was the lack of high aspect ratio ribbon at the time the investigations were carried out. Production of amorphous metal ribbon was still on an experimental basis and only ribbons approximately 1.0 mm wide with an aspect ratio of 25 were available. Secondly, the bond strengths of the ribbons to the matrices selected were very low. These two factors contributed to the relatively low composite performance.

Recent advances in processing have led to the production of amorphous metal ribbons on a continuous basis up to 50 mm (2.0 in.) wide with aspect ratios approaching 1000. These advances have presented the composite materials scientist with a source of high performance ribbon material which is potentially low cost. It was the objective of this research program to evaluate the performance of currently available amorphous metal ribbons as the reinforcement in resin matrix composites.

## II. RESULTS AND DISCUSSION

### A. Selection of Amorphous Metal Ribbon

#### 1. Evaluation of Available Ribbon Materials

Since it was directed that commercially available ribbon material be utilized in the program, only Allied Chemical Corporation was in a position to be a ribbon supplier. Other companies such as General Electric, Westinghouse Electric, and Allegheny Ludlum Industries were also involved in amorphous metal ribbon fabrication but only in experimental quantities.

As a first step in the ribbon selection process, an assessment of the minimum ribbon aspect ratio desired was made. The primary consideration was that the ribbon aspect ratio be sufficiently high to allow the composite in-plane properties to approach isotropy. The composite elastic moduli may be predicted utilizing the micromechanics analysis of Halpin and Thomas (Refs. 16,17). Their treatment yielded the following expressions:

1.  $E_{11} = E_R V_R + E_m V_m$
2.  $E_{22}/E_m = (1 + \xi \eta V_R)/(1 - \eta V_R)$
3.  $\eta = (E_R/E_m - 1)/(E_R/E_m + \xi)$

where  $E_{11}$  and  $E_{22}$  are axial and transverse composite moduli  
 $E_R$  is the ribbon modulus  
 $E_m$  is the matrix modulus  
 $V_R$  and  $V_m$  are ribbon and matrix volume fraction respectively  
 $\xi$  is a reinforcement geometry factor.

For the prediction of the transverse modulus of a ribbon reinforced composite,  $\xi = 2(w/t)$  where  $w/t$  is the ribbon aspect ratio. Using these relationships, plots of  $E_{22}/E_{11}$  vs ribbon aspect ratio were generated for various ratios of  $E_R/E_m$  and  $V_R = 0.4, 0.5$ , and  $0.6$ . As shown in Fig. 1, the most dramatic gains in transverse properties are achieved up to an aspect ratio of 100. It can also be discerned that, for a given ratio of  $E_{22}/E_{11}$ , a greater ribbon aspect ratio is required for systems having greater  $E_R/E_m$ . In other words, lower modulus matrix systems require a greater ribbon aspect ratio to achieve the same degree of isotropy as higher modulus matrix systems. Ribbon volume fraction does not strongly affect the transverse/longitudinal property ratio, but it will have a strong effect on absolute properties. For the ribbon materials under consideration, an upper limit of 165 GPa ( $24 \times 10^6$  psi) was placed on ribbon elastic



modulus after discussions with L. Davis of Allied Chemical Corporation. Assuming a matrix modulus of 3.45 GPa ( $0.5 \times 10^6$  psi) and 50% ribbon volume fraction, a plot of  $E_{22}$  vs ribbon aspect ratio was generated (Fig. 2). The transverse composite modulus increases from 41.7 to 75.9 GPa (6.0 to 11.0 Msi) as the aspect ratio increases from 10 to 100. A further increase in aspect ratio to 200 only increases the transverse modulus to 80 GPa (11.6 Msi). The modulus ratio,  $E_{22}/E_{11}$ , equals 0.9 at aspect ratio of 100. It was concluded that a ribbon aspect ratio of 100 represented a reasonable target value from the standpoint of composite elastic modulus.

A similar assessment was then made of the effect of ribbon aspect ratio on composite tensile strength. The composite tensile strength may be predicted from the following relations (Ref. 18):

$$\sigma_{11} = \sigma_R V_R + \sigma_m V_m$$

$$\sigma_{22} = \sigma_m V_m + \sigma_R V_R (1 - l_t/w)$$

where  $\sigma_{11}$  and  $\sigma_{22}$  are the composite axial and transverse tensile strengths  
 $\sigma_R$  is the ribbon tensile strength  
 $\sigma_m$  is the matrix tensile strength  
 $V_R$  and  $V_m$  are ribbon and matrix volume fractions  
 $w$  is the ribbon width  
 $l_t$  is the critical transfer length.

The equation for  $\sigma_{22}$  is derived assuming that the transverse cross section of a ribbon reinforced composite is equivalent to an uniaxially aligned short fiber composite. Further, constant interface shear stress and linear transfer of stress from matrix to ribbon is assumed. The critical transfer length,  $l_t$ , is given by  $l_t = \sigma_{Rt}/2\tau$  where  $t$  is the ribbon width and  $\tau$  is the shear strength at the matrix-ribbon interface. Using these relationships, plots of  $\sigma_{22}/\sigma_{11}$  vs ribbon aspect ratio were generated for several values of ribbon to matrix bond shear strength (Fig. 3). This plot shows that for a bond strength of 41.4 MPa (6.0 ksi), a ribbon aspect ratio of 100 would yield a transverse to longitudinal strength ratio of approximately 0.7. Note for lower values of bond strength, the ribbon aspect ratio required to give similar  $\sigma_{22}/\sigma_{11}$  ratios increases dramatically. Since typical resin to metal adhesive bond strengths generally do not exceed 41.4 MPa (6.0 ksi), this plot indicates that a ribbon aspect ratio of 100 is the minimum which should be considered to achieve a reasonable degree of isotropy.

The results of these two analyses indicated that a ribbon aspect ratio of at least 100 was required to achieve reasonably high transverse to longitudinal mechanical property ratios. A list of the commercially available amorphous metal ribbon materials was obtained from Allied Chemical Corporation and is shown in

Table 3. Note that alloys 2826, 2826 MB, and 2605 SC are available in aspect ratios greater than 100. The alloy 2826 MB offers a considerable advantage in mechanical properties and thus is preferred. It should also be mentioned that the titanium base alloy 2204 possesses the highest specific properties, and would be the optimum ribbon selection were it not for the very low aspect ratio currently available.

Based on these results, alloy 2826 MB was selected as the ribbon material for the program. Several lots of this material were purchased throughout the program. A listing of the various lots purchased is presented in Table 4 and a comment as to the ribbon use is included.

## 2. Evaluation of 2826 MB Ribbon Mechanical Properties

### a. Materials and Tensile Test Procedure

The initial lot of ribbon ordered from Allied Chemical was utilized to characterize the ribbon mechanical behavior. The as-cast ribbon width was 25.4 mm (1.0 in.). The parent ribbon was subsequently slit to 6.35 mm (0.25 in.) width by a vendor retained by Allied. This yielded four sections of ribbon which were wound on reels and identified with respect to transverse position in the 25.4 mm (1.0 in.) parent ribbon. The reels were labeled 1-4 as a sequence from one ribbon edge to the other. The average ribbon cross sectional areas were calculated from the weight of ribbon sections of a given length and a known density of 8.02 gm/cm<sup>3</sup>. This data is listed in Table 5. Note that the ribbon aspect ratio, w/t, determined from these measurements is approximately 160. Metallographic examination showed that the ribbon thickness varied considerably over a given cross section (Fig. 4).

Specimens having a 50 mm (2.0 in.) gage length were cut from each reel and tensile tested at a constant crosshead speed of 0.127 mm/min (0.005 in./min). Critical alignment was maintained by utilizing a slide tray fixture in which both the specimen and grips were mounted prior to testing. To calculate the tensile strength, the average ribbon cross sections listed in Table 5 were utilized.

### b. Tensile Strength of As-Received Ribbon

The ultimate tensile strengths determined for the ribbons utilizing the described procedure are plotted in Fig. 5 as a function of cumulative percent failed. It is evident that a significant variation in average tensile strength was associated with position in the original parent ribbon. Ribbons taken from the center of the parent (reels 2 and 3) were, on the average, significantly weaker than those taken from the outer edges (reels 1 and 4). The standard deviation in strength values was in the range of 10-15%.

### c. Effect of Gage Length on Tensile Strength

The possible effect of ribbon gage length on tensile properties was investigated utilizing the higher strength ribbon from reels 1 and 4. Specimens having gage lengths of 50.8, 127 and 254 mm (2.0, 5.0, and 10.0 in.) were tensile tested as described previously. The results are presented in Fig. 6 as a plot of tensile strength vs cumulative percent failed. It is apparent that the ribbon is not sensitive to gage length over the range measured. The data appear to fall into a bimodal format with one-third of the population failing at tensile stresses below 1900 MPa (275 ksi) and the other two-thirds above that value.

It had originally been expected that, for two reasons, there might be a gage length effect. First, statistically, it is expected that, if failure is controlled by the presence of a distributed population of initiation sites, the longer gage length would generally fail at lower stresses. This would be particularly true of a material with the large spread in strength observed in Fig. 6. Because of the uniform state of stress applied in the tensile test, it would make no difference if the strength controlling flaws were located throughout the ribbon bulk, only on the surface, or in the extreme, only on the outer edges. In each of these cases, the lack of dependence on gage length is unexpected.

A second gage length effect could relate to the probability of initiating failure from the ribbon edges. A longer gage length would tend to minimize any nonaxiality in the test and thus reduce the tendency for edge initiated fracture. This type of an effect would tend to increase ribbon strength with increasing gage length.

### d. Effect of Elevated Temperature Exposure on Ribbon Tensile Strength

The crystallization temperatures of commercially available amorphous ribbons are in the range of 400-500°C (752-932°F). Degradation of tensile properties is usually observed at considerably lower temperatures. Since the present program is concerned with resin matrix composite applications, exposure temperatures of 200, 300, and 400°C (392, 572, and 752°F) were selected. These would cover the maximum temperature ranges expected for composite fabrication utilizing thermosetting and thermoplastic matrices. Tensile specimens from reel #1 were exposed for 2 hrs at these temperatures under argon atmosphere. The tensile strengths determined at room temperature as a function of elevated temperature exposure are plotted in Fig. 7.

It is evident from this plot that elevated temperature exposure significantly reduces the ribbon tensile strength. After 200°C (392°F) exposure, the ribbon tensile strength is reduced 15% with respect to the as-received value. After 300°C (572°F) exposure, a 25% reduction in strength is observed. It is also noted that ribbons exposed to 300 and 400°C (572 and 752°F) were sufficiently embrittled to cause the gage sections to explode at failure in the tension test. These results suggest that fabrication procedures utilizing similar time cycles will be limited to approximately 200°C.

#### e. Variation in Tensile Strength as a Function of Reel Position

The tensile strengths of the as-received ribbon reported in Fig. 5 were significantly lower than projected by Allied Chemical for ribbon of this composition. An average tensile strength of at least 2410 MPa (350 ksi) had been anticipated while the best average strength measured was 1920 MPa (278 ksi). Two hypotheses to explain the observed results were considered.

The first hypothesis concerned the possibility that edge defects introduced during the slitting operation reduced the axial tensile strength. Observations in the SEM showed that the slit edges contained considerably more defects than as-cast edges. As shown in Fig. 8, the cast edge is relatively smooth with some protuberances while the slit edge contains a considerable number of irregular voids, presumably a result of the brittle fracture mode induced during the slitting operation. Such defects could act as sites for premature failure initiation. Thus, a ribbon with two slit edges would have a higher probability for low strength failure than a similar gage length ribbon with only one slit edge. Although this is a plausible argument which supports the data in Fig. 5, subsequent testing produced a contradictory result. As will be discussed in the following paragraph, sections of the ribbon having significantly higher strengths did not exhibit location dependent strength across the width. Specimens from reel #1 and reel #2 had equivalent tensile strengths. Thus, it was concluded that the edge condition characteristic of slitting was not a significant factor in affecting ribbon tensile strength.

The second hypothesis was associated with the observation that the outermost ribbon cross sections had significantly less variation in thickness than the central sections. It was reasoned that this observation was indicative of a casting instability during ribbon processing. To investigate this possibility, reels 1 and 2 were rewound so that specimens taken from the opposite ends of the 305 m (1000 ft) reels could be compared. The average cross sectional areas determined were  $26.6 \times 10^{-2} \text{ mm}^2$  ( $4.13 \times 10^{-4} \text{ in}^2$ ) and  $26.4 \times 10^{-2} \text{ mm}^2$  ( $4.10 \times 10^{-4} \text{ in}^2$ ) for reel #1 and #2 respectively. Comparing these values with the data in Table 5 indicates that the cross sectional area across the parent ribbon width was more uniform at this end of the reel. The ribbon tensile strengths were determined and are compared in Fig. 9 with those previously determined. It is evident that the average ribbon strength has increased dramatically from previous levels of 1500-1800 MPa (218-260 ksi) to greater than 2760 MPa (400 ksi). Also, there was no location dependent tensile strength (reel #1 vs reel #2) for the high strength ribbon sections. Observations of polished ribbon cross sections,

Fig. 10, showed that the cross sections of the high strength ribbons were significantly more uniform than those of the low strength ribbons. A significant difference in ribbon surface appearance was also detected. High strength ribbon material had a very smooth surface appearance while low strength ribbon material had a mottled surface appearance. Observations in the SEM, Fig. 11, showed that the low strength ribbon material was covered with void craters indicating poor contact of the ribbon with the casting chill block during fabrication. Chemical analysis of both high strength and low strength ribbon sections was also performed. As shown in Table 6, there was no macrosegregation of either metal or metalloid constituent to a particular section. It was concluded from these observations that casting instability during processing was responsible for the low ribbon strengths originally observed. Discussions with Allied Chemical indicated that this was most likely due to wheel erosion with time as casting progressed. Thus, it was expected that ribbon tensile strength would remain at high levels until that point at which instability occurred. Subsequent ribbon monitoring demonstrated that this was the case with the majority of the 305 m length exhibiting tensile strengths in excess of 2410 MPa (350 ksi).

The other ribbons listed in Table 4 were purchased in as-cast form at later dates and no strength variations such as described in this section were encountered. The ribbons were of high quality and possessed consistently high strengths. Tensile strength data will be presented in later sections where this ribbon material was utilized for composite fabrication.

#### f. Observations of Tensile Fracture Surfaces

Fracture surfaces from both high strength and low strength ribbons were viewed in the SEM. A specific fracture mechanism was not isolated since preferential fracture nucleation sites could not be identified. In general, all the fracture surfaces exhibited the veining pattern typical of metallic glass fracture. Some areas of high plasticity characterized by ductile tearing were also located. It appeared that the veining pattern was somewhat finer and that regions of ductile tearing were more prevalent for the higher strength ribbon. (Compare Figs. 12 and 13 with Figs. 14 and 15.) However, the number of observations was not sufficient to make a quantitative statement.

#### g. Determination of Ribbon Elastic Modulus

The elastic modulus was determined from load (P) - elongation ( $\Delta L$ ) curves by plotting the  $\Delta L/P$  as a function of specimen gage length. Such a plot exhibits linear behavior, where the slope is inversely proportional to the elastic modulus. Using this technique, the elastic modulus was calculated as 165 GPa (24 Msi).

The modulus was also measured using extensional wave velocity measurements. In this technique the pulse velocity is determined over a given path length and  $E$  is calculated from the relationship  $E = \rho V^2$ . The elastic modulus determined in this manner was 158.6 GPa (23.0 Msi). This value is within 6.9 GPa (1 Msi) of the value reported by Allied Chemical for this material. Davis (Ref. 18) has pointed out that such measurements on ferromagnetic metallic glasses should be carried out under a saturating magnetic field to negate the so-called " $\Delta E$  effect" which results in reduced elastic modulus determinations. However, in this material, the magnitude of any such effect appears to be within the error of measurement.

## B. Selection of Matrix Material

### 1. Preliminary Screening of Matrix Candidates

#### a. Materials

Due to the ribbon format and metallic characteristics of the amorphous metal reinforcement, two types of resin systems were considered as matrix candidates. These were commonly utilized epoxy resins in liquid form and epoxy based adhesives in solid film form. The adhesive films were included since they were developed specifically for bonding metals. Also, the solid film form could offer unique advantages in fabricating composite prepreg material. The liquid resins evaluated were Shell Epon 828, PR-286 supplied by 3M Co., and FR-7015 supplied by Fiber Resin Corporation. The FR-7015 is a 2 part room temperature cure system while the others are cured at 177°C (350°F). The adhesive films evaluated included FM-300 $\mu$ , FM-1000, and FM-1046 supplied by American Cyanamid, AF-42 supplied by 3M Company, and EA-9649R supplied by Hysol Corporation. All the films are unsupported and are cured at 177°C (350°F).

#### b. Ribbon/Matrix Bond Strength Determination

The primary property of interest for developing a ribbon reinforced composite is the ribbon/matrix bond strength. This value coupled with the matrix shear strength will determine efficiency of load transfer from matrix to ribbon. The ribbon/matrix bond strength was determined utilizing single overlap shear specimens, Fig. 16, having an adherend length of 63.5 mm (2.5 in.) and bond overlap length of 3.2 to 12.7 mm (0.13 to 0.5 in.) depending on the bond strength. The ribbon was solvent cleaned prior to bonding. Glass scrim cloth was inserted in the liquid epoxy lap joints to stabilize resin flow during curing. The specimens were mounted in a slide tray alignment fixture and tested to failure in tension at a crosshead speed of 0.25 mm/min (0.01 in./min). The results of the lap shear testing are presented in Table 7. The superiority of the epoxy based

adhesive films over liquid epoxies is clearly evident. The ribbon/matrix bond strength is an order of magnitude greater for the film adhesives. One contribution to the difference in bond strength measured by the lap shear test is the lower peel strength of the epoxies compared to the epoxy nylons. There is always a bending moment in the single lap shear test which will tend to decrease the bond strength measured, and the degree of decrease is related to the peel strength. Thus, the measured bond strength will be reduced the greatest for the epoxies in this type of test. However, the large magnitude of the difference measured indicates that the adhesive films clearly represent a better choice of matrix material than liquid epoxies. This conclusion was reinforced by observations of the bond failure mode. For the liquid epoxy systems, the failure was adhesive, i.e. at the ribbon/matrix interface, while for the epoxy-nylon adhesive films, the failure was cohesive or partially cohesive, i.e. failure through the matrix and/or ribbon.

#### c. Effect of Ribbon Cleaning Procedures on Ribbon/Matrix Bond Strength

In the adhesive bonding of iron based materials, it is generally observed that a well cleaned surface forms an excellent bond with epoxy based systems. For this reason, surface treatments are relatively simple utilizing either acid or alkaline based cleaning systems. A review of the adhesive bonding procedures for steels shows that the cleaning procedures developed to date rely primarily on solutions of common laboratory reagents (Refs. 19,20). Cleaning agents which are commercially available in bulk form have not been widely used. For this reason, our initial investigation of ribbon surface treatment involved the evaluation of the relative bond strength associated with acid and alkaline cleaning solutions prepared from laboratory reagents. Due to the simplicity of the cleaning procedures utilized, however, it was felt that commercially available acidic and alkaline cleaners for steels should be obtained and compared with the cleaning solutions prepared from laboratory reagents. The commercial cleaners offer the advantages of having the components precombined as a single powder or liquid which is simply mixed with water. After discussions with local suppliers, the following METEX compounds supplied by McDermid Co. were selected. Following is a brief summary of the technical merits of these products as listed by the producer.

##### METEX T-103

This solution is a soap-free, moderately alkaline metal cleaner recommended as a heavy duty soak cleaner for steels. It exhibits excellent penetration into deep recesses, rapid wetting of metal surfaces even when oily, complete and rapid displacement and emulsification of oily soils.

#### METEX S-1645

This solution is a blend of surfactants, detergents, inhibitors, and acids offering tremendous cleaning power at low concentration and temperature. It is extremely effective in removing soils that are difficult to remove with alkaline cleaning systems.

#### METEX M-629

This solution is an acid salt which is used primarily to strip chromium from nickel. Its primary advantage is in producing an activated nickel surface after cleaning. Due to the composition of 2826 MB, the producer felt this may offer an advantage in surface preparation for bonding. In particular, it was recommended as a second step after cleaning with T-103.

In assessing the utility of these solutions, an overall scheme of composite tape preparation was a foremost consideration. In particular, it was felt that a maximum bath time of 5 sec was amenable with a rapid drum winding process. For this reason, concentrated solutions as recommended by the manufacturer were utilized. The relative cleaning success was assessed qualitatively by testing for a water-break-free condition and quantitatively by the measurement of bond strength. Following is a listing of the procedures utilized. All treatments start with solvent cleaned ribbon material.

##### a. 2 Part Acid Solution

- (1) immerse for 5 sec in a bath of 4 parts sodium dichromate, 10 parts sulfuric acid, 20 parts distilled water held at 75°C
- (2) rinse in distilled water
- (3) rinse in ethyl alcohol and wipe dry.

##### b. 3 Part Base Solution

- (1) immerse for 5 sec in a bath of 6.4 parts sodium metasilicate, 3.2 parts sodium hydroxide, 0.5 parts sodium pyrophosphate, 32 parts distilled water heated to 70-80°C.
- (2) rinse in distilled water
- (3) rinse in ethyl alcohol and wipe dry.

##### c. METEX T-103

- (1) immerse for 5 sec in a bath containing 9 gm T-103/100 ml distilled water heated to 85-90°C
- (2) rinse in distilled water
- (3) rinse in ethyl alcohol and wipe dry.



d. METEX S-1645

- (1) immerse for 5 sec in a bath containing 5 ml S-1645/100 ml distilled water heated to 55°C
- (2) rinse in distilled water
- (3) rinse in ethyl alcohol and wipe dry.

e. METEX M-629

- (1) immerse for 5 sec in bath containing 20 gm M-629/100 ml distilled water heated to 80°C
- (2) rinse in distilled water
- (3) rinse in ethyl alcohol and wipe dry.

f. METEX T-103/METEX M-629

- (1) immerse for 5 sec in T-103 bath as described in (b)
- (2) rinse in distilled water
- (3) immerse for 5 sec in M-629 bath as described in (e)
- (4) rinse in distilled water
- (5) rinse in ethyl alcohol and wipe dry.

Only treatment (b) resulted in a 100% water-break-free surface. Treatment (a) exhibited an initial water break-free-surface which continuously degraded after approximately 5 min. Treatments (c) and (f) produced a partial water-break-free surface while (d) and (e) resulted in no water-break-free surface. It is also noted that treatment (a) resulted in a weight loss of approximately 1.3%, while no weight loss was produced with the other treatments.

The relative effectiveness of the surface treatments in promoting good bonding was evaluated for the two commonly utilized liquid epoxy resins, PR-286 and EPON 828, and one film adhesive, EA-9649R. A similar assessment for the other adhesive films was complicated by the fact that the ribbons failed prior to bond failure, for the minimum reasonable bond length, 3.2 mm (0.13 in.). Therefore, any significant improvement in ribbon/matrix bond strength using the FM-300 $\mu$ , FM-1000, FM-1046, or AF-42 would be immeasurable by this simple procedure. Although the measured bond strength was significantly lower for the EA-9649R, it was felt that it would be a useful screening agent for the general class of materials being considered. It should be noted that EA-9649R is a lower peel strength system than the other films, and as described previously would be expected to exhibit lower bond strength in a lap shear test.

The bond strength was determined using single overlap shear specimens as outlined previously. The results of testing are listed in Table 8. It is evident that the ribbon surface treatments significantly improve the bond strength of the liquid epoxies with the ribbon material when compared to solvent cleaned surfaces. In particular, the alkaline clean procedure (b) is correlated with optimum bonding. The optimum bond strength produced, however, is still significantly lower than that associated with the adhesive films. For the EA-9649R bond material, it is evident that the alkaline treatments provide a 25% increase in bond strength over solvent cleaned specimens as measured by this test, while the acidic treatments decrease the bond strength. Note that the use of M-629 as a secondary treatment with T-103 has negated the positive effect of using T-103 alone. Although both alkaline treatments provided the same relative increase in bond strength, it was observed that the T-103 solution was not rinsed as effectively in distilled water as the 3 part base. Residual T-103 solution was expelled from ribbon surfaces in the alcohol rinse.

It was concluded from these data that the 3 part base alkaline clean procedure represented the optimum ribbon surface preparation. However, it also seemed apparent that the degree of enhancement in bond strength can be correlated with the bond strength observed for solvent cleaned surfaces. Liquid epoxies had very low bond strengths with solvent cleaned ribbon surfaces and exhibited great improvements in ribbon/matrix bond strength when the ribbons were surface treated. The EA-9649R adhesive film exhibited moderate bond strength with solvent cleaned ribbons, and the sensitivity to surface treatment was much reduced. It is also very likely that an adhesive film such as FM-1000, having a very high bond strength with solvent cleaned ribbon material, would show even less sensitivity to surface treatment. It was clear, however, that even with the optimum ribbon surface preparation, the bond strengths associated with the liquid epoxies were significantly less than those observed with the adhesive films without ribbon surface treatment.

## 2. Evaluation of Adhesive Films

Based on the bond strength data, it was concluded that the epoxy based adhesive films offered the best choice of matrix material for fabricating ribbon reinforced composites. In selecting the optimum film, ribbon/matrix bond strength was considered the most important parameter. Other parameters of interest include matrix properties, film thickness, film flow properties, and handleability.

### a. Materials

A variety of adhesive films was selected which represented an extensive range of matrix systems. A description of these adhesive films is presented in Table 9. FM-1000 and FM-1046 were selected as representative epoxy-nylons, and are characterized by high peel strength, low stiffness, and low use temperature,

60°C (140°F). FM-150 is at the opposite end of the scale possessing low peel strength, high modulus, and a 177°C (350°F) capability. EA-9649R and AF-147 are toughened epoxies which exhibit better peel strength than FM-150 while maintaining similar temperature capabilities. AF-163 is a toughened epoxy which exhibits high peel strength, but only has a high temperature capability of approximately 120°C (250°F). The epoxy-nylons exhibit low flow during hot pressing and behave like a thermoplastic. In contrast, all the other systems have a component which melts and therefore exhibit high flow. Thus, although the epoxy adhesive films are much thicker than the epoxy nylons, equivalent ribbon volume fractions in composites may be achieved due to the difference in flow properties. It should be mentioned that all the films evaluated were unsupported. Also, the maximum cure temperature was limited to 177°C (350°F) due to the degradation of ribbon properties documented at temperatures above 200°C (392°F).

#### b. Determination of Ribbon/Matrix Bond Shear Strength

The primary property of interest for developing a ribbon reinforced composite is the ribbon/matrix bond strength. This value will determine the amount of ribbon overlap needed for optimizing translation of load from the matrix to the ribbon, and therefore will dictate composite construction parameters to a large extent. The ribbon/matrix bond shear strength was determined for the adhesive films in Table 9 utilizing single overlap shear specimens, Fig. 16, having an adherend length of 63.5 mm (2.5 in.) and bond overlap length of 3.2 mm (0.13 in.). Since ribbon surface treatment was previously shown to have a significant effect on the magnitude of bond strength developed when using epoxies as bonding agents, all the ribbon adherends were alkaline cleaned prior to bonding. The cured specimens were mounted in a slide tray alignment fixture and tested in tension to failure at 0.25 mm/min (0.01 in./min). The results of the lap shear testing are listed in Table 10. Included are the ribbon/matrix bond strength and the specimen failure mode. Schematic representations of the possible failure modes are shown in Fig. 17. It is evident that the FM-150 and EA-9649R exhibit significantly lower bond strengths than the other matrix candidates. Adhesive failures at the ribbon/matrix interface, Fig. 17c, correlated with the low bond strength observed. All the other matrix candidates exhibited cohesive failures, but other observations allowed a ranking of their performance. Note that ribbons bonded with AF-147 exhibited cohesive failure through the adhesive film midplane in the bond as characterized in Fig. 17b. Observation of the bond showed that it was very porous and of generally poor quality. It appeared that the adhesive did not wet the metal surface properly. In the case of FM-1046, one adhesive failure was observed in four samples tested. For these reasons, the AF-147 and FM-1046 are judged inferior to the FM-1000 and AF-163. Both the FM-1000 and AF-163 have true bond strengths with the ribbon in excess of the value measured since all failures occurred in the ribbon adherends as in Fig. 17a.

### c. Determination of Laminate Interlaminar Shear Properties

Another matrix controlled parameter which is of potential importance is the level of interlaminar shear strength developed in a composite. To determine the value of composite interlaminar shear strength, 60 layer laminates were constructed and hot pressed to yield composites having a ribbon volume fraction of approximately 60%. The hot pressing procedures were determined from the curing characteristics of the films as established using an Audrey dielectric analyzer. Several layers of the film were compressed at 0.69 MPa (100 psi) between two platens which were heated at a rate of approximately 2.5 C/min up to the manufacturer's suggested curing temperature, and then held for 1 hr at this temperature. The dielectric change in the adhesive films was continuously monitored as a function of time and temperature. The plots of dissipation factor vs time determined in this manner are presented in Figs. 18-20. Two generic curves were observed for the matrix systems studied. The epoxy nylons generally exhibited a single broad peak characteristic of curing as shown in Fig. 18. The other systems exhibited a double peak, Figs. 19 and 20, due to the presence of a low temperature melting peak, a minimum at which point gelation begins, and finally a gel peak. A listing of these temperatures for the systems investigated is presented in Table 11.

The epoxy nylons behaved like thermoplastic materials and it was found that optimum pressing conditions were more easily determined from experiment rather than attempting to pinpoint an optimum pressing temperature from the data in Fig. 18. The hot press procedure utilized is listed in Table 12. The primary difference in the two systems was that appreciable flow was observed when using FM-1000 whereas very little flow was available with the FM-1046. To achieve ribbon volume fraction of 0.60, 6.9 MPa (1000 psi) pressure was required when using the FM-1046 whereas only 1.38 MPa (200 psi) was required when using the FM-1000. Careful analysis of the curves in Fig. 18 reveals a secondary peak located at A for the FM-1000 which is not present in FM-1046. This could be characteristic of a delayed curing reaction in the FM-1000 which gives rise to considerably more flow.

For the other systems investigated, the hot press procedures were determined directly from the data in Figs. 19 and 20. Due to the thickness of these adhesive films, considerable flow was required prior to curing to achieve the required ribbon volume fraction. This was achieved by pressing at a temperature between the melting peak and the initiation of gel. The procedure followed was to heat the loaded die to this intermediate temperature plateau, press to stops at this temperature, and then raise the hot press temperature to the final cure temperature. The hot pressing schedules utilized are listed in Table 12.

The composites thus fabricated were then tested in three point bend at a span/depth of 5.0. Plots of calculated shear stress as a function of crosshead deflection are presented in Fig. 21. It is evident that widely varying behavior is associated with the various matrix selections, and this factor complicates the definition of the composite interlaminar shear strength. According to ASTM D2344 the short beam shear strength is defined at the ultimate failure load of the composite. However, there is no alternate definition to use for systems where extensive shear deformation occurs prior to failure. To resolve this problem, the following procedure was utilized. A tangent line to the load vs crosshead deflection curve was drawn. Then a secant to the curve was constructed having 75% of the slope of the tangent curve. The interlaminar shear strength was then defined as the shear stress associated with the load corresponding to the intersection of the secant line with the load deflection curve. In the case of FM-150 and EA-9649R, such a secant line was beyond the composite failure load, and the normal interlaminar shear strength associated with maximum load was recorded. For the other composites where extensive shear deformation occurred, this procedure allowed the definition of a comparative interlaminar shear strength at a point on the load vs deflection curve beyond initial bendover due to shear deformation. The values of interlaminar shear strength thus determined, as well as those calculated from the maximum load, are presented in Table 13. Also listed is the deflection observed at maximum load.

By using the secant method for defining the interlaminar shear strength, three strength regimes are defined. Composites utilizing FM-150 and EA-9649R as matrix materials have clearly superior interlaminar shear strengths. Intermediate interlaminar shear strength is associated with AF-147, FM-1000, and AF-163 as matrix materials. Finally, composites utilizing FM-1046 as the matrix material exhibit low interlaminar shear strength. When the maximum load criterion is utilized, the dispersion in composite interlaminar shear strength is greatly reduced so that distinct groupings of composites exhibiting similar behavior no longer exist. This is because the extensive deformation associated with the lower stiffness films increases the shear stress to levels approaching that observed in the high modulus films. For this reason, the secant method for defining interlaminar shear strength is preferred. This is particularly true if one is attempting to separate systems using incipient shear failure to define the interlaminar shear strength.

The composite failure modes observed could also be categorized. The FM-150 and EA-9649R composites exhibited catastrophic shear failure characterized by delamination at the specimen midplane at relatively low crosshead deflection. The AF-147 composites also failed by delamination, but only after considerable deformation. The FM-1000, FM-1046, and AF-163 exhibited matrix shear flow such that the laminate deformed to the shape of the loading apparatus. No delaminations occurred at the ribbon/matrix interfaces. In the case of the AF-163,

maximum load was defined by ribbon failure on the tension side of the bend specimen. In the case of FM-1000 and FM-1046, no evidence of any failure occurred, but the load did reach a maximum. However, considerable side loading was occurring at this point due to the large deflection so it is difficult to attach undue significance to this point.

#### d. Matrix Selection

In summarizing the ribbon/matrix bond strength and composite interlaminar shear strength data, the following correlation results. High composite interlaminar shear strength at incipient shear failure is achieved in brittle epoxy-novalac systems characterized by FM-150 and EA-9649R. However, the ribbon/matrix bond shear strength associated with these systems is low. High ribbon/matrix bond strength is achieved with a toughened epoxy such as AF-163 or an epoxy nylon, FM-1000. However, matrix shear flow decreases the composite interlaminar shear strength at incipient shear failure to only moderate levels.

Since the ribbon/matrix bond strength was considered most critical to constructing composites with high structural integrity, FM-1000 and AF-163 were favored over the other films. From a fabrication standpoint, the much lower resin flow associated with FM-1000 presented an advantage in maintaining ribbon alignment during hot processing. Both films exhibited excellent handleability. For these reasons, FM-1000 was selected as the matrix material for subsequent composite fabrication.

### C. Composite Fabrication Procedures

#### 1. Fabrication of Prepreg Tape

In order to fabricate large numbers of composite plates, it was necessary to formulate a composite tape fabrication procedure. Toward this end, a low speed winder was constructed which had the capability of winding ribbons up to 0.5 in. wide onto a 12 in. diameter rotating drum. The drum rotation and drum traverse were controlled separately allowing a continuous range of ribbon spacing to be obtained. A photograph of this apparatus is presented in Fig. 22.

The first step in the drum winding process involved covering the drum with a release paper over which a strip of the adhesive film was taped. Ribbon was then wound over the adhesive film with a controlled spacing as shown in Fig. 22. The primary problem in tape fabrication was to devise a method for adhering the ribbon to the adhesive film. Two approaches were investigated. The first involved painting the tape with a primer solution compatible with the adhesive film while the second approach utilized the heat sensitive nature of the film.

#### a. Prepreg Bonding by Primer Application

After covering the drum with a strip of adhesive film, the film was lightly painted with tack primer BR 1009-8. The ribbon was subsequently wound over the painted film before the primer dried. The BR 1009-8 developed a sufficient tack in 1 hr at room temperature to bond the ribbon to the adhesive film. The composite tape was then cut from the drum and could be laid out for cutting into the desired piece size. Handleability was good although ribbons could easily be peeled off the film. It was also observed that the bond seemed to degrade slightly if the tape was allowed to stand unused for a 24 hr period.

The effect of primer application on cured bond shear strength was determined utilizing single overlap shear specimens. It was found that the bond strength values varied considerably from 11.1 to 26.4 MPa (1610 to 3830 psi). The magnitude of bond strength could be correlated with the amount of primer applied. Very light applications resulted in good bonds, while excess primer severely degraded bond quality. This observation coupled with the fact that primer application could not be rigidly controlled prompted the consideration of other methods of bonding the ribbons to the adhesive film.

#### b. Prepreg Bonding by Heat Application

Since the FM-1000 behaved very much like a thermoplastic, it was felt that a controlled amount of heating could serve to initiate bonding of the ribbons to the film without causing any extensive film curing. An attempt was first made to bond the ribbon to the adhesive film on the winder by resistance heating of the ribbon. This was accomplished by connecting the two ribbon ends to an AC voltage source, and increasing the voltage until the ribbons were heated to a temperature which softened the adhesive film to initiate bonding. It was found that hot spots developed along the ribbons using this technique which produced two undesirable results. Bonding was very uneven, and the heat generated at the hot spot locations was sufficient to embrittle the ribbon material. This particular bonding method was therefore abandoned.

The use of radiant heat sources to bond the ribbon to the adhesive film was then investigated. A technique was developed which allowed the fabrication of composite tape material exhibiting excellent handleability. The following procedure was utilized. After winding ribbon over a strip of FM-1000 adhesive film, a heat gun was traversed over the film at a controlled rate. This provided sufficient tack of the ribbon on the film to allow cutting of the composite tape and removal from the mandrel. The tape was then laid out on a bench and pressed with a heated flat iron. This served to embed the ribbon in the film providing excellent handleability.

This process was subsequently refined so that the tape could be processed while remaining on the mandrel. First, the mandrel was spring loaded so that once the ribbon was wound onto the adhesive film, a radial load could be gradually applied to insure intimate contact of the ribbon with the film. Once this was accomplished, bonding could be achieved by simply passing the heated flat iron over the ribbon surface at a slow rate. A heated iron with a radius matching the mandrel was also fabricated, but this method of heat application offered no significant advantage over a standard heated flat iron. An example of a ribbon composite tape fabricated in this manner is shown in Fig. 23. Handleability and drape are both very good.

## 2. Composite Construction and Hot Pressing Procedure

Plies of the proper dimensions were cut from the prepreg tape material. Two approaches to composite construction were then utilized depending on the complexity of the stacking pattern and ribbon width utilized. For a simple stacking pattern where one-half the ribbon width was overlapped from layer to layer and where the ribbon width was at least 12.7 mm (0.5 in.), the plies were simply stacked in closed steel dies for subsequent hot pressing. When narrower ribbons were used or when a more complex stacking pattern was desired, the plies were laid up on a steel plate with the ribbon ends of each ply successively taped together to maintain alignment. The center section between the taped ends of this construction was then hot pressed using a ram of suitable size. In all cases, the hot pressing schedule outlined in Table 12 for the FM-1000 adhesive film was utilized.

## D. The Effect of Composite Construction Parameters on Tensile Properties

### 1. Evaluation of Ribbon Surface Treatment

It was pointed out in section B1c that the degree of improvement in ribbon/matrix bond strength associated with ribbon cleaning depended on the intrinsic bond strength of the adhesive film with the ribbon. No discrimination could be made using lap shear tests between solvent cleaned and alkaline cleaned ribbon bonded with FM-1000 since all failures occurred in the ribbon adherends as shown in Fig. 17a.

To determine whether the alkaline surface treatment would provide any significant advantage in composite properties, composites were fabricated from solvent cleaned and alkaline cleaned 6.35 mm ribbon from reel #1 in combination with the FM-1000 adhesive film and tested in tension in both the longitudinal and transverse orientation. Seven layer composites were constructed via hand lay-up using the ribbon stacking pattern presented in Fig. 24. Final composite dimensions were approximately 38.1 x 127 x 0.64 mm (1.5 x 5 x 0.025 in.). Tensile specimens 10.2 mm (0.4 in.) wide were cut from the composite plates, and



doublers were bonded to the ends producing a gage length of 50.8 mm (2.0 in.). Standard resistance strain gages were bonded to both sides of the specimens. Tensile tests were conducted at a crosshead speed of 0.25 mm/min (0.01 in./min). The data obtained are listed in Table 14. It is evident from this data that equivalent translation of ribbon properties to the composite was obtained using either solvent cleaned or alkaline cleaned ribbons. Any difference in bonding would be evident particularly in the transverse ribbon orientation, but it is evident that the strength observed scales with the ribbon volume fraction. Also, the transverse failure modes were characterized by ribbon failure with no ribbon pullout indicating excellent bonding in both cases. It was concluded from these results that a ribbon surface treatment other than solvent cleaning was unnecessary when bonding the ribbons with FM-1000.

## 2. The Effect of Ribbon Spacing and Volume Fraction on Composite Properties

Several composites were constructed using the ribbon stacking pattern depicted in Fig. 24 and hot pressed using the standard fabrication cycle. Final composite dimensions were 38.1 x 127 x t mm (1.5 x 5 x t in.) with ribbons oriented either parallel or transverse to the composite long axis. Ribbon spacings of 2.5 mm (0.1 in.) and 0.5 mm (0.02 in.) were utilized, and the ribbon volume fraction was varied by pressing to stops. Tension specimens 10.2 mm (0.4 in.) wide were cut from the composite plates and doublers were bonded to the ends producing a gage length of 50.8 mm (2.0 in.). Standard resistance strain gages were bonded to both sides of the specimens. Tensile tests were conducted at a constant crosshead speed of 0.25 mm/min (0.01 in./min).

The results of tensile testing these composites are listed in Table 15. The ribbon volume fractions were determined from density measurements assuming a ribbon density of 8.02 gm/cm<sup>3</sup> and matrix density of 1.15 gm/cm<sup>3</sup>. The average ribbon tensile strengths determined for specimen locations adjacent to the ribbon sections utilized for composite fabrication are listed in Table 16.

A comparison of the longitudinal properties with a rule of mixture calculation is presented in Table 17. The contribution of the matrix to the composite strength and modulus was considered negligible. It is evident that the measured values are closely approximated by the rule of mixture values. The longitudinal tensile fracture surfaces were characterized by a relatively flat fracture surface with little evidence of ribbon pullout. The crack propagated through the matrix and ribbon with little deviation. A typical example is shown in Fig. 25. The ribbons are easily discerned at the higher magnifications by the veining pattern characteristic of amorphous metal fractures.

Comparison of the transverse tensile properties listed in Table 15 indicate that ribbon overlap is very important in achieving optimum transverse properties. Note that a 20% increase in ribbon volume fraction has resulted in a 90% increase in transverse tensile strength (compare composite 3297 with 3300). This correlation is more readily seen in a comparison of transverse to longitudinal property ratios presented in Table 18. Where equivalent volume fractions for the longitudinal and transverse orientation were not available from the data in Table 15, the longitudinal tensile strengths were calculated from the rule of mixtures utilizing the ribbon tensile strength and ribbon volume fraction associated with the transverse composite. Similarly, the longitudinal modulus values were calculated assuming a ribbon modulus of 165 GPa (24 Msi). It may be seen in Table 18 that decreasing the ribbon spacing from 2.5 mm to 0.5 mm increased the strength ratio from 0.38 to 0.52. The modulus ratios for these ribbon spacings were equivalent.

Observation of the composite fracture surfaces demonstrated that the increase in transverse strength with decreased ribbon spacing correlated with a change in composite fracture mode. With the 2.5 mm (0.1 in.) ribbon spacing, a mixed fracture mode of ribbon pullout and ribbon failure was observed. An area of complete pullout is shown in Fig. 26a. Note the smooth surface feature of the ribbons indicating that these ribbons were pulled out of an overlap region with no ribbon fracture occurring. The deep crevices mark the void space left behind as the ribbons in the alternating layers of the seven layer composite were pulled out. An example of the mixed failure mode is shown in Fig. 26b where a smooth ribbon edge characteristic of pullout is observed adjacent to a fractured ribbon. Complete ribbon failure in the transverse cross section is shown in Fig. 27. Note that the fracture surface appears identical to that observed in longitudinal tensile failures.

The dual fracture mode associated with the 2.5 mm ribbon spacing was better understood after examination of polished ribbon cross sections. A typical transverse composite cross section is presented in Fig. 28. It can be seen that ribbon overlap was significantly reduced in region A in comparison with region B due to a small amount of ribbon sliding which occurred during the hot pressing operation. Region A is now a preferential fracture site where composite failure could occur by ribbon pullout. In the composites fabricated with the 0.5 mm in-ply ribbon spacing, overlap was sufficient to prevent cracks from propagating around ribbon ends. Rather, the fracture path was forced through ribbon cross sections. Presented in Fig. 29 is a composite cross section characteristic of the 0.5 mm ribbon spacing. It can be seen that ribbon sliding during fabrication does not significantly reduce the ribbon overlap. The preferential fracture site in this case is at point O where the crack only has to propagate through three

ribbon cross sections. Observations of the fracture surface in the SEM, Fig. 30, confirm that this is the case. The outermost ribbon has a smooth surface characteristic of a ribbon edge and the other three are fractured. This indicates that the fracture process involved propagation of a crack at the edge of the outermost ribbon and then ribbon failure through the cross section remaining.

It was concluded from these observations that the inferior transverse strength associated with the 2.5 mm (0.1 in.) in-ply ribbon spacing was due to the presence of ribbon pullout caused by poor ribbon overlap at specific sites. With the 0.5 mm (0.02 in.) in-ply ribbon spacing, no pullout was observed but rather fracture proceeded through the cross section at a plane of weakness delineated by the gap between ribbons. The increase in ribbon cross sections fractured increased the tensile strength.

One could rationalize from this analysis that the optimum overlap configuration would be a staggered lay-up which would have sufficient overlap to prevent crack propagation around the ribbon ends and increase the net number of ribbon cross sections in the crack path. The critical overlap or critical transfer length is defined by the stress level at which interface failure and ribbon failure are balanced. This length may be defined by loading a ribbon which has one end embedded in a matrix as shown in Fig. 31. Using a simple shear lag approach, the balance of stresses neglecting edge effects is  $2\tau lb = \sigma b t$  where  $\tau$  is the interface shear stress and  $\sigma$  is the tensile stress in the ribbon. The critical transfer length is then  $l_t = \sigma_r t / 2\tau$  where  $\tau$  is the ribbon/matrix bond strength in shear and  $\sigma_r$  is the ribbon fracture strength. Thus, for embedded ribbon lengths less than  $l_t$ , ribbon pullout is predicted, whereas at lengths greater than  $l_t$ , ribbon fracture is predicted. For the 2826 MB/FM-1000 composites in Table 15, calculation of the critical overlap length assuming a ribbon strength of 2480 MPa (360 ksi), bond shear strength of 34.5 MPa (5 ksi), and average ribbon thickness of  $4.1 \times 10^{-2}$  mm ( $1.6 \times 10^{-3}$  in.) yields  $l_t = 1.46$  mm (0.058 in.). For a 2.5 mm (0.01 in.) ribbon spacing, the ribbon overlap assuming perfect lay-up would be 2.03 mm (0.080 in.) and ribbon failure would be predicted. However, as shown in Fig. 28, ribbon sliding reduced the overlap to less than 0.4 mm (0.016 in.) at specific sites and pullout would be predicted and was observed.

### 3. The Effect of Ribbon Stacking Sequence on Composite Transverse Tensile Properties

#### a. Experimental Results

The concept developed in the previous section for optimizing the transverse tensile properties of ribbon reinforced composites was that a critical transfer length can be defined and that the ribbon overlap must be maintained greater than this critical transfer length. To test the validity of this concept, a

series of composites were constructed at relatively constant ribbon volume fraction utilizing various ribbon widths and stacking sequences. A constant ribbon spacing of 0.5 mm (0.02 in.) was utilized to minimize the effect of this parameter. The physical and mechanical properties of the 2826 MB ribbon obtained from Allied Chemical Corp. for this study (Fig. 32) are listed in Table 19. Also included is the critical transfer length calculated using the listed properties and assuming a ribbon/matrix bond strength of 34.5 MPa (5 ksi). Four composite lay-up patterns were designed and these are shown schematically in Fig. 33. Also shown in Fig. 33 are the expected fracture paths and resultant fraction of ribbons broken,  $f_{br}$ , assuming that the overlap in processed composites was greater than the critical transfer length. Due to the limitations of transfer length, lay-up (a) was used with the 3.175 mm (0.125 in.) ribbon, lay-ups (a) and (c) were used with the 6.35 mm (0.25 in.) ribbon, and all stacking sequences were used with the 13.0 mm (0.51 in.) ribbon. The composites were constructed and hot pressed according to the procedures outlined in section C. Tensile specimens were prepared for testing as described in the previous section, and were tested at a constant crosshead speed of 0.25 mm/min. (0.01 in./min). In all specimens, the ribbons were oriented transverse to the tensile axis.

The tensile properties determined for these composites are listed in Table 20. It is evident that the transverse composite modulus increased as the ribbon aspect ratio increased at relatively constant ribbon volume fraction. Changes in the overlap pattern had relatively little effect at constant ribbon aspect ratio. Modulus ratios  $E_{22}/E_{11}$  of approximately 0.8, 0.9, and 1.0 were achieved for ribbon aspect ratios of 93, 155, and 380 respectively assuming that the axial modulus could be calculated from the rule of mixtures.

A significantly greater effect of ribbon aspect ratio and composite lay-up pattern on the composite strength data is evident. It is most convenient to compare results based on the strength ratio,  $\sigma_{22}/\sigma_{11}$ . The value of  $\sigma_{11}$  was calculated from the simple rule of mixtures using the ribbon volume fraction measured for the transverse composite, and the ribbon strength determined for ribbon specimens removed from the reels adjacent to sections utilized for composite fabrication. The ribbon strength data are listed in Table 21, and the calculated strength ratios are listed in Table 22. The low value of  $\sigma_{22}/\sigma_{11}$  for composites fabricated with ribbons 3.18 mm (0.125 in.) wide suggests that the overlap with this ribbon was insufficient. From Table 19 it is seen that the critical transfer length is approximately 1.48 mm (0.058 in.). Since the ribbon width is 3.18 mm (0.125 in.), then the maximum spacing between ribbons which could be tolerated to still achieve reinforcement is 0.25 mm (0.010 in.). The average ribbon spacing in the composite was 0.48 mm (0.019 in.) and thus, ribbon pullout would be expected. Observation of the fracture surface, Fig. 34, confirmed that ribbon pullout was the primary failure mechanism which correlates

with the low strength observed. The other composites had sufficient overlap for reinforcement and significantly greater strength ratios were observed. It is also evident that as the overlap decreased, the strength ratio was increased. The reason for this, as is demonstrated in Fig. 33, is that a greater number of ribbon cross sections were aligned with the fracture plane by decreasing the overlap. Such a result is contingent on the requirement that an overlap greater than the critical transfer length remains, so that ribbon fracture will occur. Observations of the fracture surfaces indicated that the anticipated fracture mode depicted in Fig. 33 had occurred. As shown in Fig. 35, composite fracture occurred along the plane of weakness defined by the ribbon gaps resulting in a flat fracture perpendicular to the tensile axis. Note that on the back side of the specimens, fracture occurs at approximately 1/2 of a ribbon width for the 0.5w overlap pattern, and at approximately 1/4 of a ribbon width for the 0.2w overlap pattern. This coincides with the anticipated fracture path for these lay-ups in Fig. 33. The fracture surfaces were also observed in the SEM. As seen in Fig. 36, four ribbon fractures and two cast edges are present on the fracture surface of the specimen constructed with the 0.5w overlap pattern. This is in agreement with Fig. 33a. In the case of the 0.2w overlap pattern, Fig. 37, seven ribbon fractures and one cast edge are observed. As shown in Fig. 33d, eight ribbon fractures are expected for a perfect lay-up. It is apparent that one layer had insufficient overlap so as to allow the crack to circumvent it. Thus, a fracture efficiency of 0.7 occurred rather than 0.8.

It was concluded from these results that significant improvements in transverse composite modulus and strength could be achieved by varying the ribbon aspect ratio and repeat pattern. The modulus depended primarily on ribbon aspect ratio while the strength was dependent on the composite construction parameters. A modulus ratio,  $E_{22}/E_{11}$ , of 1.0 and strength ratio,  $\sigma_{22}/\sigma_{11}$ , of 0.76 were achieved using 13 mm (0.51 in.) wide ribbon material.

#### b. Comparison of Experimental Results with the Theory of Ribbon Reinforcement

##### (1) Elastic Modulus

The elastic moduli may be predicted utilizing the following expressions developed by Halpin and co-workers (Refs. 16,17).

$$E_{11} = E_R V_R + E_m V_m$$

$$E_{22}/E_m = (1 + \xi \eta V_R)/(1 - \eta V_R)$$

$$\eta = (E_R/E_m - 1)/(E_R/E_m + \xi)$$

where  $E_{11}$  and  $E_{22}$  are composite moduli

$E_R$  is the ribbon modulus

$E_m$  is the matrix modulus

$V_R$  and  $V_m$  are ribbon and matrix volume fraction respectively

$\xi$  is a reinforcement geometry factor.

For the prediction of the transverse modulus of a ribbon reinforced composite,  $\xi = 2$  ( $w/t$ ) where  $w/t$  is the ribbon aspect ratio. A comparison of the experimental modulus ratios with those calculated using these equations is presented in Table 23. Reasonable agreement between the experimental values and those calculated using this analysis is observed.

It should be realized that construction parameters such as ribbon overlap, spacing, and stacking sequence are not included in the equations used for predicting elastic properties. Rather, the material properties and in particular, the ribbon aspect ratio, are the parameters of key importance. Note that a ribbon aspect ratio of 93 yields 80% isotropy in elastic modulus while a ribbon aspect ratio of 380 yields complete isotropy in elastic modulus.

## (2) Tensile Strength

The composite tensile strength parallel to the long direction of the ribbons may be predicted by a simple rule of mixtures:

$$\sigma_{11} = \sigma_r V_r + \sigma_m V_m$$

where  $\sigma_r$  and  $\sigma_m$  are the ribbon and matrix tensile strengths, and  $V_r$  and  $V_m$  are the respective volume fractions. This expression may be used only when the critical volume fraction for reinforcement is less than the composite volume fraction. Two approaches to predict the transverse tensile strength of ribbon reinforced composites have been presented in the literature (Refs. 5,7,8,11,12,15). The first of these is based on the assumption that the transverse cross section of a ribbon reinforced composite is equivalent to an uniaxially aligned short fiber composite. Assuming linear transfer of load to the reinforcing phase, then the composite tensile strength parallel to the short fiber axis is given by (Ref. 21):

$$\sigma_c = \sigma_f V_f (1 - l_t/l) + \sigma_m' V_m$$

where  $l$  is the fiber length,  $l_t$  is the critical transfer length,  $\sigma_f$  and  $\sigma_m'$  are stress in fiber and matrix at the composite failure strain, and  $V_f$  and  $V_m$  are the respective volume fractions. Assuming equivalency of the transverse ribbon composite cross section to uniaxially aligned short fibers, then the transverse ribbon composite strength is given by

$$\sigma_{22} = \sigma_r V_r (1 - l_t/w) + \sigma_m' V_m \quad (1)$$

where  $w$  is the ribbon width. A primary difference between the uniaxial short fiber composite and the transverse ribbon cross section is the fact that the short fiber composite possesses a completely random overlap pattern whereas the

ribbon reinforced composite is generally constructed with a specific overlap pattern. This equation, then, is considered as an upper bound of the transverse strength which may be obtained in a ribbon reinforced composite.

A second approach to predicting the transverse tensile strength of ribbon reinforced composites utilizes the capability to predict the failure mode of a ribbon reinforced composite. An important consequence of a continuous planar reinforcement is the existence of a specific fracture initiation site at the gap between ribbons on the exterior surfaces. Since the failure always initiates on the specimen surface at a gap between ribbons, one ribbon layer is automatically discounted as reinforcement. Thus, the maximum composite strength possible would be  $\sigma_c = (N-1/N)(\sigma_r V_r) + \sigma_m' V_m$ , where  $N$  is the number of ribbon layers. This assumes that advancing crack always encounters a critical overlap length and all plies except the surface fail by ribbon fracture. This situation is virtually impossible to achieve, and in fact, most ribbon composites are laid up with a specific overlap pattern. The equation to predict strength remains the same, but now  $N$  becomes the number of layers in the repeat pattern,  $n$ . As a first approximation,  $n$  may be calculated as  $w/\ell_o$  where  $w$  is the ribbon width and  $\ell_o$  is the overlap from layer to layer. If the transfer length is known to be less than the overlap utilized, then a first approximation of the transverse composite tensile strength is given by:

$$\sigma_{22} = (n-1/n) \sigma_r V_r + \sigma_m' V_m.$$

Since ribbon reinforced composites exhibit a specific registry, and failure modes can be predicted as in Fig. 33, a more exact analysis based on the fracture mode is possible. Equations of the following form have been suggested to assess the transverse tensile strength (Ref. 12):

$$\sigma_{22} = f_{br} \sigma_r V_r + f_{po} \sigma_{r\ell^*} V_r + \sigma_m' V_m \quad (2)$$

This consists of three parts. The contribution from ribbons fractured is  $f_{br} \sigma_r V_r$  where  $f_{br}$  is the fraction of ribbons broken,  $\sigma_r$  is the ribbon fracture stress, and  $V_r$  is the ribbon volume fraction. The second term is the strength contribution from pullout where  $f_{po}$  is the fraction of ribbons pulled out,  $\sigma_{r\ell^*}$  is the ribbon stress corresponding to the average pullout length  $\ell^*$ , and  $V_r$  is the ribbon volume fraction. The third term is the matrix contribution at the composite failure strain. Assuming constant shear stress at the interface and linear load transfer to the fibers,  $\sigma_{r\ell^*}$  is simply defined as  $(\ell^*/\ell_t) \sigma_r$  where  $\ell_t$  is the critical transfer length and  $\ell^*$  is the average ribbon pullout length.

The experimental strength ratios are compared with those calculated using these expressions in Table 23. The values calculated from Eq. (1) are those expected from an uniaxially aligned short fiber composite, and therefore represent an upper bound of strength ratio which could be achieved. Values calculated

using Eq. (2) assume that ribbon sliding during fabrication is nonexistent so that the fracture paths depicted in Fig. 33 occur. It is evident that the experimental strength ratios are in good agreement with those calculated using Eq. (2). This suggests that transverse composite properties may be predicted knowing the critical transfer length and lay-up pattern utilized. The upper bound values calculated from Eq. (1) are also useful since they pinpoint the limiting values achievable with a given ribbon material. It is clear that 0.51 in. wide ribbon material offers significant advantages in this respect.

### c. Composites Design

The results of the previous discussion suggest several techniques which should be followed to obtain maximum transverse strength in ribbon reinforced composites. First, the ratio  $l_t/w$  must be minimized. Of the variables under our control, this can be accomplished by maximizing the ribbon/matrix interface shear strength and the ribbon aspect ratio utilized. The second critical factor involves optimizing the lay-up pattern. To obtain the highest transverse properties, the number of layers in the repeat pattern and the number of ribbons fractured should be maximized. This can be accomplished by selecting a ribbon overlap only slightly greater than the critical transfer length and by minimizing the ribbon spacing. Thus, matrix and ribbon selection as well as the construction parameters must be optimized to obtain maximum transverse strength properties.

### 4. Investigation of 0/90 Lay-up Patterns

The results of the previous section demonstrated that the transverse to longitudinal strength ratio was a function of the ribbon width and stacking pattern utilized. In general, an increase in transverse composite strength was achieved by varying the ribbon stacking pattern to increase the fraction of ribbons breaking. It was reasoned that further efficiency in ribbon fracture could be achieved by selective placement of  $90^\circ$  layers in composite cross sections.

For a simple stacking pattern using  $0.5w$  overlap for successive layers, the expected fracture mode in transverse tension is for one-half of the ribbons to fail. Thus,  $\sigma_{22}/\sigma_{11}$  would be approximately equal to 0.5. However, as seen in Table 23, an experimental value of 0.26 was obtained when using 0.125 in. ribbon ( $w/t = 93$ ). This was observed since ribbon pullout occurred rather than ribbon fracture. This is schematically represented in Fig. 38a. Note for the wider ribbons having the same stacking pattern, composites 3410 and 3418, the values of  $\sigma_{22}/\sigma_{11}$  were slightly greater than the calculated value of 0.5. In both cases, one-half of the ribbons failed. Assuming that it was desired to use a ribbon material which was not available in ribbon widths sufficient to produce ribbon fracture in this simple lay-up pattern, then an alternate solution would be to use a 0/90 lay-up. This is shown in Fig. 38b. Note that in this case, failure of the composite has to result in failure of one-half the



ribbon cross sections, i.e. all ribbons aligned parallel to the principal stress. Thus, the fraction of ribbons breaking,  $f_{br}$ , equals 0.5 and the ratio of composite strength to that of an unidirectional laminate,  $\sigma_{0/90}/\sigma_0$ , would be predicted as approximately 0.5, just as in the case of conventional cross ply composites.

To demonstrate this point, the 0.125 in. wide ribbon was utilized to fabricate 0/90 composites. Our first attempts utilized FM-1000 as the matrix material. However, it was found that the resin flow during hot pressing was too great to fabricate such a composite. FM-1046 was then used as a substitute matrix since this material exhibits very little flow during processing. Reasonably good ribbon alignment was maintained during fabrication resulting in satisfactory composites. Tensile coupons were cut from the composite plates and tested in tension as described in section D2. The results of these tests are listed in Table 24 along with those for an unidirectional composite having the 0.5w overlap pattern. The ratios of the transverse strength and modulus to those for an unidirectional laminate are presented in Table 25. The strength ratio increases from 0.2 for the simple unidirectional lay-up pattern to 0.46 for the 0/90 lay-up. The predicted value of 0.5 was not reached due to more extensive sliding between the ribbons in the zero layers as revealed through metallographic observations. This reduced the total fracture length of ribbons resulting in decreased contribution to the composite strength. Although the strength of the 0/90 lay-up pattern is significantly greater than the transverse strength observed for the unidirectional ribbon composite, the 0/90 strength is considerably reduced with respect to the longitudinal direction. The results are not significantly different than those expected for a fiber reinforced composite.

The 0/90 lay-up essentially offers an alternate lay-up for ribbon material which has less than the critical ribbon width required to prevent pullout. This could become important in considering more advanced ribbon material for composite fabrication, i.e. titanium base, where processing difficulties have limited casting of ribbons with aspect ratios less than 50.

The use of 0/90 lay-ups may also be extended to include ribbons having dimensions significantly greater than the critical width. One advantage of this is that the fraction of ribbons breaking in transverse tension can be improved with respect to the optimized unidirectional lay-up pattern. The latter point is demonstrated in Fig. 39. In Fig. 39a, an unidirectional lay-up with 0.2w overlap is depicted. The advancing crack will circumvent every fifth layer resulting in a fraction of ribbons failing equal to 0.8. This would be the approximate strength ratio,  $\sigma_{22}/\sigma_{11}$ , of the composite. In Fig. 39b, a 0/90 lay-up is presented where the overlap to the fracture plane is maintained greater than 0.2w for the 90° layers. It is evident that a crack will initiate at a ribbon gap on the outside surface and result in ribbon failure in all succeeding layers. Thus,  $f_{br} = 0.88$ , which represents an increase in the transverse strength with a small reduction in longitudinal properties when compared to the unidirectional lay-up. A composite was fabricated using the lay-up pattern presented in Fig. 39b with 13 mm (0.51 in.) wide 2826MB ribbon. FM-1046 adhesive film

was used as the matrix to minimize ribbon sliding. The tensile properties determined for this composite are listed in Table 24. The ratios of the tensile strength and modulus to those for an unidirectional laminate are presented in Table 25. Also included are the results for an unidirectional composite utilizing the overlap pattern shown in Fig. 39a. Comparison of these values with the calculated values based on the fracture paths shown in Fig. 39 shows that the predicted properties were not achieved for the 0/90 composite. Observation of the fracture surface showed that the actual fracture path produced a jog between layers 5 and 7 in Fig. 39b which allowed the crack to pass through two ribbon gaps thus reducing  $f_{br}$ . This was apparently caused by the greater transfer length when using FM-1046 as compared to FM-1000. An attempt was made to fabricate a similar composite using the FM-1000 adhesive film. The increased resin flow associated with this film, however, resulted in unsatisfactory composites. The  $0^\circ$  layers experienced various degrees of expulsion from the lay-up since the primary resin flow pattern occurred between the  $90^\circ$  oriented ribbons. Due to the processing difficulties, no further effort was expended in 0/90 fabrication. This is not considered a serious drawback since the theoretical transverse strength achievable with the complex 0/90 lay-up pattern was only 10% greater than that which has been achieved with low overlap unidirectional lay-ups.

In summary, two specific examples of the use of 0/90 lay-ups in ribbon reinforced composites were presented. Specific advantages in achieving improved transverse mechanical properties were discussed. However, the fabrication difficulties associated with the 0/90 lay-up may outweigh the possible advantages for use with wide ribbon materials.

#### E. Physical and Mechanical Properties of 2826 MB/FM-1000 Composites

Based on the results of the construction parameter study, a composite system was selected to be utilized in a broad based assessment of composite physical and mechanical properties. The 13 mm (0.51 in.) wide 2826 MB ribbon was selected in conjunction with FM-1000 as the matrix since this combination minimized the ratio of critical transfer length to ribbon width. A stacking sequence utilizing the 0.5w overlap pattern was selected since this would provide the greatest margin for error in the lay-up pattern associated with ribbon sliding during fabrication. Also this would simplify interpretation of the results, particularly with regard to fracture mode.

##### 1. 2826 MB Ribbon Tensile Properties

Approximately 4 kg of 2826 MB ribbon nominally 13mm wide was purchased from Allied Chemical Corporation for the test program. The ribbon was cast continuously in one production run and was designated lot RB776-1PF455 by the vendor.

Throughout composite fabrication, ribbon samples were removed to monitor tensile strength and dimensional stability. The cross sectional areas determined by weight measurement varied approximately 2% around a mean value of  $2.24 \times 10^{-2} \text{ mm}^2$  ( $8.80 \times 10^{-4} \text{ in.}^2$ ). The ribbon width was 13.2 mm (0.52 in.), and the average thickness was 0.043 mm ( $1.69 \times 10^{-3} \text{ in.}$ ) which corresponds to a ribbon aspect ratio of 308. Metallographic examination revealed that the ribbon cross sections were very uniform indicative of high quality ribbon material. Ten groups of five ribbon samples were tensile tested to monitor ribbon strength and these results are plotted in Fig. 40. The average ribbon strength determined from this data was 2570 MPa (373 ksi).

## 2. Thermal Expansion Characteristics

### a. Ribbon Thermal Expansion Behavior

The thermal expansion characteristics parallel and perpendicular to the long axis of the ribbon were determined using a quartz dilatometer. Ribbon sections were coiled inside silica glass collars and their expansion characteristics on heating and cooling were monitored. A heating rate of  $2^\circ\text{C}/\text{min}$  was utilized. The ribbon thermal expansion behavior was first determined over a temperature range of  $25\text{--}500^\circ\text{C}$  to define the crystallization phenomena. The plots of thermal strain as a function of temperature are presented in Figs. 41 and 42 for the longitudinal and transverse orientation respectively. The onset of crystallization is marked by a decrease in specimen volume which occurred at approximately  $400^\circ\text{C}$ . It also appears that there is a difference in expansion behavior for the two orientations up to the crystallization temperature. However, it is felt that this is due to difficulty in specimen mounting, particularly in the longitudinal orientation. For this reason, the data obtained for the transverse orientation are considered more representative of the ribbon.

Subsequently, specimens were monitored on a more sensitive scale between  $25^\circ\text{C}$  and  $170^\circ\text{C}$  to characterize the ribbon expansion behavior in the temperature regime of interest to composite thermal expansion. Plots of thermal strain as a function of temperature are presented in Figs. 43 and 44 for the longitudinal and transverse orientations respectively. Note that some hysteresis was recorded in the longitudinal orientation while the heating and cooling traces are nearly coincident for the transverse orientation. It is felt that this observation is again related to difficulties associated with the measuring technique in the longitudinal orientation. The average coefficients of expansion determined from the data are listed in Table 26. Assuming that the transverse orientation yields values most representative of the ribbon material, then the average ribbon coefficient of thermal expansion,  $\alpha_T$ , is  $11.2 \times 10^{-6} \text{ }^\circ\text{C}^{-1}$ .

### b. Composite Thermal Expansion Behavior

An 18 layer composite of dimensions 38.1 x 127 x 1.22 mm (1.5 x 5.0 x .048 in.) was constructed using an 0.3w overlap pattern, and was hot pressed in the normal manner. The ribbon volume fraction was calculated as 0.62. Specimens of dimensions 6.35 x 25 mm (0.25 x 1.0 in.) were cut from the composite plate in orientations of 0, 45, and 90° to the long axis of the ribbons. The thermal expansion behavior of these specimens was determined in the quartz dilatometer over a temperature range of 25-150°C. The specimens were cycled twice since "settling" of the specimen generally occurs during the first cycle. Typical second cycle plots of thermal strain as a function of temperature for these specimens are presented in Figs. 45, 46 and 47. The thermal expansion coefficients,  $\alpha$ , determined from this data for the cooling cycle are listed in Table 27. Since the cooling cycle is characterized by a much slower rate of change in temperature, the  $\alpha$  determined on this cycle is considered more accurate. A comparison of these values indicates that the in-plane thermal expansion coefficient,  $\alpha$ , of the composite is virtually isotropic. The composite thermal expansion coefficient is only slightly greater than that measured for the ribbon material averaging  $12.7 \times 10^{-6} \text{ }^{\circ}\text{C}^{-1}$ . The ribbon controls the thermal expansion behavior because of its high modulus with respect to the matrix.

## 3. Composite Mechanical Properties

### a. Interlaminar Shear Strength

The composite interlaminar shear properties were determined using 60 layer laminates which were constructed from the 13.2 mm (0.52 in.) 2826 MB ribbon and were hot pressed in the normal manner. The laminate dimensions were 13.2 x 150 x t mm (0.52 x 6.0 x t in.) where the thickness, t, was approximately 4.0 mm (0.160 in.). These laminates were cut into specimens of dimensions 13.2 x 38 x t mm (0.25 x 1.5 x t in.) and tested in three point bend at a span/depth of 5.0.

The composite interlaminar shear strength was determined at 21°C (70°F) and 82°C (180°F) in three point bending as described previously. Typical load-deflection curves for these two test temperatures are presented in Fig. 48. At room temperature, a plateau is observed in the load-deflection curve which corresponded to matrix shear failure. The interlaminar shear strength was defined using the load corresponding to the 75% secant intersection with this curve. At 82°C (180°F), the load increased continuously with deflection until the sample impinged on the loading pins. As seen in Fig. 48, the bending modulus was significantly reduced. For these samples, the interlaminar shear strength was calculated using the load corresponding to a deflection of 2.5 mm (0.1 in.). The composite interlaminar shear strengths,  $\tau_{\text{max}}$ , calculated using these loads are listed in Table 28. The average interlaminar shear strength

at 21°C (70°F) was 47.1 MPa (6830 psi) while at 82°C (180°F), the average inter-laminar shear strength decreased to only 2.56 MPa (371 psi). Observation of the specimens during deformation showed that those tested at room temperature deformed to the shape of the loading nose while those tested at 82°C (180°F) deformed in a similar manner but then exhibited a partially recoverable deformation on unloading. No delamination was observed in any of the specimens. Photographs of the tested specimens are shown in Fig. 49.

These results indicate that the FM-1000 matrix has extensively softened at 82°C (180°F) even in the cured or postcured condition. This phenomena severely limits the elevated temperature shear properties of the composite.

#### b. Tensile Properties

A test program was formulated to address the effect of ribbon orientation and test temperature on composite tensile properties. Two lay-up patterns were utilized. The simple 0.5w overlap pattern was first considered since this was least sensitive to error in lay-up pattern associated with ribbon sliding during fabrication, and simplified interpretation of specimen fracture surfaces. The more complex 0.3w overlap pattern was included to demonstrate the effect of overlap on tensile properties particularly as a function of test temperature. Schematic transverse cross sections of these two lay-up patterns are presented in Fig. 50. Note that the 0.5w pattern is an 8 layer composite while the 0.3w pattern is a 9 layer composite.

Composite panels of dimensions 38 x 127 x t mm (1.5 x 5.0 x t in.) and 76 x 152 x t mm (3.0 x 6.0 x t in.) were hot pressed according to the schedule outlined previously. Ribbon volume fractions were determined from density measurements assuming no porosity and using a density of 8.02 gm/cm<sup>3</sup> for the 2826 MB ribbon and 1.15 gm/cm<sup>3</sup> for the FM-1000 matrix. Tensile specimens 6.35 mm (0.25 in.) in width were cut from the panels, and fiberglass doublers were bonded to the specimens providing a gage section of 50 mm (2.0 in.) for the 0 and 90° specimens and 38 mm (1.5 in.) for the 45° specimens. Resistance strain gages were bonded to both sides of the specimens for determination of the elastic modulus and failure strain. Tensile testing was performed at a constant crosshead speed of 0.25 mm/min (0.01 in/min). Following is a summary of the results.

##### (1) Ribbons Oriented at 0° to the Tensile Axis

Two composite panels, 3555 and 3486, were fabricated utilizing the 0.5w and 0.3w overlap patterns respectively. Since it was anticipated that the longitudinal composite tensile properties,  $\sigma_{11}$  and  $E_{11}$ , could be predicted by the simple rule of mixtures, the density of the individual tensile specimens cut from these panels was determined to provide an accurate measure of ribbon

volume fraction in each specimen. The longitudinal tensile properties determined at room temperature are listed in Table 29 along with the rule of mixture values calculated assuming a ribbon tensile strength of 2570 MPa (373 ksi) and ribbon tensile modulus of 165 GPa (24 Msi). It is evident from the data in Table 29 that the composite modulus measured is closely approximated by the rule of mixtures modulus calculation. However, it is also evident that the composite strengths are significantly greater than that predicted by the rule of mixtures. The data can be more closely approximated assuming a ribbon strength of 2900 MPa (420 ksi).

Typical stress-strain curves for specimens from each panel are presented in Fig. 51. Linear elastic behavior is observed up to a strain level of approximately 0.01, and then a slightly decreased modulus is observed to failure. The failure strains varied between 0.017 and 0.0196. As shown in Fig. 52, tensile fractures were generally flat and occurred at 90° to the tensile axis.

#### (2) Ribbons Oriented at 90° to the Tensile Axis

Several composite panels were fabricated utilizing both the 0.5w and 0.3w overlap patterns. The transverse tensile properties of these composites were determined at room temperature, 54°C (130°F) and 82°C (180°F). The results are listed in Tables 30 and 31.

The average room temperature tensile strength was 807 MPa (117 ksi) for the 0.5w overlap pattern and 947 MPa (137 ksi) for the 0.3w overlap pattern. However, there was a significant difference in ribbon volume fraction in the composite panels. To compare the panels on an equivalent basis, the ratio of these tensile strengths to a calculated longitudinal strength,  $\sigma_{90}/\sigma_0$ , was determined. An average ribbon strength of 2900 MPa (420 ksi) was assumed since previous longitudinal tensile data could be closely approximated using this value. The calculated strength ratios are listed in Table 32. On this basis, it can be seen that the calculated strength ratio for the 0.5w overlap averages 0.48 while that for the 0.3w overlap averages 0.51. Reviewing Fig. 50, it is apparent that assuming perfect lay-ups and the fracture paths predicted, a ratio of 0.5 is expected for the 0.5w overlap pattern while a ratio of 0.67 is expected for the 0.3w overlap pattern. Good agreement is observed for the simple 0.5w overlap pattern, whereas a significant discrepancy exists for the more complex 0.3w overlap pattern. An explanation for these results was formulated by correlating the strength data with observations of the specimen fracture surfaces. For the 0.5w overlap pattern, the fracture mode was exactly as depicted in Fig. 50. For the 0.3w overlap pattern, the fracture mode varied significantly from that depicted in Fig. 50. In general, rather than 6 of 9 ribbons fracturing in the cross section, only 5 of 9 ribbons fractured due to imperfections in the repeat pattern. The expected strength ratio for this case is 0.55 which is in reasonable agreement with the results obtained.

The data in Tables 30 and 31 show that there is a significant reduction in transverse tensile strength with increased test temperature. It is also evident that the degree of reduction is more severe for the more complex overlap pattern. This is more easily seen in Fig. 53, a plot of the percent of room temperature transverse tensile strength retained as a function of test temperature. Note that an average of 55% of the room temperature strength is retained at 82°C (180°F) for the 0.5w overlap pattern, whereas only 26% of the room temperature strength is retained at 82°C (180°F) for the 0.3w overlap pattern.

Observations of the specimen fracture surfaces showed that the occurrence of pullout increased with test temperature and was dependent on the overlap pattern. Specimens constructed with the 0.5w overlap pattern showed some evidence of ribbon pullout when tested at 54°C (130°F). As shown in Fig. 54a, a one ply pullout was observed for specimen 3549-2 while tensile failure equivalent to that observed at room temperature is typified by specimen 3550-2. The pullout susceptibility increased at 82°C (180°F) such that a typical fracture surface exhibited two ribbons pulled out and two ribbons fractured. Typical failures showing the degree of pullout are shown in Fig. 54b. Note that this is consistent with a strength retained of slightly greater than 50% of the room temperature tensile strength. As shown in Fig. 55, specimens constructed utilizing the 0.3w overlap pattern exhibited extensive pullout with some ribbon fracture when tested at 54°C (130°F), while at 82°C (180°F) complete pullout was observed.

These results indicate that the decrease in tensile properties associated with increased test temperature is due to a decreased bond strength as well as extensive softening of the resin. The primary effect of decreased bond strength is to increase the critical overlap required to prevent pullout. Data provided by the manufacturer indicate a 40% reduction in lap shear strength at 82°C (180°F). A more complex overlap pattern provides less overlap length with respect to the critical overlap, and allows the instability associated with pullout to occur at lower stress levels.

The elastic properties were also determined at 70°F and are listed in Tables 30 and 31. A wide variation in elastic modulus and failure strain is observed with no apparent correlation to ribbon volume fraction as was observed for the longitudinal elastic modulus. Examination of the test specimens indicated that the location of the strain gage pairs on the surfaces of the specimens influenced the strain measured as a function of load. For the specimens listed in Table 30, the gages were bonded to the specimens so that the gages did not overlay any of the gaps between ribbons. This is schematically shown in Fig. 56a. Note that this resulted in a modulus measurement in excess of 110 GPa (16 Msi). However, based on the volume fraction measured and a ribbon modulus of 165 GPa (24 Msi), the maximum possible composite modulus is 99 GPa (14.4 Msi). For the

specimen listed in Table 31, the strain gages were bonded to the specimens such that one gage always overlayed a ribbon gap (Fig. 56b). In this case a modulus between 76 and 93 GPa (11.0 and 13.5 Msi) was measured compared to a maximum possible composite modulus of 109 GPa (15.8 Msi). Comparison of the failure strains also indicates distinctly different specimen behavior for the two strain gage locations. For the specimens with the gages overlaying ribbon gaps listed in Table 31, strain gage operation ceased prior to actual specimen failure. It was presumed that this was caused by contraction of the matrix material in the gap which resulted in gage debonding.

Typical stress-strain behavior for the two gage locations is shown in Fig. 57. When neither strain gage overlayed a ribbon gap, specimen 3549-1, an extensive range of linear behavior is observed and then as the failure load was approached, the apparent elastic modulus of the specimen increased. When one gage overlayed a ribbon gap, specimen 3504-2, a relatively short linear range is observed followed by a much more rapid increase in strain as the load increases.

These results indicate that nonuniform deformation occurs along the length of the specimen when tested in transverse tension. Greater deformation occurs at the ribbon gap locations, and this condition is aggravated as the failure load is approached.

### (3) Ribbons Oriented at $45^\circ$ to the Tensile Axis

Composite panels of dimensions 76 x 152 mm (3 x 6 in.) were fabricated utilizing both the 0.5w and 0.3w overlap patterns, and tensile specimens were cut from the panels at an angle  $\theta$  of  $45^\circ$  to the axis of the ribbons. The tensile properties determined at room temperature,  $54^\circ\text{C}$  ( $130^\circ\text{F}$ ), and  $82^\circ\text{C}$  ( $180^\circ\text{F}$ ) are listed in Tables 33 and 34. Also listed in the tables is the strength of a specimen cut from each plate with the ribbons oriented at  $90^\circ$  to the tensile axis.

The ratio of the  $90^\circ$  tensile strengths determined at room temperature compared to a calculated longitudinal strength,  $\sigma_{90}/\sigma_0$ , is approximately 0.5 for both lay-ups. The transverse fracture modes were identical to those observed and discussed in the previous section. However, it is evident that the ratio of the room temperature tensile strength with ribbons oriented at  $45^\circ$  to the  $90^\circ$  tensile strength,  $\sigma_{45}/\sigma_{90}$ , is markedly different for the two lay-up patterns. For the 0.5w overlap pattern, this ratio is approximately 1.0 while for the 0.3w overlap pattern,  $\sigma_{45}/\sigma_{90}$  is approximately 1.31. The reason for this discrepancy is related to the specimen fracture mode. In the case of the 0.5w overlap pattern, the specimens fractured along the plane of weakness, i.e. at  $45^\circ$  to the tensile axis. In the case of the 0.3w overlap pattern, the fracture plane was



predominantly perpendicular to the tensile axis with some outer ply pullout along the  $45^\circ$  plane. The latter fracture path increases the volume fraction of ribbon material fractured thus increasing the strength. Typical tensile fractures for both overlap patterns are shown in Fig. 58.

Significant reductions in tensile strength were observed for testing at  $54^\circ\text{C}$  ( $130^\circ\text{F}$ ) and  $82^\circ\text{C}$  ( $180^\circ\text{F}$ ). A plot of the room temperature tensile strength retained as a function of test temperature is presented in Fig. 59. At  $82^\circ\text{C}$  ( $180^\circ\text{F}$ ), an average of 47% of room temperature strength is retained for the 0.5w overlap pattern while 32% of room temperature strength is retained for the 0.3w overlap pattern. This dependence of strength on overlap pattern is similar to that observed with ribbons oriented at  $90^\circ$  to the tensile axis.

Observations of the fracture surfaces showed that those specimens constructed with the 0.5w overlap pattern exhibited increased evidence of pullout as the test temperature was increased (Fig. 60). Some ribbon fracture was still evident at  $82^\circ\text{C}$  ( $180^\circ\text{F}$ ). In the case of the 0.3w overlap pattern, Fig. 61, a change in fracture plane accompanied the increased susceptibility to pullout. Specimens tested at  $54^\circ\text{C}$  ( $130^\circ\text{F}$ ) fractured along the plane of weakness at  $45^\circ$  to the tensile axis in contrast to the room temperature fracture at  $90^\circ$  to the tensile axis. Extensive pullout with some ribbon fracture was observed. This change in fracture plane coupled with the increased susceptibility to pullout decreased the tensile strength. Specimens tested at  $82^\circ\text{C}$  ( $180^\circ\text{F}$ ) showed complete pullout with no ribbon fracture further decreasing the tensile strength.

The elastic properties determined at  $70^\circ\text{F}$  are also listed in Tables 33 and 34. A wide variation in elastic modulus and failure strain are evident. As discussed previously, this variation was due to the location of the strain gages relative to the gaps between ribbons on the specimen surface.

Typical stress-strain curves for the two overlap patterns are presented in Fig. 62. The data for the specimens constructed with the 0.5w overlap pattern represent strain gage locations which overlay, 3551-2, or do not overlay, 3551-11, ribbon gaps. Specimen 3488-4 was constructed with the 0.3w overlap pattern and exhibits much greater failure strain for an equivalent modulus.

#### c. Effect of Thermal Fatigue on Transverse Tensile Strength

An eight ply composite panel of dimensions  $38.1 \times 127 \text{ mm}$  ( $1.5 \times 5.0 \text{ in.}$ ) was constructed utilizing the 0.5w overlap pattern with ribbons oriented at  $90^\circ$  to the long dimension of the panel. The panel was hot pressed using established procedures. The panel was cycled between room temperature and  $82^\circ\text{C}$  ( $180^\circ\text{F}$ ) a total of 500 times. A plot of the thermal cycle utilized is presented in Fig. 63.

After this thermal cycling, there was no visual degradation of the panel. Tensile specimens 6.35 mm (0.25 in.) wide were cut from the panel and fiberglass doublers were bonded to the specimens providing a gage length of 50.8 mm (2.0 in.). The specimens were tested in tension at a crosshead speed of 0.25 mm/min (0.01 in./min). The tensile strengths determined are listed in Table 35. Also included are the ribbon volume fraction determined from density measurements and the predicted composite strength for this ribbon stacking pattern. It can be seen that the average tensile strength measured was very close to the expected composite strength. It was concluded from these results that the composite transverse tensile strength was unaffected by the thermal fatigue cycle utilized.

#### d. Effect of Moist Environment on Transverse Tensile Strength

An eight ply composite panel of dimensions 38.1 x 127 mm (1.5 x 5.0 in.) was fabricated utilizing the 0.5<sub>w</sub> overlap pattern with ribbons oriented at 90° to the long direction of the panel using established procedures. Tensile specimens 6.35 mm (0.25 in.) wide were cut from the panel, ribbon volume fractions were determined by density measurement, and fiberglass doublers were bonded to the specimens to provide a gage length of 50.8 mm (2.0 in.). These specimens were exposed to 95% relative humidity at 60°C (140°F) for 21 hrs. Weight gain measurements indicated that saturation occurred in less than 4 hrs. On removing the specimens from the chamber it was noted that small irregular patches of rust had formed on the outer ply ribbon surfaces. The specimens were sealed in plastic bags until tensile testing was performed. The results of tensile testing are listed in Table 36 along with the predicted tensile strength of the specimens. It is evident that exposure to moist environment has severely degraded the composite transverse tensile strength. All specimens failed by ribbon pullout indicating that the ribbon/matrix bond strength was severely degraded. There was some evidence of corrosion product along the edges of the interior ply ribbons, but to a much less extent than observed on the outer ply ribbon surfaces. Photographs of the failed specimens are shown in Fig. 64.

These results indicated that the 2826 MB/FM-1000 composite system has very low resistance to moisture exposure. Also, since most resin systems absorb moisture to some extent, the fact that the ribbons rust in moist environment indicates that this will be a general characteristic of resin matrix composites reinforced with 2826 MB ribbon. Exposure of the ribbon to the identical conditions in the humidity chamber showed that the same degree of rusting occurred in 2 hrs on ribbon material as was observed on the composite outer plys in 21 hrs.

## e. Compression Properties

### (1) Compression Testing

ASTM standard D3410-75 was selected as the test method for determining the composite compressive properties. To determine the required test specimen thickness,  $h$ , to insure composite beam failure in lieu of buckling, the Euler equation was utilized. The buckling load for a rectangular beam with both ends fixed is  $P = 4\pi^2 EI/L^2$  where  $E$  is the beam elastic modulus,  $I$  is equal to  $bh^3/12$ , and  $L$  is the specimen gage length. Since the strength,  $\sigma$ , is given by  $P/bh$ , the minimum beam thickness to prevent buckling is given by  $h = [3 \sigma L^2/\pi^2 E]^{1/3}$ . The minimum composite thickness to prevent buckling was calculated for ribbons oriented at  $0^\circ$  and  $90^\circ$  to the compression axis assuming that the compression strength and modulus were equivalent to those in tension. The results of tension testing have shown that reasonable values of the tensile properties for a ribbon volume fraction of 0.60 are  $\sigma_0 = 1740$  MPa (252 ksi),  $\sigma_{90} = 868$  MPa (126 ksi),  $E_0 = E_{90} = 99$  GPa (14.4 Msi). Assuming these values, then  $h_0 = 1.85$  mm (.073 in.) and  $h_{90} = 1.31$  mm (.052 in.). For composite thicknesses greater than these in the respective orientations, beam failure would occur prior to buckling.

Specimens of sufficient thickness were subsequently fabricated utilizing standard procedures. For the longitudinal ribbon orientation, 26 layer laminates of dimensions 6.35 x 152.4 mm (0.25 x 6.0 in.) were constructed utilizing the 6.35 mm (0.25 in.) ribbon. The laminate thickness was 2.08 mm (0.082 in.) and ribbon volume fraction was 0.52. For the transverse ribbon orientation, a 24 ply composite panel of dimensions 38.1 x 127 mm (1.5 x 5.0 in.) was constructed utilizing the 0.5w overlap pattern with 13.2 mm (0.52 in.) wide ribbons oriented at  $90^\circ$  to the long direction of the panel. The resultant composite thickness was 1.57 mm (0.062 in.) and the ribbon volume fraction was 0.60. Specimens 6.35 mm (0.25 in.) wide were cut from this panel. Doublers were bonded to the longitudinal and transverse specimens in accordance with standard D3410-75. Strain gages were bonded to both sides of the gage sections and wired to provide individual readout. Compression testing was then performed at a constant crosshead speed of 0.25 mm/min (0.01 in./min).

The failure stress and modulus values determined at room temperature are listed in Table 37. Also included is the predicted composite tensile strengths. It is evident that the compressive failure stress is significantly lower than the tensile strength predicted for similarly constructed composites. Examination of the specimens showed that this was due to a buckling failure mode in both the longitudinal and transverse specimens. In the case of the transverse specimens, the buckling failure was located at the plane of weakness where the gaps between ribbons were aligned. Since the Euler buckling stress

for uniform beams of these dimensions was 1860 MPa (270 ksi) and 1260 MPa (182 ksi) for the longitudinal and transverse ribbon orientations respectively, it was concluded that the buckling observed was a true composite failure mechanism in these ribbon reinforced composites. Typical stress strain curves for the longitudinal and transverse ribbon orientations are presented in Figs. 65 and 66 respectively.

#### f. Mechanical Fatigue Properties

##### (1) Longitudinal Ribbon Orientation

An eight ply composite panel 76.2 x 152 mm (3.0 x 6.0 in.) was fabricated utilizing the 0.5w overlap pattern with ribbons oriented parallel to the long dimension of the panel. Tensile specimens 6.35 mm (0.25 in.) wide were cut from this panel, and the density of the individual specimens was measured to determine the ribbon volume fraction. Fiberglass doublers were bonded to the specimens providing a gage length of 76.2 mm (3.0 in.). The specimens were tested at a maximum to minimum stress ratio of 0.1. The test parameters and the cycles to failure are listed in Table 38. Since the ribbon volume fractions varied considerably, the ratio of the maximum stress to the composite strength calculated from the rule of mixtures is also listed.

This data shows that this composite system has very poor fatigue resistance. Note that a  $10^6$  cycle life was achieved with ribbons in the longitudinal orientation for a maximum stress to composite strength ratio,  $\sigma_{\max}/\sigma_c$ , of only 0.11. For a system such as AS-graphite reinforced epoxy, this ratio is typically in the range of 0.6 to 0.7 for the longitudinal fiber orientation.

It was felt that the poor fatigue resistance of the previously discussed samples might in part be due to the fact that the amorphous metal ribbons were notch sensitive, and that the specimen cutting operation induced defects along the specimen length in those areas where a ribbon was cut. To assess this possibility, composite laminates were fabricated using the as-received 13 mm ribbon. The laminate dimensions were 13.5 x 152 mm (0.53 x 6.0 in.). Doublers were bonded to the as-pressed laminates providing a gage section of 76.2 mm (3.0 in.) that was 13.5 mm wide and wherein none of the ribbons had been cut. The specimens were tested using a stress ratio of 0.1 as before. The data for these specimens is also included in Table 38. These results indicate that the composite laminates fabricated from as-received ribbons have better fatigue resistance than specimens cut from a composite panel. A  $10^6$  cycle fatigue life was achieved for a maximum stress to composite strength ratio of 0.19. Although this represents a considerable improvement in fatigue life, even in the as-received condition the ribbon fatigue resistance is low.

## (2) Transverse Ribbon Orientation

Eight ply composite panels of dimensions 38.1 x 127 mm (1.5 x 5.0 in.) were fabricated utilizing the 0.5w overlap pattern with ribbons oriented at 90° to the long dimension of the panel. Specimens 6.35 mm (0.25 in.) in width were cut from the panels and fiberglass doublers were bonded to the specimens to provide a gage section of 50.8 mm (2.0 in.). Specimens were tested in tension-tension fatigue with a maximum to minimum stress ratio of 0.1. The test parameters and the cycles to failure are listed in Table 39. Also included are several static tension tests which are listed as 1 cycle failures.

The data listed in Table 39 indicate that with ribbons oriented at 90° to the tensile axis, the composite fatigue resistance is similar to that observed with ribbons oriented at 0° to the tensile axis. The 10<sup>6</sup> cycle fatigue limit was achieved for a maximum stress to composite strength ratio,  $\sigma_{\max}/\sigma_c$ , of 0.16. This ratio is greater than that observed for the longitudinal specimens cut from panels but is less than that observed for the uncut longitudinal laminates.

## (3) Summary

The fatigue results are summarized in Fig. 67 as a plot of the ratio of  $\sigma_{\max}$  to  $\sigma_c$  as a function of cycles to failure for both the transverse and longitudinal ribbon orientation. These data indicate that for a ribbon volume fraction of 0.60 with a simple overlap pattern, the fatigue limit is 345 MPa (50 ksi) for the longitudinal orientation while the fatigue limit is 138 MPa (20 ksi) with ribbons oriented transversely. These values are less than 20% of the composite static strength. In comparison with fiber reinforced composites, the fatigue resistance of these amorphous metal ribbon reinforced composites is low.

Examination of the fractured specimens, Fig. 68, showed that the fracture mode was similar to that observed in static tension. Flat fractures perpendicular to the tensile axis were observed with failure along the plane of weakness for the transverse specimens. However, delamination and a step-like fracture surface were observed for the longitudinal laminates.

### g. Assessment of Composite Impact Resistance and Fracture Toughness

Composite impact resistance and fracture toughness were assessed utilizing the instrumented pendulum impact test. The test apparatus consisted of a standard 31.2 joule (23 ft-lb) capacity pendulum impact machine equipped with an instrumented tup which permitted the generation of load-time traces describing

the impact event. Continuous load measurement was achieved through the use of strain gages mounted on the tup and a calibration to translate strain into load. The strain gage output is monitored on an oscilloscope producing a load-time trace which was then photographically recorded.

The composite specimens tested were all non-standard width and depth. However, all specimens were notched in accordance with the specifications of ASTM standard E-23 for impact testing of subsize Charpy specimens. To insure uniform impact loading for specimens of different depth, shims were fabricated to position the specimen impact face properly with respect to the bottom of the pendulum swing.

Composite specimens were tested with ribbons oriented parallel and transverse to the specimen long axis and are referred to as the longitudinal and transverse orientation respectively. The specimen dimensions were nominally 40 x 6.35 x h mm (1.57 x 0.25 x h in.) where h is the beam depth. For the longitudinal orientation, laminates were constructed using 6.35 mm (0.25 in.) wide ribbon to beam depths of 1.59, 3.18, and 6.35 mm (0.062, 0.125, 0.250 in.). For the transverse orientation, a 24 ply composite panel of dimensions 38.1 x 127 x 1.59 mm (1.5 x 5 x 0.062 in.) was fabricated utilizing the 0.5w overlap pattern with ribbons oriented at 90° to the long dimension of the panel. Specimens of the appropriate dimensions were cut from these composite panels and notched as specified in the standard. Several dummy specimens were run initially and it was found that the optimum tup velocity was 1.06 m/sec (3.48 ft/sec). This eliminated impulse peaks from the load-time traces.

A summary of the specimens tested at a tup velocity of 1.06 m/sec (3.48 ft/sec) and the data recorded is presented in Table 40. Typical load-time traces obtained for the various specimen geometries are shown in Figs. 69 and 70. Interpretation of the impact response of composites is generally complicated since it often depends on specimen geometry and the resultant imposed stress state. It is well known from beam theory that the failure mode in three point bending is dependent on the test span-to-depth ratio. In general, for high longitudinal strength composites, tensile failures are observed at large span-to-depth ratios while shear failures are observed at low span-to-depth ratios. Thus, the impact energy measured can depend to a large extent on the test span-to-depth ratio. To assess the relative role of this phenomena in the test results reported, the maximum flexural stress at failure was calculated using the equation  $\sigma_{\max} = 3/2 (PS/bh^2)$  where P is the load at failure, S is the span, b is the beam width, and h is beam depth. For our purpose, the net beam depth minus the notch was utilized.

The values of maximum flexural stress at failure are compared with the energy per unit area absorbed in Table 41. It is evident that the test span-to-depth,  $S/h$ , has a strong influence on the flexural stress at failure. For the longitudinal specimens, as  $S/h$  decreased from 31.5 to 7.95, the flexural stress at failure decreased from 1450 MPa (210 ksi) to 869 MPa (126 ksi). This is typically observed in most composite systems and indicates a significant contribution of shear failure in the composites. It should be noted that the predicted flexural strength of the beam is 1540 MPa (223 ksi) based on a ribbon strength of 2560 MPa (372 ksi) measured for the 6.35 mm (0.25 wide ribbon. This compares reasonably well with the flexural strength determined at the highest  $S/h$ . Although the data in Table 41 indicated a change in the stress state at failure as a function of test geometry, the energy absorbed per net section area was not strongly affected. The energy per unit area increased approximately 15% over the same range of  $S/h$ . This result was consistent with the observed failure mode. All specimens exhibited tensile failure of ribbons in the plane of impact with very little interlaminar failure as shown in Fig. 71.

Presented in Fig. 72 is a comparison of the effect of test geometry on the impact energy between the longitudinally reinforced composite and unreinforced metals tested similarly (Ref. 22). The data for the composite specimens was normalized to the same specimen width as the alloys assuming a linear dependence of impact energy on specimen width. Both the notched unreinforced metals and composite specimens exhibit relatively equivalent dependence of energy dissipated on net specimen depth. However, the composite absorbs equivalent impact energy only at the smaller net specimen depths tested.

With the ribbons oriented transversely, an average flexural strength of 869 MPa (126 ksi) was measured. This correlates with a calculated tensile strength of 869 MPa (126 ksi) for the composite based on a ribbon strength of 2900 MPa (420 ksi). The average energy per unit area absorbed for the transverse specimen was 56900 joule/m<sup>2</sup> (27.1 ft-lb/in<sup>2</sup>) compared to 74500 joule/m<sup>2</sup> (35.4 ft-lb/in<sup>2</sup>) for longitudinal specimens of the same test geometry, i.e.  $S/h = 31.5$ . Observation of the fracture surfaces of the transverse specimens, Fig. 73, also indicated a more irregular fracture plane in comparison with the longitudinal specimens. This was caused by a certain degree of ribbon sliding during fabrication which forced the crack to deviate significantly about the plane of weakness. This factor no doubt contributed to an increase in energy measured for the transverse specimens. Thus, an even greater difference in energy absorbed between the two orientations would be expected for a perfect transverse lay-up.

Finally, as a measure of resistance to crack growth, values of  $K_{ID}$  were calculated for the composite specimens. These data are listed in Table 42 along with values determined for Charpy V-notch specimens of Ti-6Al-4V and 6061-T6 in a previous investigation (Ref. 22). The 2826 MB/FM-1000 composites

longitudinally reinforced exhibit a fracture toughness,  $K_{ID}$ , similar to that observed for 6061-T6 aluminum alloy. With ribbons in the transverse orientation, the fracture toughness is half that observed for the longitudinal orientation.

#### h. Room Temperature Creep Properties

The transverse composite creep and stress rupture properties were determined at room temperature. Specimens 6.35 mm (0.25 in.) wide were cut from composite panels of dimensions 38.1 x 127 mm (1.5 x 5.0 in.) which had been fabricated with ribbons oriented transverse to the long axis. Fiberglass doublers were bonded to the specimen ends resulting in a gage section of 50.8 mm (2.0 in.). These specimens were mounted in wedge grips and loaded in uniaxial tension in lever arm creep machines.

To obtain a measure of the composite transverse creep behavior, an extensometer was mounted on the gage section of the first sample tested, and the strain was monitored as a function of time for several stress levels. The data obtained are shown in Fig. 74. The calculated transverse strength of the specimen was 846 MPa (123 ksi). Note that at a stress level of 690 MPa (100 ksi), the creep rate was  $4.9 \times 10^{-6} \text{ hr}^{-1}$ . At a stress level of 758 MPa (110 ksi), the creep rate increased to  $8.0 \times 10^{-6} \text{ hr}^{-1}$ . On loading the composite to a stress level of 793 MPa (115 ksi), the specimen failed in 0.25 hr. There was no indication of an accelerated creep rate prior to failure at the final stress level.

Subsequently, a series of specimens were loaded at several stress levels and the time to failure was determined. The results of these stress-rupture tests are listed in Table 43. Also listed is the ratio of the stress level to the calculated composite strength. Two specimens were also tensile tested and indicate that the calculated strengths were in good agreement with the true composite strength. These results show rupture times in excess of 100 hrs were achieved at a stress level equivalent to 90% of the composite ultimate tensile strength. This result coupled with the very low creep rate observed indicates that the resistance to creep is high at room temperature.



### III. ASSESSMENT OF AMORPHOUS RIBBON REINFORCED RESIN MATRIX COMPOSITES

The results of this investigation have demonstrated that amorphous metal ribbon properties can be effectively translated into a resin matrix composite. The utility of the ribbon format was also demonstrated since transverse to longitudinal strength and modulus ratios approaching unity were achieved using currently available materials. The strength and modulus properties achieved could be readily predicted using relatively simple models coupled with existing theories. Several deficiencies were also identified and directly related to the use of amorphous metal ribbons in resin matrices. These included poor moisture resistance, low composite compression strength, and poor composite fatigue properties.

To assess the performance of amorphous metal ribbon reinforced composites relative to fiber reinforced composites, the static tensile data generated in this report, as well as properties projected for future amorphous metal ribbon materials, were compared with quasi-isotropic AS-3501 graphite/epoxy. The quasi-isotropic properties are utilized for comparison since a primary advantage of the ribbon reinforcement is composite transverse to longitudinal property ratios which approach unity.

Presented in Fig. 75 is a plot of composite transverse specific strength as a function of ribbon tensile strength. The series of lines drawn on the figure correspond to composite densities of 3.0, 4.0, 5.0, and 6.0 gm/cm<sup>3</sup> (0.108, 0.144, 0.180, 0.217 lb/in<sup>3</sup>). Furthermore, it is assumed that the ribbon volume fraction is 0.60, and that a stacking pattern providing a 75% ribbon fracture efficiency is achieved. As indicated on the figure, the density of titanium base ribbon reinforced composites is approximately 3.0 gm/cm<sup>3</sup> (0.108 lb/in<sup>3</sup>) while that of iron base ribbon reinforced composites is approximately 5.0 gm/cm<sup>3</sup> (0.180 lb/in<sup>3</sup>). The following assessment is made based on the use of such ribbon materials. The data point presented as current technology represents the transverse specific properties which can be achieved using currently available 2826 MB ribbon material. The transverse specific strength of composites fabricated using this system is only 15% lower than that of quasi-isotropic AS-3501 graphite/epoxy. It should be noted that the longitudinal specific strength of the ribbon reinforced composite exceeds the quasi-isotropic graphite/epoxy. Since an increase in iron base amorphous metal ribbon strength to 3450 MPa (500 ksi) is feasible, the potential to exceed the specific strength of quasi-isotropic graphite/epoxy exists. From the standpoint of using titanium base ribbons, current ribbon strength is approximately 1860 MPa (270 ksi). Thus, it is apparent from Fig. 75 that if titanium base ribbons

were available in ribbon widths of 13 mm (0.5 in), so that the desired stacking pattern could be constructed, composite transverse specific strength equivalent to quasi-isotropic graphite/epoxy would be achieved. Further improvements in ribbon tensile strength would result in further gains in specific properties. In summary, this analysis indicates that composite specific strength properties exceeding those of quasi-isotropic graphite/epoxy can be achieved using either iron base or titanium base ribbons with further ribbon development work. It is evident that the greatest potential for improvement lies in titanium ribbon development.

Presented in Fig. 76 is a plot of composite transverse specific modulus as a function of ribbon elastic modulus. The assumptions are that the ribbon aspect ratio,  $w/t$ , is 300, ribbon volume fraction is 0.60, and the matrix modulus is 0.2 Msi. Note that the composite transverse specific modulus using either titanium base or iron base ribbons is approximately 30% lower than that observed for quasi-isotropic AS-3501 graphite/epoxy. It is also noted that composite longitudinal modulus is essentially equivalent to the transverse modulus for ribbons of this aspect ratio. This deficiency in specific modulus is one which cannot be overcome within the framework of existent amorphous metal ribbon technology. This is due to the fact that the elastic modulus to density ratio of most metallic materials is invariant. Thus, improvements in ribbon modulus will be achieved concurrently with increases in density so that improvement in specific modulus properties is not foreseen. As indicated in Fig. 76, dramatic improvements in specific modulus could be achieved with ceramic ribbon material. However, the difficulties associated with processing, handleability, and cost make this a questionable technology.

Because of the low specific modulus of amorphous metal ribbon reinforced composites, it is felt that these composites will not be in a competitive position for most traditional composite applications, particularly in the aerospace industry. The advantages of the composite lie in the high biaxial strength properties, potential low cost, and perhaps the unusual soft magnetic properties offered by the ribbons. Potential composite applications will probably be limited. A summary of composite mechanical properties demonstrated in this investigation, as compared to selected engineering materials, is presented in Table 44.

#### REFERENCES

1. R. M. Gray: Symp. of Met. Soc. AIME, May 1969, DMIC Mem. 243, p 52.
2. M. J. Hordon: J. Comp. Mat., Vol. 7, p 521 (1973).
3. M. J. Hordon: Final Report, Contract N00019-72-C-0445, Naval Air Systems Command, Nov. 1972.
4. M. J. Hordon: Final Report, Contract N62269-73-C-0306, Naval Air Development Center, March 1974.
5. E. Anderson, B. Lux and C. Crussard: Rev. Met., Vol. 2, p 165 (1972).
6. E. Anderson: J. Mat. Sci., Vol. 8, p 676 (1973).
7. J. T. A. Pollock and J. Arthur: Mat. Sci. and Eng., Vol. 18, p 209 (1975).
8. E. Anderson and R. Bode: Proceedings of the Symposium on Failure Modes in Composites, Boston, MA, p 289 (1972).
9. T. B. Lewis: 25th Annual SPI Conference, Section 8-D, p 1, 1970.
10. L. A. Goettler, T. B. Lewis, and L. E. Nielson: Am. Chem. Soc., Div. of Polymer Chem., Vol. 14, No. 1, p 436 (1973).
11. T. B. Lewis and L. E. Nielsen, U.S. Patent 3,790,438 (1974).
12. J. Rexer, E. Anderson, G. Fourty, C. Bournazel, and J. Corteville: Proceedings of the 1975 ICCM, p 758.
13. D. J. Goldwasser and B. H. Kear: Mat. Sci. and Eng., Vol. 23, p 237 (1976).
14. D. J. Goldwasser, E. P. Ostocka and B. H. Kear: Mat. Sci. and Eng., to be published.
15. J. Rexer and E. Anderson: Polymer Eng. and Sci., Vol. 19, No. 1, p 1 (1979).
16. J. E. Ashton, J. C. Halpin and P. H. Petit: Primer on Composite Materials: Analysis, Technomic Publications, Stamford, CT (1969).
17. J. C. Halpin and R. L. Thomas: J. Comp. Mat., Vol. 2, p 488 (1968).

18. L. Davis: 1976 ASM Seminar on Metallic Glasses, Niagara Falls, NY, Sept. 18-19.
19. C. V. Cagle: Handbook of Adhesive Bonding, McGraw Hill Book Co., New York, (1973).
20. J. Shields: Adhesives Handbook, CRC Press, Cleveland, OH (1971).
21. A. Kelly and G. J. Davies: Met. Rev., Vol. 10, No. 37, p 20 (1965).
22. K. M. Prewo: Development of Impact Resistant Metal Matrix Composites, AFML-TR-75-216, March 1976.

Table 1

Comparison of Unidirectionally Reinforced  
Resin Matrix Composites

	$\sigma_{11}$		$E_{11}$		$\sigma_{22}/\sigma_{11}$	$E_{22}/E_{11}$
	MPa	(ksi)	GPa	(Msi)		
<u>Fiber Reinforced</u> (UTRC data)						
AS graphite/epoxy	1450	(210)	117	(17)	0.043	0.09
Boron/epoxy	1460	(212)	207	(30)	0.062	0.10
SiC/epoxy	1410	(205)	221	(32)	0.045	0.10
E-glass/epoxy	1100	(160)	39.3	(5.7)	0.02	0.25
<u>Ribbon Reinforced</u> (Ref. 11)						
E-glass/AF-42	1140	(165)	39.3	(5.7)	0.56	0.72
E-glass/surllyn A652	1050	(153)	37.2	(5.4)	0.45	0.82
Graphite/nylon 6	662	(96)	-	-	0.64	-

Table 2

Summary of Metal Ribbon Reinforced Resin  
Matrix Composites Data

		$\sigma_{11}$		$E_{11}$		$\sigma_{22}/\sigma_{11}$	$E_{22}/E_{11}$
		MPa	(ksi)	GPa	(Msi)		
C steel/epoxy	(Ref. 12)	1210	(175)	120	(17.4)	0.60	0.90
302 SS/surlyn A	(Ref. 9)	690	(100)	117	(17)	0.60	0.71
Al/surlyn A	(Ref. 10)	165	(24)	41.3	(6.0)	0.79	0.88
Al/PV butaryl	(Ref. 10)	172	(25)	44.1	(6.4)	0.68	0.94
2605A/P-1700	(Ref. 13)	1180	(171)	77.9	(11.3)	0.06	0.54
2826/epon 828	(Ref. 14)	669	(97)	51.7	(7.5)	0.12	0.63

Table 3

Commercially Available Amorphous Metal Ribbons  
(Allied Chemical)

<u>Alloy</u>	<u>Composition</u> (atomic %)	<u>Nominal</u> <u>Aspect</u> <u>Ratio</u>	<u>Density</u>		<u>Elastic</u> <u>Modulus</u>		<u>Tensile</u> <u>Strength*</u>	
			<u>gm/cm<sup>3</sup></u>	<u>(lb/in<sup>3</sup>)</u>	<u>GPa</u>	<u>(10<sup>6</sup> psi)</u>	<u>MPa</u>	<u>(ksi)</u>
2204	Ti <sub>50</sub> Be <sub>40</sub> Zr <sub>10</sub>	17	4.13	(0.149)	105.5	(15.3)	1860	(270)
2605	Fe <sub>80</sub> B <sub>20</sub>	42	7.48	(0.27)	169.6	(24.6)	1720	(250)
2605A	Fe <sub>78</sub> Mo <sub>2</sub> B <sub>20</sub>	27	7.40	(0.267)	172.4	(25)	2720	(395)
2826	Fe <sub>40</sub> Ni <sub>40</sub> P <sub>14</sub> B <sub>6</sub>	30-500	7.76	(0.28)	124.1	(18)	1720	(250)
2826A	Fe <sub>32</sub> Ni <sub>36</sub> Cr <sub>14</sub> P <sub>12</sub> B <sub>6</sub>	47	7.76	(0.28)	137.9	(20)	1900	(275)
2826MB	Fe <sub>40</sub> Ni <sub>38</sub> Mo <sub>4</sub> B <sub>18</sub>	100-500	8.02	(0.29)	165.5	(24)	2410	(350)
2605SC	Fe <sub>81</sub> B <sub>13.5</sub> Si <sub>3.5</sub> C <sub>2</sub>	500	7.30	(0.263)	165.5	(24)	>690	(100)

\*as-cast

Table 4

## Summary of 2826 MB Ribbon Purchased for the Research Program

Manufacturer's Designation	Width		Edge Condition	Quantity Ordered		Price	Delivery Date	Use
	mm	(in.)		Kg	(lb)			
Reel #1,2,3,4	6.35	(0.25)	slit	2.52	(5.55)	\$630/kg	9/78	<ul style="list-style-type: none"> <li>• Ribbon mechanical property evaluation</li> <li>• Lap shear tests</li> <li>• Composite construction parameter study</li> </ul>
Run LPF375	3.18	(0.125)	as-cast	0.27	(0.59)			
Run LPF385	13.0	(0.51)	as-cast	0.36	(0.80)	\$330/kg	3/79	<ul style="list-style-type: none"> <li>• Composite construction parameter study</li> </ul>
RB 776-LPF455	13.2	(0.52)	as-cast	4.0	(8.8)	\$300/kg	7/79	<ul style="list-style-type: none"> <li>• Task III evaluation of composite physical and mechanical properties</li> </ul>



Table 5

## Ribbon Dimensional Parameters

Ribbon Source	Width		Thickness		Aspect Ratio	Cross Sectional Area	
	mm	(in.)	$10^{-3}$ mm	( $10^{-3}$ in.)		( $10^{-2}$ mm <sup>2</sup> )	( $10^{-4}$ in <sup>2</sup> )
Reel #1	6.55	(0.26)	40.6	(1.60)	161	26.6	(4.13)
Reel #2	6.35	(0.25)	39.1	(1.54)	162	24.8	(3.84)
Reel #3	6.35	(0.25)	39.4	(1.55)	161	24.9	(3.86)
Reel #4	6.35	(0.25)	41.1	(1.62)	154	26.1	(4.04)

Table 6

Chemical Composition of Ribbon Cross Sections  
Exhibiting Varying Strength

<u>Sample #</u>	<u>Tensile Strength</u> MPa (ksi)	<u>Chemical Composition, at. %</u>			
		<u>Fe</u>	<u>Ni</u>	<u>Mo</u>	<u>B</u>
2-5	1380 (200)	41.4	38.2	4.1	16.3
2-6	1380 (200)	42.8	38.1	3.1	16.0
2-3-E	2930 (425)	42.9	38.0	3.1	15.9
2-6-E	3000 (435)	40.4	39.3	4.1	16.2

Table 7

**Summary of Bond Shear Strengths for Various Bonding Materials  
with Solvent Cleaned 2826 MB Ribbon**

<u>Material</u>	<u>Basic Type</u>	<u>Supplier</u>	<u>Bond Strength</u>	
			<u>MPa</u>	<u>(psi)</u>
PR-286	epoxy-liquid	3M	2.9	(415)
Epon 828	epoxy-liquid	Shell	3.0	(430)
FR-7015	epoxy-liquid	Fiber Resin Corp.	7.5	(1090)
FM-300 $\mu$	epoxy/nylon-film	American Cyanamid	30.8	(4470)
FM-1000	epoxy/nylon-film	American Cyanamid	32.5*	(4710)
FM-1046	epoxy/nylon-film	American Cyanamid	29.6**	(4300)
AF-42	epoxy/nylon-film	3M	28.4**	(4120)
EA-9649R	epoxy/novalac-film	Hysol	13.4	(1940)

\*100% adherend failures

\*\*80% adherend failures

Cure Cycles

PR-286	4 hrs 177°C (350°F)
Epon 828/Sonite	2 hrs 100°C (212°F), 2 hrs 150°C (302°F), 2 hrs 130°C (350°F)
FR-7015	48 hrs 25°C (77°F)
FM-300 $\mu$	1 hr 177°C (350°F)
FM-1000	"
FM-1046	"
AF-42	"
EA-9649R	"

Table 8

Summary of Bond Shear Strengths for Various Ribbon Surface  
Treatments and Bonding Materials with 2826 MB Ribbon

<u>Bond Material</u>	<u>Ribbon Treatment</u>	<u>Bond Shear Strength</u>	
		MPa	(psi)
PR-286-liquid	Solvent clean	2.86	(415)
	a. 2 part acid	4.25	(615)
	b. 3 part base	5.25	(760)
Epon 828/Sonite-liquid	Solvent clean	2.96	(430)
	a. 2 part acid	5.2	(750)
	b. 3 part base	11.3	(1640)
EA-9649R-film	Solvent clean	13.3	(1930)
	b. 3 part base	17.0	(2470)
	c. METEX T-103	16.6	(2410)
	d. METEX S-1645	10.9	(1580)
	e. METEX M-629	12.4	(1800)
	f. T-103/M-629	12.7	(1840)

Table 9

## Summary of Adhesive Films Investigated

<u>Designation</u>	<u>Supplier</u>	<u>Type</u>	<u>Film Thickness</u>		<u>Cure Temp.</u>
			mm	(in)	
FM-1000	American Cyanamid	epoxy-nylon	0.076	(0.003)	177°C (350°F)
FM-1046	"	epoxy-nylon	0.038	(0.0015)	177°C (350°F)
FM-150	"	epoxy-novalac	0.23	(0.009)	177°C (350°F)
EA-9649R	Hysol	toughened epoxy (epoxy-novalac base)	0.25	(0.010)	177°C (350°F)
AF-147	3M	toughened epoxy	0.23	(0.009)	177°C (350°F)
AF-163	3M	toughened epoxy	0.31	(0.012)	135°C (275°F)

Table 10

Results of Lap Shear Testing Using Various Adhesive Films  
with Alkaline Cleaned 2826 MB Ribbon

<u>Matrix</u>	<u>Bond Strength</u>		<u>Failure Mode</u>
	MPa	(ksi)	
FM-1000	34.2	(5.0)	Cohesive: ribbon failure
FM-1046	31.4	(4.6)	75% Cohesive: ribbon failure
FM-150	16.7	(2.4)	Adhesive: ribbon/matrix interface
EA-9649R	17.0	(2.5)	Adhesive: ribbon/matrix interface
AF-147	33.2	(4.8)	Cohesive: matrix failure
AF-163	35.6	(5.2)	Cohesive: ribbon failure

Table 11

Curing Characteristics of Adhesive Films Investigated as  
Determined Using the Audrey Dielectric Analyzer

<u>Adhesive</u>	<u>Melting Peak</u>		<u>Initiation of Gelation</u>		<u>Gel Peak</u>	
	<u>°C</u>	<u>(°F)</u>	<u>°C</u>	<u>(°F)</u>	<u>°C</u>	<u>(°F)</u>
FM-1000	None		-		66	(151)
FM-1046	None		-		112	(234)
FM-150	114	(237)	175	(347)	177	(350)
EA-9649R	80	(176)	157	(315)	177	(350)
AF-147	70	(158)	134	(273)	177	(350)
AF-163	95	(203)	108	(226)	121	(250)

Table 12

Hot Pressing Procedures Utilized for Preparing Ribbon Reinforced  
Laminates Using the Indicated Matrix Materials

<u>Adhesive Film</u>	<u>Hot Pressing Schedule</u>
FM-1000 } FM-1046 }	<ul style="list-style-type: none"> <li>• Apply 0.35 MPa at 149°C (50 psi at 300°F)</li> <li>• Apply 0.69-1.38 MPa at 163°C (100-200 psi at 325°F)</li> <li>• Hold pressure for 1 hr at 177°C (350°F)</li> </ul>
FM-150	<ul style="list-style-type: none"> <li>• Initiate pressure application to remove excess resin at 127°C (260°F)</li> <li>• Press to stops at 149°C (300°F)</li> <li>• Hold for 1 hr at 177°C (350°F)</li> </ul>
EA-9649R	<ul style="list-style-type: none"> <li>• Initiate pressure application at 121°C (250°F)</li> <li>• Press to stops at 135°C (275°F)</li> <li>• Hold for 1 hr at 177°C (350°F)</li> </ul>
AF-147	<ul style="list-style-type: none"> <li>• Initiate pressure application at 107°C (225°F)</li> <li>• Press to stops at 121°C (250°F)</li> <li>• Hold for 1 hr at 177°C (350°F)</li> </ul>
AF-163	<ul style="list-style-type: none"> <li>• Initiate pressure application at 102°C (215°F)</li> <li>• Press to stops at 104°C (220°F)</li> <li>• Hold for 1 hr at 135°C (275°F)</li> </ul>



Table 13

Interlaminar Shear Strength of 60 Layer Laminates Tested  
in Three Point Bend at Span/Depth = 5

<u>Composite</u>	<u>Matrix</u>	<u>V<sub>r</sub></u>	Shear Stress, $\tau$				Crosshead Deflection	
			<u>75% Secant</u>		<u>Maximum</u>		<u>at <math>\tau_{max}</math></u>	
			MPa	(ksi)	MPa	(ksi)	mm	(in)
C3347	FM-1000	0.65	51.4	(7.45)	75.9	(11.0)	3.25	(.128)
C3387	FM-1000	0.67	50	(7.25)	ND		ND	
C3372	FM-1046	0.57	36.5	(5.30)	64.1	(9.30)	5.08	(.200)
C3388	FM-1046	0.68	15.2	(2.20)	50.3	(7.30)	3.91	(.154)
C3358	FM-150	0.61	84.8	(12.3)	84.8	(12.3)	0.61	(.024)
C3393	EA-9649R	0.61	80	(11.6)	80	(11.6)	0.79	(.031)
C3368	AF-147	0.61	56.4	(8.18)	68.3	(9.90)	1.78	(.070)
C3369	AF-163	0.58	44.4	(6.44)	65	(9.43)*	3.30	(.130)
C3386	AF-163	0.78	51.9	(7.53)	70.3	(10.2)	1.14	(.045)

ND - not determined

\* - Ribbon Failure

Table 14

Tensile Test Results for 2826 MB/FM-1000 Composites Comparing  
Solvent Cleaned and Alkaline Cleaned Ribbon

<u>Composite</u>	<u>Ribbon Treatment</u>	<u>Orientation</u>	<u>V<sub>r</sub>*</u>	<u>UTS</u>		<u>Modulus</u>		<u>Failure Strain %</u>
				MPa	(ksi)	GPa	(msi)	
3301	Alkaline	Longitudinal	0.34	908	(132)	60.1	(8.71)	1.58
			0.39	1029	(149)	64	(9.28)	1.67
3300	Alkaline	Transverse	0.39	565	(81.9)	58.2	(8.44)	1.15
			0.39	554	(80.4)	56.4	(8.18)	1.15
3341	Solvent	Longitudinal	0.40	1206	(175)	68.4	(9.92)	1.80
			0.36	960	(139)	62.8	(9.11)	1.55
3346	Solvent	Transverse	0.46	683	(99.1)	65	(9.43)	1.25
			0.46	659	(95.5)	64.9	(9.41)	1.21

\*calculated from density measurements

Table 15

## Tensile Test Results for 2826 MB/FM-1000 Composites

Composite #	Ribbon Orientation	Ribbon Spacing mm (in.)	Density gm/cm <sup>3</sup>	V <sub>r</sub>	Composite Properties		Failure Strain %
					UTS MPa (ksi)	Modulus GPa (Msi)	
3296	Longitudinal	2.5 (0.10)	3.17 3.39	0.29 0.33	736 (107) 767 (111)	51.0 (7.40) 57.6 (8.35)	1.46 1.40
3297	Transverse	2.5 (0.10)	3.42 -	0.33 0.33	293 (42.5) 296 (42.9)	47.2 (6.85) 48.9 (7.09)	0.71 0.62
3301	Longitudinal	0.5 (0.02)	3.47 3.81	0.34 0.39	910 (132) 1030 (149)	59.1 (8.57) 64.0 (9.28)	1.58 1.67
3300	Transverse	0.5 (0.02)	- 3.82	0.39 0.39	565 (81.9) 554 (80.4)	58.2 (8.44) 56.4 (8.18)	1.15 1.15
3341	Longitudinal	0.5 (0.02)	- 3.65	0.40* 0.36	1210 (175) 960 (139)	68.4 (9.92) 62.8 (9.11)	1.80 1.55
3346	Transverse	0.5 (0.02)	- 4.34	0.46 0.46	683 (99.1) 659 (95.5)	65.0 (9.43) 64.9 (9.41)	1.25 1.21
3342	Transverse	0.5 (0.02)	6.07 -	0.71 0.71	1010 (146) 971 (141)	95.1 (13.8) 94.7 (13.7)	1.31 >1.26**

\*metallographic cross section

\*\*strain gage debonded

Table 16

Summary of 2826 MB Ribbon Tensile Strength Data from Reel  
Locations Associated with Composite Fabrication

<u>No. of Specimens</u>	<u>Reel #</u>	<u>Tensile Strength</u>		<u>Standard Deviation</u>		<u>Composite</u>
		MPa	(ksi)	MPa	(ksi)	
32	1	2480	(360)	206	(29.9)	3296, 3297, 3300, 3301
15	1	2790	(405)	301	(43.7)	3341, 3342, 3346

Table 17

Comparison of Longitudinal Tensile Properties with  
Rule of Mixture Calculation

<u>Composite #</u>	<u>V<sub>r</sub></u>	<u>Composite Properties</u>		<u>Rule of Mixtures</u>		
		<u>UTS, <math>\sigma_{ll}</math></u> MPa	<u>Modulus, E<sub>ll</sub></u> GPa	<u><math>\sigma_{ll}^*</math></u> MPa	<u>E<sub>ll</sub><sup>**</sup></u> GPa	<u>E<sub>ll</sub><sup>**</sup></u> (Msi)
3296	0.29	736	51.0	720	48.0	(6.96)
	0.33	767	57.6	819	54.6	(7.92)
3301	.34	910	59.1	842	56.2	(8.16)
	0.39	1030	64.0	968	64.5	(9.36)
3341	0.40	1206	68.4	1117	66.2	(9.60)
	0.36	960	62.8	1005	59.6	(8.64)

\* $\sigma_r$  from Table XVI\*\*assuming  $E_r = 165$  GPa (24 Msi)

Table 18

Transverse to Longitudinal Property Ratios  
for 2826 MB/FM-1000 Composites

$V_r$	$\sigma_{11}$		$\sigma_{22}$		$E_{11}$		$E_{22}$		$\sigma_{22}/\sigma_{11}$	$E_{22}/E_{11}$
	MPa	(ksi)	MPa	(ksi)	GPa	(Msi)	GPa	(Msi)		
0.33	767	(111)	294	(42.7)	57.6	(8.36)	48	(6.96)	0.38	0.83
0.39	1030	(149)	560	(81.2)	64.1	(9.28)	57.3	(8.31)	0.54	0.90
0.46	1280	(186)*	671	(97.3)	76.1	(11.0)	65	(9.42)	0.52	0.86
0.71	1980	(288)*	989	(144)	117	(17.0)	94.9	(13.8)	0.50	0.77

\*calculated from rule of mixtures

Table 19

2826 MB Ribbon Parameters and Calculated Critical  
Transfer Length with FM-1000 Adhesive Film

Ribbon Properties					
Width mm	(in)	Thickness mm	(10 <sup>-3</sup> in)	Aspect Ratio	
				MPa	UTS (ksi)
3.18	(0.125)	0.034	1.34	3010	(436)
6.35	(0.25)	0.041	1.61	2560	(372)
13.0	(0.51)	0.034	1.34	2360	(343)
				Modulus	
				GPa	(Msi)
				165	(24)
				165	(24)
				165	(24)
				Critical Transfer Length	
				mm	(10 <sup>-2</sup> in)
				1.48	(5.8)
				1.52	(6.0)
				1.17	(4.6)

Table 20

## Transverse Tensile Test Results for 2826 MB/FM-1000 Composites

Composite No.	Ribbon Width mm (in)	Ribbon Aspect Ratio	Nominal Ribbon Overlap*	V <sub>r</sub>	Composite Properties		
					UTS MPa (ksi)	Modulus GPa (Msi)	Failure Strain %
3415	3.18 (0.125)	93	(a) 0.5w	0.59	439 (63.7) 482 (69.9)	81.4 (11.8) 75.6 (11.0)	0.88 1.24
3410	6.35 (0.25)	160	(a) 0.5w	0.66	902 (131) 841 (122)	92.2 (13.4) 91.2 (13.2)	>1.0** >0.94**
3396	6.35 (0.25)	160	(c) 0.3w	0.61	986 (143) 979 (142)	100 (14.5) 96.5 (14.0)	>1.25** 1.41
3418	13.0 (0.51)	380	(a) 0.5w	0.60	857 (124)	106 (15.3)	0.79
3419	13.0 (0.51)	380	(b) 0.4w	0.61	915 (133) 844 (122)	106 (15.4) 101 (14.6)	0.88 0.89
3420	13.0 (0.51)	380	(c) 0.3w	0.62	1100 (159) 1040 (151)	94.5 (13.7) 91.3 (13.3)	1.32 1.26
3421	13.0 (0.51)	380	(d) 0.2w	0.63	1140 (166) 1100 (159)	104 (15.0) 103 (14.6)	1.21 1.21

\*Fig. 33, w = ribbon width

\*\*strain gage debonded



Table 21

Summary of 2826 MB Ribbon Tensile Strength Data from Reel  
Locations Associated with Composite Fabrication

<u>Ribbon Width</u> mm (in)	<u>Reel #</u>	<u>No. of Specimens</u>	<u>Tensile Strength</u>		<u>Standard Deviation</u>		<u>Composite</u>
			MPa	(ksi)	MPa	(ksi)	
3.18 (0.125)	1PF375	10	3010	(436)	87.2	(12)	3415
6.35 (0.25)	4	20	2740	(398)	221	(32.1)	3396
6.35 (0.25)	2	15	2560	(372)	227	(32.9)	3410
13.0 (0.51)	1PF385	15	2360	(343)	268	(38.8)	3418 3419 3420 3421

Table 22

## Summary of Calculated Composite Strength and Modulus Ratios

Composite	$\frac{\text{Ribbon Width}}{\text{mm}}$ (in)	Nominal Ribbon Overlap*	$\frac{\text{RibbonTensileStrength}}{\text{MPa}}$ (ksi)	$V_r$	$\frac{\sigma_{22}/\sigma_{11}^{**}}{\text{}}$	$\frac{E_{22}/E_{11}^{***}}{\text{}}$
3415	3.18 (0.125)	0.5w	3010 (436)	0.59	0.26	0.81
3410	6.35 (0.25)	0.5w	2560 (372)	0.66	0.52	0.84
3396	6.35 (0.25)	0.3w	2740 (398)	0.61	0.59	0.97
3418	13.0 (0.51)	0.5w	2360 (343)	0.60	0.61	1.05
3419	13.0 (0.51)	0.4w	2360 (343)	0.61	0.61	1.02
3420	13.0 (0.51)	0.3w	2360 (343)	0.62	0.73	0.91
3421	13.0 (0.51)	0.2w	2360 (343)	0.63	0.76	1.0

\*Fig. 33, w = ribbon width

\*\* $\sigma_{11} = \sigma_r V_r$ \*\*\* $E_{11} = E_r V_r + E_m V_m$ ,  $E_r = 165$  GPa and  $E_m = 1.38$  GPa

Table 23

Comparison of Experimental and Calculated Transverse Composite Property Ratios

Ribbon Aspect Ratio	$V_r$	Ribbon Overlap	$E_{22}/E_{11}$		$\sigma_{22}/\sigma_{11}$	
			Experimental	Calculated*	Experimental	Calculated**
93	0.59	0.5w	0.81	0.80	0.26	0.53
160	0.66	0.5w	0.84	0.89	0.52	0.76
160	0.61	0.3w	0.97	0.89	0.59	0.76
380	0.60	0.5w	1.05	0.94	0.61	0.91
380	0.61	0.4w	1.02	0.94	0.62	0.91
380	0.62	0.3w	0.91	0.95	0.73	0.91
380	0.63	0.2w	1.0	0.95	0.76	0.91
						0.80

\*Halpin-Tsai equations

\*\*(1)  $\sigma_{22} = (1 - k_c/w) \sigma_r V_r + \sigma_m' V_m$  (upper bound)\*\*\* (2)  $\sigma_{22} = f_{br} \sigma_r V_r + f_{po} \sigma_{rl}' V_r + \sigma_m' V_m$

Table 24

## Transverse Tensile Properties for 2826 MB/FM-1046 Composites

<u>Composite</u>	<u>Ribbon Width</u> mm (in)		<u>Stacking</u> <u>Pattern</u>	<u>V<sub>r</sub></u>	<u>UTS</u>		<u>Modulus</u>		<u>Failure</u> <u>Strain</u> %
					MPa	(ksi)	GPa	(Msi)	
3423	3.18	(0.125)	Fig. 32a	0.51	336	(48.7)	58.5	(8.48)	>1.0*
				0.49	306	(44.4)	52.9	(7.68)	>1.22*
3424	3.18	(0.125)	0/90	0.44	600	(87.0)	64.7	(9.38)	1.36
				0.42	577	(83.7)	58.5	(8.48)	1.46
3435	13.0	(0.51)	Fig. 39b	0.56	852	(124)	69.1	(10.0)	>1.08*
				0.57	913	(132)	81.5	(11.8)	1.02

\*strain gage debonded

Table 25

Ratio of Transverse Composite Tensile Strength to Axial  
Unidirectional Laminate Composite Tensile Strength

<u>Composite</u>	<u>Ribbon Width</u> mm (in)	<u>V<sub>r</sub></u>	<u>Stacking</u> <u>Pattern</u>	<u><math>\sigma_T/\sigma_{Lam}</math></u>	<u><math>E_T/E_{Lam}</math></u>
3423	3.18 (0.125)	0.50	Fig. 33a	0.21	0.67
3424	3.18 (0.125)	0.43	0/90	0.46	0.86
3421	13.0 (0.51)	0.63	Fig. 39a	0.76	1.0
3435	13.0 (0.51)	0.56	Fig. 39b	0.67	0.80

\*Longitudinal properties calculated from rule of mixtures  
Ribbon strength from Table XIX

Table 26

Average Thermal Expansion Coefficients  
for 2826MB Ribbon

<u>Ribbon Orientation</u>	<u>Run #</u>	<u>Initial Temp. °C</u>	<u>Final Temp. °C</u>	$\frac{\alpha_{avg}}{10^{-6} \text{ } ^\circ\text{C}^{-1}}$
Longitudinal	1	22	152	9.08
	2	24	171	9.56
Transverse	1	25	166	10.75
	2	26	165	11.70

Table 27

Composite Thermal Expansion Coefficients as a  
Function of Ribbon Orientation

<u>Specimen</u>	<u>Ribbon Orientation</u>	<u>Initial Temp °C</u>	<u>Final Temp °C</u>	$\frac{\alpha_{avg}}{10^{-6}C^{-1}}$
3500-0-2	0°	163	26	13.4
3500-0-3	0°	142	26	11.2*
3500-45-1	45°	150	28	13.5
3500-45-2	45°	161	29	12.1
3500-90-1	90°	150	28	11.8
3500-90-2	90°	155	28	12.5

\*specimen delaminated

Table 28

Interlaminar Shear Properties of  
2826 MB/FM-1000 Laminates

Specimen #	Density		$V_r$	Test Temp		$\tau_{max}$	
	gm/cm <sup>3</sup>	(lb/in <sup>3</sup> )		°C	(°F)	MPa	(psi)
3544-1	5.29	(0.191)	0.60	21	(70)	48.9	(7090)
-2				82	(180)	2.65	(385)
-3*				21	(70)	47.9	(6940)
3545-1	5.23	(0.189)	0.59	21	(70)	45.8	(6640)
-2				82	(180)	2.70	(392)
-3*				82	(180)	2.31	(335)
3546-1	5.37	(0.194)	0.61	21	(70)	45.8	(6640)
-2				82	(180)	2.61	(378)
-3*				82	(180)	2.50	(363)

\*Postcured 1 hr at 177°C (350°F)



Table 29

Composite Tensile Properties with Ribbons Oriented  
at 0° to the Tensile Axis

Specimen #	Composite Properties					Rule of Mixtures	
	Density gm/cm <sup>3</sup> (lb/in <sup>3</sup> )	V <sub>r</sub> %	UTS, $\sigma_{ll}$ MPa (ksi)	Modulus E <sub>ll</sub> GPa (Msi)	Failure Strain %	$\sigma_{ll}^*$ MPa (ksi)	E <sub>ll</sub> ** GPa (Msi)
3555-1	4.90 (0.177)	54.6	1480 (215)	88.6 (12.9)	1.70	1400 (203)	90.3 (13.1)
3555-4	4.48 (0.162)	48.5	—	81.5 (11.8)	—	—	80.0 (11.6)
3555-6	4.20 (0.152)	44.4	1260 (183)	73.1 (10.6)	1.80	1140 (165)	73.8 (10.7)
3486-1	3.88 (0.140)	39.8	1250 (181)	—	—	1020 (148)	—
3486-2	3.90 (0.141)	40.0	1120 (163)	—	—	1030 (149)	—
3486-3	4.13 (0.149)	43.4	1320 (191)	71.3 (10.3)	1.96	1120 (162)	71.7 (10.4)
3486-4	3.85 (0.139)	39.4	1170 (170)	64.6 (9.36)	1.92	1020 (148)	65.2 (9.46)
3486-5	4.19 (0.151)	44.3	1250 (181)	72.1 (10.5)	1.81	1140 (165)	73.1 (10.6)

\*assuming  $\sigma_R = 2570$  MPa (373 ksi)

\*\*assuming  $E_R = 165$  GPa (24 Msi)

Table 30

Composite Tensile Properties with Ribbons Oriented at 90°  
to the Tensile Axis, Ribbon Overlap was 0.5w

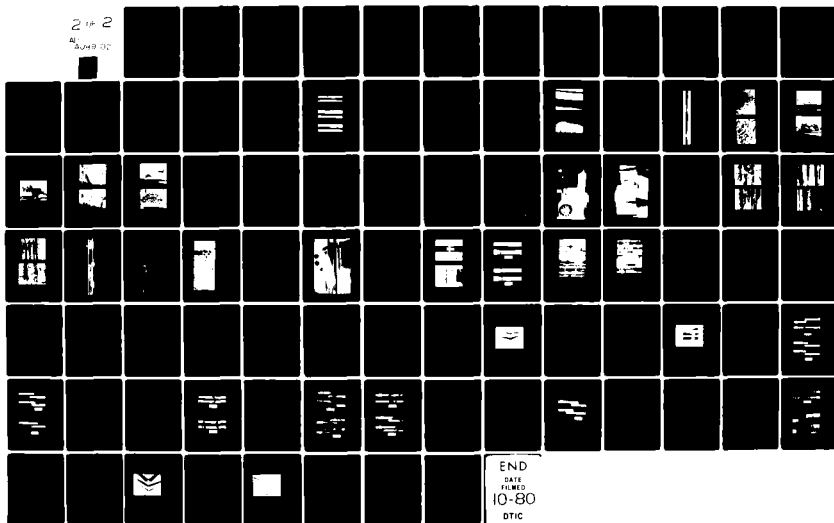
<u>Specimen #</u>	<u>V<sub>r</sub></u>	<u>Test Temp.</u> <u>°C</u> ( <u>°F</u> )	<u>UTS, <math>\sigma_{22}</math></u> <u>MPa</u> ( <u>ksi</u> )	<u>Modulus, E<sub>22</sub></u> <u>GPa</u> ( <u>Msi</u> )	<u>Failure</u> <u>Strain</u> <u>%</u>
3549-1	0.55	21 (70)	790 (115)	113 (16.4)	0.66
3549-4	0.57	21 (70)	787 (114)	112 (16.3)	0.68
3550-1	0.60	21 (70)	818 (119)	111 (16.1)	0.69
3550-4	0.60	21 (70)	829 (120)	143 (20.3)	0.56
3549-2	0.55	54 (130)	646 (93.7)	-	-
3549-5	0.57	54 (130)	688 (99.8)	-	-
3550-2	0.60	54 (130)	739 (107)	-	-
3549-3	0.55	82 (180)	391 (56.7)	-	-
3550-3	0.60	82 (180)	518 (75.4)	-	-
3550-5	0.60	82 (180)	438 (63.5)	-	-

AD-A089 102

UNITED TECHNOLOGIES RESEARCH CENTER EAST HARTFORD CONN F/G 11/4  
EVALUATION OF AMORPHOUS RIBBON REINFORCED RESIN MATRIX COMPOSIT--ETC(U)  
APR 80 J R STRIFE, K M PREWO F33615-78-C-5063  
UNCLASSIFIED UTRC/R80-914389-18 AFWAL-TR-80-4060 NL

2 1/2 2

AL 3449 02



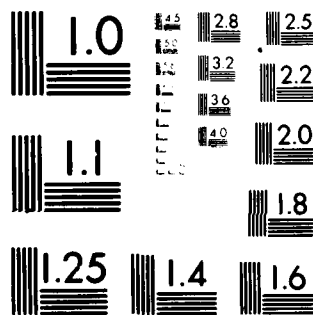


Table 31

Composite Tensile Properties with Ribbons Oriented  
at 90° to the Tensile Axis  
Ribbon Overlap was 0.3w

Specimen #	$V_r$	Test Temp		UTS, $\sigma_{22}$		Modulus, $E_{22}$		Failure
		°C	(°F)	MPa	(ksi)	GPa	(Msi)	Strain*
								%
3503-1	0.63	21	(70)	943	(137)	76.2	(11.0)	>0.95*
3503-2	0.64	↓	↓	866	(126)	81.2	(11.8)	>1.37*
3504-2	0.63			932	(135)	92.1	(13.4)	>1.13*
3504-3	0.65			1040	(151)	89.6	(13.0)	>1.28*
3504-4	0.65			979	(142)	93.2	(13.5)	>1.21*
3504-5	0.66			982	(142)	-	-	-
3509-2	0.65	↓	↓	965	(140)	83.2	(12.1)	>0.74*
3509-3	0.64			867	(126)	-	-	-
3503-4	0.64	54	(130)	503	(73.0)	-	-	-
3503-5	0.65	↓	↓	585	(84.8)	-	-	-
3509-5	0.63	↓	↓	443	(64.2)	-	-	-
3503-3	0.64	82	(180)	270	(39.2)	-	-	-
3509-1	0.65	↓	↓	239	(34.6)	-	-	-
3509-4	0.64	↓	↓	217	(31.5)	-	-	-

\*strain gage failure

Table 32

Calculated Transverse to Longitudinal Strength Ratios at 70°F

Specimen #	$V_r$	$\sigma_0^*$		$\sigma_{90}$		$\sigma_{90}/\sigma_0$	Overlap Pattern
		MPa	(ksi)	MPa	(ksi)		
3549-1	0.55	1590	(231)	790	(115)	0.50	0.5w ↓
3549-4	0.57	1650	(239)	787	(114)	0.48	
3550-1	0.60	1740	(252)	818	(119)	0.47	
3550-4	0.60	1740	(252)	829	(120)	0.48	
3503-1	0.63	1830	(265)	943	(137)	0.52	0.3w ↓
3503-2	0.64	1850	(269)	866	(126)	0.47	
3504-2	0.63	1830	(265)	932	(135)	0.51	
3504-3	0.65	1880	(273)	1040	(151)	0.55	
3504-4	0.65	1880	(273)	979	(142)	0.52	
3504-5	0.66	1910	(277)	982	(142)	0.51	
3509-2	0.65	1880	(273)	965	(140)	0.51	
3509-3	0.64	1850	(269)	867	(126)	0.47	

\*simple rule of mixtures assuming  $\sigma_r = 2900$  MPa

Table 33

Composite Tensile Properties with Ribbons Oriented at 45°  
to the Tensile Axis, Ribbon Overlap was 0.5w

Specimen #	$V_r$	Test Temp.		UTS, $\sigma$		Modulus, E		Failure Strain %
		°C	(°F)	MPa	(ksi)	GPa	(Msi)	
3551-2	0.47	21	(70)	732	(106)	80.9	(11.7)	0.98
3551-5	0.48	21	(70)	664	(96.3)	84.8	(12.3)	0.83
3551-8	0.52	21	(70)	791	(115)	110	(16.0)	0.68
3551-11	0.54	21	(70)	654	(109)	117	(17.0)	0.64
3551-3	0.47	54	(130)	624	(90.6)	-	-	-
3551-6	0.50	54	(130)	506	(73.4)	-	-	-
3551-9	0.52	54	(130)	575	(83.4)	-	-	-
3551-4	0.49	82	(180)	328	(47.5)	-	-	-
3551-7	0.51	82	(180)	318	(46.1)	-	-	-
3551-10	0.55	82	(180)	409	(59.3)	-	-	-
3551-1 (90°)	0.50	21	(70)	724	(105)	-	-	-

Table 34

Composite Tensile Properties with Ribbons Oriented at  
45° to the Tensile Axis, Ribbon Overlap was 0.3w

Specimen #	$V_r$	Test Temp.		UTS, $\sigma$		Modulus, E		Failure
		°C	(°F)	MPa	(ksi)	GPa	(Msi)	Strain %
3488-1	0.60	21	(70)	1120	(162)	83.3	(12.1)	1.42
3488-4	0.60	21	(70)	1220	(177)	92.4	(13.4)	1.44
3488-5	0.60	21	(70)	1110	(161)	106	(15.4)	1.05
3488-6	0.60	21	(70)	1040	(151)	80.3	(11.6)	>1.42*
3488-7	0.58	54	(130)	604	(87.5)	-	-	-
3488-8	0.58	54	(130)	569	(82.6)	-	-	-
3488-10	0.58	54	(130)	578	(83.8)	-	-	-
3488-2	0.60	82	(180)	370	(53.7)	-	-	-
3488-3	0.60	82	(180)	334	(48.4)	-	-	-
3488-11(90°)	0.60	21	(70)	750	(124)	89	(12.9)	1.02

\*strain gage failure



Table 35

## Transverse Tensile Strength after Thermal Fatigue

<u>Specimen #</u>	<u>Density</u> (gm/cm <sup>3</sup> )	<u>V<sub>r</sub></u>	<u>UTS</u>		<u>Predicted</u> <u>UTS*</u>	
			MPa	(ksi)	MPa	(ksi)
3605-1	5.28	0.60	881	(128)	869	(126)
-2	5.48	0.63	842	(122)	910	(132)
-3	5.90	0.69	995	(144)	1000	(145)
-4	5.69	0.66	958	(139)	958	(139)
-5	5.39	0.62	<u>892</u>	<u>(129)</u>	<u>896</u>	<u>(130)</u>
Avg			913	(132)	927	(134)

\*  $\sigma = 0.5 \sigma_R V_r$ ,  $\sigma_R = 2900 \text{ MPa (420 ksi)}$

Table 36

Transverse Tensile Strength after Exposure to Moisture

<u>Specimen #</u>	<u>Density</u> (gm/cm <sup>3</sup> )	<u>V<sub>r</sub></u>	<u>UTS</u>		<u>Predicted</u> <u>UTS*</u>	
			MPa	(ksi)	MPa	(ksi)
3602-1	5.46	0.63	138	(20.1)	910	(132)
-2	5.62	0.65	193	(28.0)	945	(137)
-3	5.62	0.65	174	(25.2)	945	(137)
-4	5.39	0.62	93.1	(13.5)	896	(130)

\*  $\sigma = 0.5 \sigma_r V_r$ ,  $\sigma_r = 2900 \text{ MPa (420 ksi)}$

Table 37

## Results of Compression Testing at Room Temperature

Specimen #	Ribbon Orientation	V <sub>r</sub>	Compression Modulus			Calculated Tensile Strength MPa (ksi)	Euler Buckling Stress MPa (ksi)
			E <sub>1</sub> *	E <sub>2</sub> *	E <sub>avg</sub>		
			GPa (ksi)	GPa (ksi)	GPa (ksi)	MPa (ksi)	MPa (ksi)
3632	Longitudinal	0.52	87.7 (12.7)	81.3 (11.8)	84.5 (12.3)	1330 (193)	1860 (270)
3634	Longitudinal	0.52	91.1 (13.2)	87.0 (12.6)	89.0 (12.9)	1330 (193)	1860 (270)
3547-1	Transverse	0.60	108 (15.6)	98.6 (14.3)	103 (15.0)	869 (126)	1260 (182)
3547-2	Transverse	0.60	110 (16.0)	89.6 (13.0)	100 (14.5)	869 (126)	1260 (182)

\*Individual modulus determinations

Table 38

Results of Tension-Tension Fatigue Testing at Room Temperature  
Ribbons Oriented at 0° to the Tensile Axis

Specimen #	Density (gm/cm <sup>3</sup> )	$V_r$	Maximum Stress		Minimum Stress		Cycles to Failure	$\sigma_{\max}/\sigma_c^*$
			MPa	(ksi)	MPa	(ksi)		
3594-7	3.87	0.40	345	(50)	34.5	(5)	18,090	0.30
-6	3.92	0.40	276	(40)	27.6	(4)	45,250	0.24
-2	3.75	0.34	207	(30)	20.7	(3)	134,740	0.19
-3	3.68	0.37	172	(25)	17.2	(2.5)	165,500	0.16
-4	3.72	0.37	138	(20)	13.8	(2)	577,800	0.13
-5	4.22	0.45	138	(20)	13.8	(2)	1,351,800**	0.11
3588-L	-	0.67	862	(125)	86.2	(12.5)	20,390	0.44
3597-L	-	0.64	862	(125)	86.2	(12.5)	21,310	0.47
3599-L	-	0.62	345	(50)	34.5	(5.0)	1,000,600***	0.19
3621-L	-	0.64	517	(75)	51.7	(7.5)	89,900	0.28
3622-L	-	0.62	345	(50)	34.5	(5.0)	1,000,500****	0.19

L - Laminate

\*  $\sigma_c = \sigma_r V_r$ ,  $\sigma_r = 2900$  MPa (420 ksi)\*\* stop test - increase  $\sigma_{\max}$  to 172 MPa (25 ksi) - failed at 455,400 cycles -  $\sigma_{\max}/\sigma_c = 0.133$ \*\*\* stop test - increase  $\sigma_{\max}$  to 517 MPa (75 ksi) - failed at 495,800 cycles -  $\sigma_{\max}/\sigma_c = 0.29$ \*\*\*\* stop test - increase  $\sigma_{\max}$  to 517 MPa (75 ksi) - failed at 77,100 cycles -  $\sigma_{\max}/\sigma_c = 0.29$

Table 39

Results of Tension-Tension Fatigue Testing at Room Temperature  
Ribbons Oriented at 90° to the Tensile Axis

Specimen #	Density (gm/cm <sup>3</sup> )	$V_r$	Maximum		Minimum		Cycles to Failure	$\sigma_{max}/\sigma_c^*$
			Stress MPa	(ksi)	Stress MPa	(ksi)		
3553-1	5.20	0.59	496	(72)	49.6	(7.2)	4,770	0.60
3553-3	5.20	0.59	414	(60)	41.4	(6.0)	1,717	0.50
3553-5	5.20	0.59	414	(60)	41.4	(6.0)	5,754	0.50
3556-1	5.29	0.60	207	(30)	20.7	(3.0)	124,970	0.24
3605-2	5.24	0.60	172	(25)	17.2	(2.5)	205,200	0.20
3605-5	5.34	0.61	172	(25)	17.2	(2.5)	141,700	0.20
3556-2	5.29	0.60	138	(20)	13.8	(2.0)	195,740	0.16
3556-5	5.29	0.60	138	(20)	13.8	(2.0)	1,695,720**	0.16
3605-4	5.40	0.62	138	(20)	13.8	(2.0)	1,293,400***	0.15
3556-4	5.29	0.60	69.0	(10)	6.90	(1.0)	2,011,640****	0.08
3553-2	5.20	0.59	765	(111)	-	-	1	-
3553-4	5.20	0.59	876	(127)	-	-	1	-
3556-3	5.29	0.60	822	(119)	-	-	1	-

\*  $\sigma_c = 0.5 \sigma_r$  where  $\sigma_r = 2900$  MPa (420 ksi)

\*\* stop test - increased  $\sigma_{max}$  to 207 MPa (30 ksi) - failed at 73,890 cycles

\*\*\* stop test - determined residual tensile strength = 696 MPa (101 ksi)

\*\*\*\* stop test - determined residual tensile strength = 907 MPa (132 ksi)

Table 40

## Results of Instrumented Impact Testing

Specimen #	Orientation	V <sub>r</sub>	Specimen		Specimen Depth mm (in.)	Maximum Load N (lb)	Impact Energy	
			Width mm (in.)	Depth mm (in.)			joules (ft-lb)	
3611	Longitudinal ↓	0.60	6.86 (0.270)	1.58 (0.062)	267 (60.0)	0.65 (0.48)		
3612		0.60	6.91 (0.272)	1.58 (0.062)	236 (53.0)	0.65 (0.48)		
3613		0.59	6.93 (0.273)	3.18 (0.125)	872 (196)	1.50 (1.11)		
3614		0.58	7.06 (0.278)	3.18 (0.125)	805 (181)	1.49 (1.10)		
3615		0.56	7.32 (0.288)	6.35 (0.248)	2680 (603)	3.10 (2.29)		
3547-3	Transverse ↓	0.60	6.25 (0.246)	1.59 (0.062)	142 (32.0)	0.47 (0.35)		
3547-4		0.60	6.27 (0.247)	1.59 (0.062)	125 (28.0)	0.49 (0.36)		
3547-5		0.60	6.15 (0.242)	1.59 (0.062)	133 (30.0)	0.34 (0.25)		
3547-6		0.60	6.25 (0.246)	1.59 (0.062)	182 (41.0)	0.50 (0.37)		

Table 41

Effect of Test Span to Depth on Energy per Unit Area Absorbed

Specimen #	Ribbon Orientation	V <sub>r</sub>	Test Span to Depth	Flexural Stress		Energy per Unit Area	
				MPa	$\sigma_{max}$ (ksi)	joule/m <sup>2</sup>	(ft-lb/in <sup>2</sup> )
3611	Longitudinal ↓	0.60	31.5	1450	(210)	74700	(35.6)
3612		0.60	31.5	1270	(184)	74200	(35.3)
3613		0.59	15.8	1170	(170)	85400	(40.7)
3614		0.58	15.8	1060	(154)	83100	(39.6)
3615		0.56	7.95	869	(126)	84400	(40.2)
3547-3	Transverse ↓	0.60	31.5	848	(123)	59800	(28.5)
3547-4		0.60	31.5	738	(107)	61200	(29.2)
3547-5		0.60	31.5	807	(117)	43400	(20.7)
3547-6		0.60	31.5	1080	(157)	63200	(30.1)

Table 42

Calculated  $K_{ID}$  Values for Charpy V-Notch Specimens

Material	Total Crack		Total Specimen		Maximum Failure Load N (lb)	K <sub>ID</sub>	
	mm	(in.)	mm	(in.)		MPa/m	(ksi/in)
2826MB/FM-1000							
<u>Longitudinal</u>							
3611	0.305	(0.012)	1.58	(0.062)	269	29.1	(26.5)
3612	0.305	(0.012)	1.58	(0.062)	238	25.6	(23.3)
3613	0.635	(0.025)	3.18	(0.125)	878	32.9	(29.9)
3614	0.635	(0.025)	3.18	(0.125)	811	29.8	(27.1)
3615	1.270	(0.050)	6.30	(0.248)	2700	46.2	(42.0)
<u>Transverse</u>							
3547-3	0.305	(0.012)	1.58	(0.062)	143	17.0	(15.5)
3547-4	0.305	(0.012)	1.58	(0.062)	125	14.8	(13.5)
3547-5	0.305	(0.012)	1.58	(0.062)	134	16.2	(14.7)
3547-6	0.305	(0.012)	1.58	(0.062)	184	21.8	(19.8)
6061-T6*	2.00	(0.079)	10.0	(0.394)	7480	34.7	(31.6)
	4.42	(0.174)	10.0	(0.394)	3740	33.0	(30.0)
Ti-6Al-4V*	2.00	(0.079)	10.0	(0.394)	29100	135	(123)
	4.42	(0.174)	10.0	(0.394)	15400	135	(123)

\*Ref. 22



Table 43

Room Temperature Stress-Rupture Data-Transverse  
Ribbon Orientation

<u>Specimen</u>	<u>V<sub>r</sub></u>	<u>Creep Stress</u>		<u>Rupture Time</u> hr	<u>Calculated UTS***</u>		<u><math>\sigma_{\text{creep}}/\sigma_{\text{UTS}}</math></u>
		MPa	(ksi)		MPa	(ksi)	
3601-1	0.66	690	(100)	>600*	958	(139)	0.72
3607-1	0.65	827	(120)	369	945	(137)	0.88
3607-2	0.60	793	(115)	162	869	(126)	0.91
3601-3	0.64	896	(130)	2.7	924	(134)	0.97
3607-3	0.63	862	(125)	0**	910	(132)	0.95
3601-2	0.66	UTS = 1000 MPa (145 ksi)			958	(139)	-
3601-4	0.61	UTS = 910 MPa (132 ksi)			883	(128)	-

\* no failure

\*\* failed on loading

\*\*\*  $\sigma_c = 0.5 \sigma_r V_r$

Table 44  
Material Property Summary

<u>Ribbon Reinforced 2826 MB/FM-1000</u>		<u><math>\pi/4</math> AS-3501 Graphite/Epoxy</u>	<u>6061-T6</u>	<u>Ti-6Al-4V</u>
$\sigma_{11}$ (ksi)	240	65	45	170
$\sigma_{22}$ (ksi)	180	65		
$E_{11}$ (Msi)	14.5	7	10	16.5
$E_{22}$ (Msi)	14.5	7		
$\epsilon_{11}$ (%)	1.6	>1.0	12	8.0
$\epsilon_{22}$ (%)	1.2	>1.0		
$\rho$ (lb/in <sup>3</sup> )	0.190	0.057	0.098	0.160

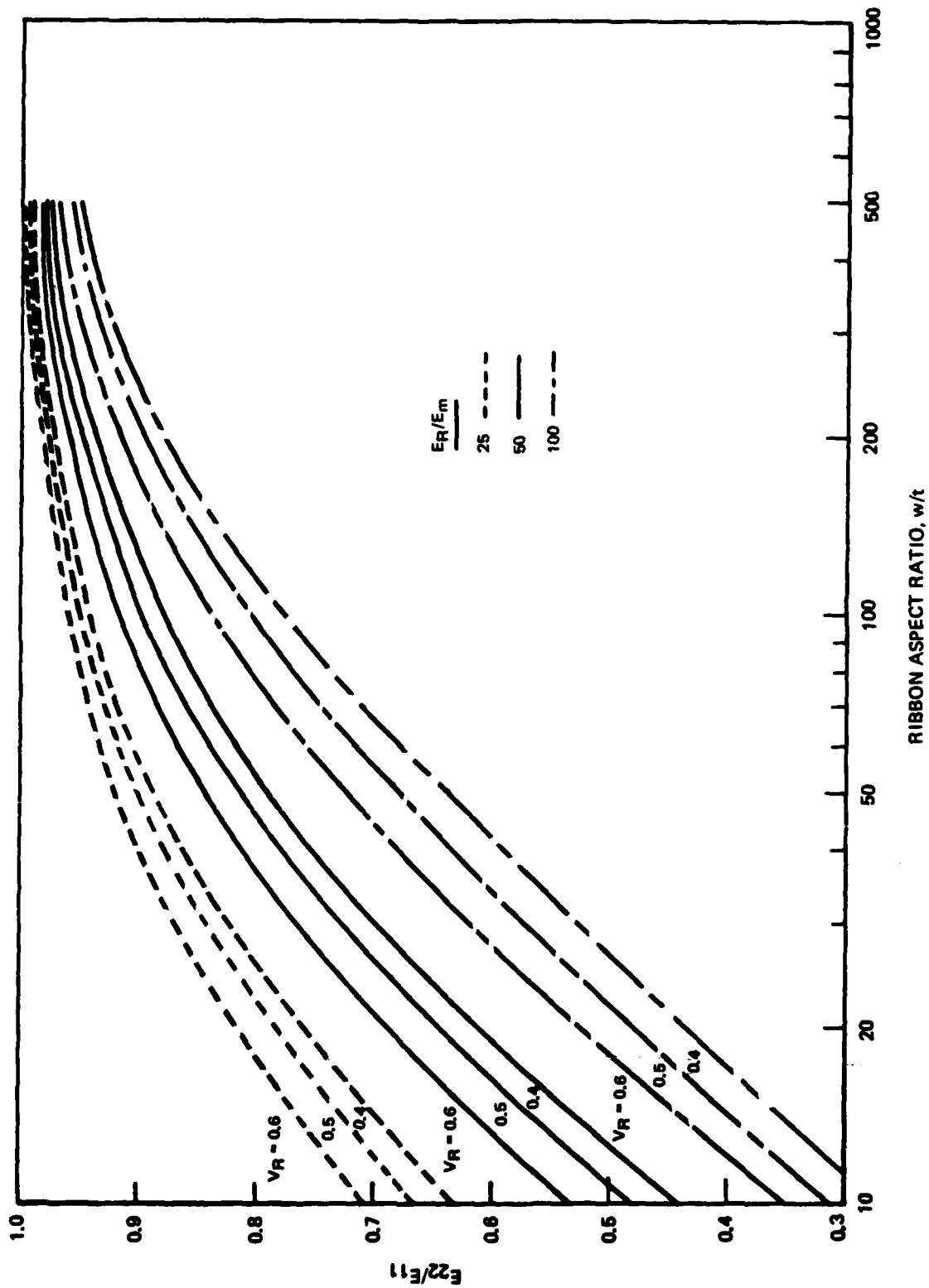


Figure 1.  $E_{22}/E_{11}$  vs Ribbon Aspect Ratio Calculated for Three Ribbon to Matrix Modulus Ratios

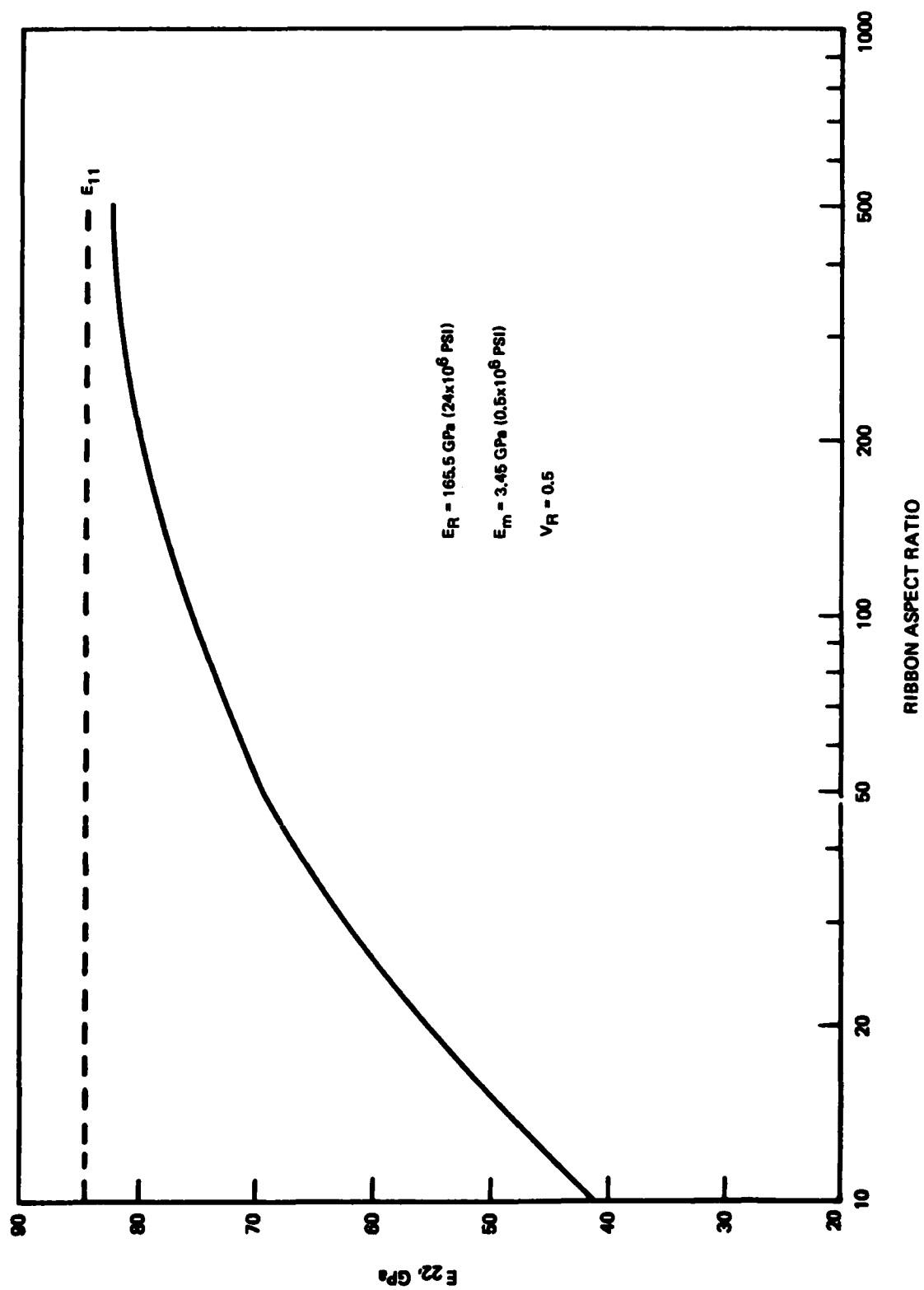


Figure 2. Calculated Transverse Composite Modulus vs Ribbon Aspect Ratio

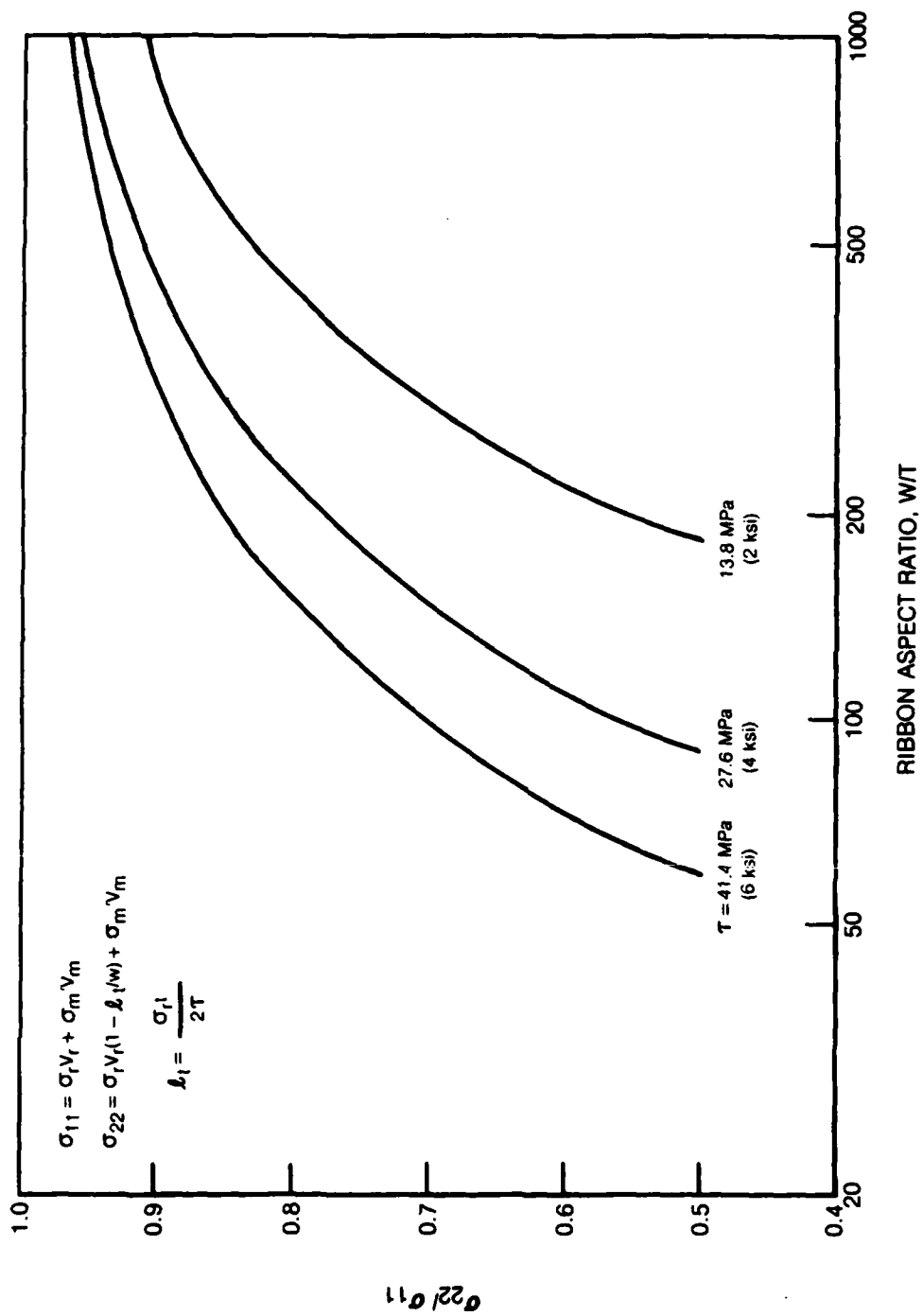
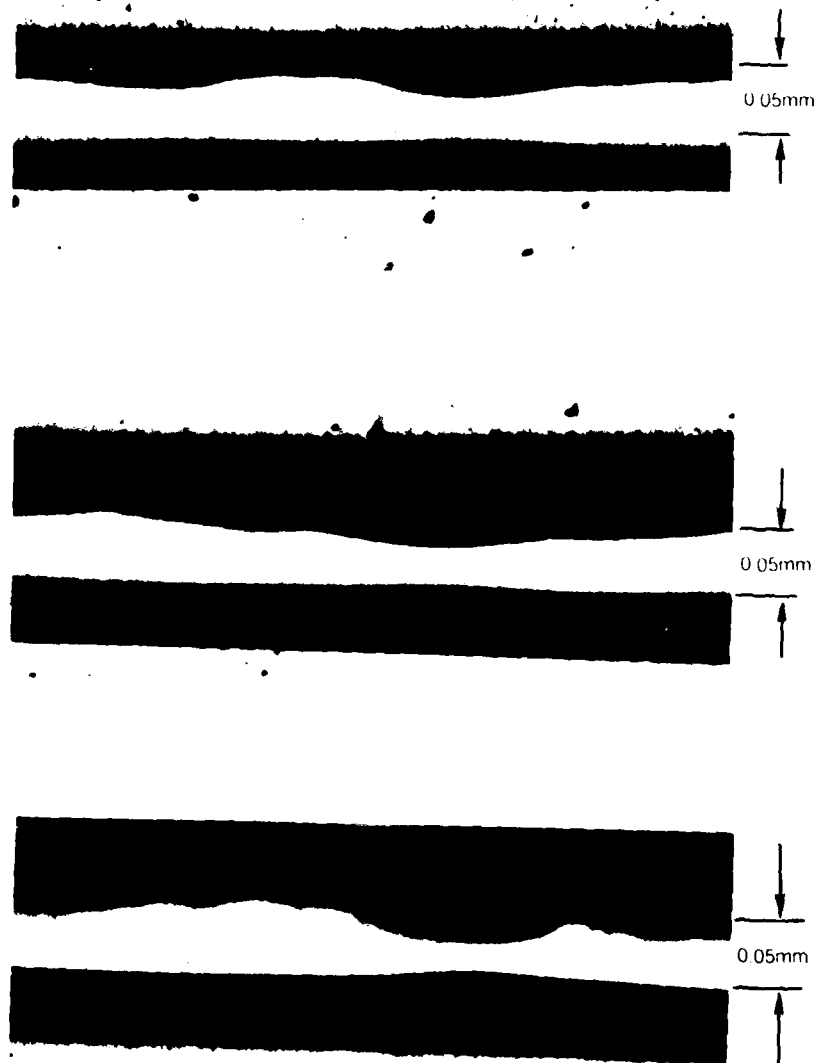


Figure 3.  $\sigma_{22}/\sigma_{11}$  vs Ribbon Aspect Ratio Calculated for Several Ribbon/Matrix Bond Strengths.



**Figure 4. Optical Micrographs of Ribbon Cross Sections. Nominal Ribbon Thickness is 0.05 mm (0.002 in)**

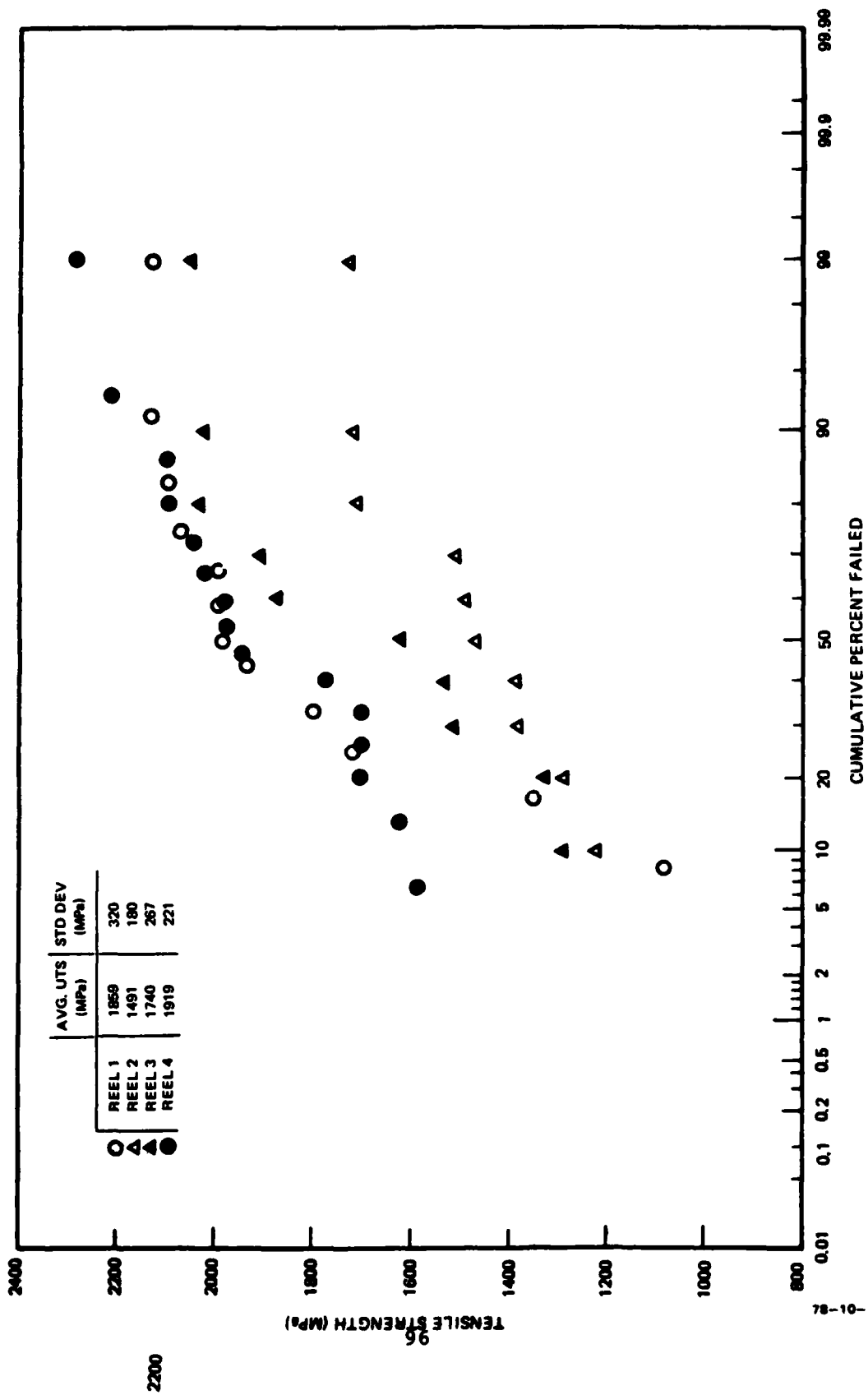


Figure 5. Tensile Properties of As-Received Ribbon

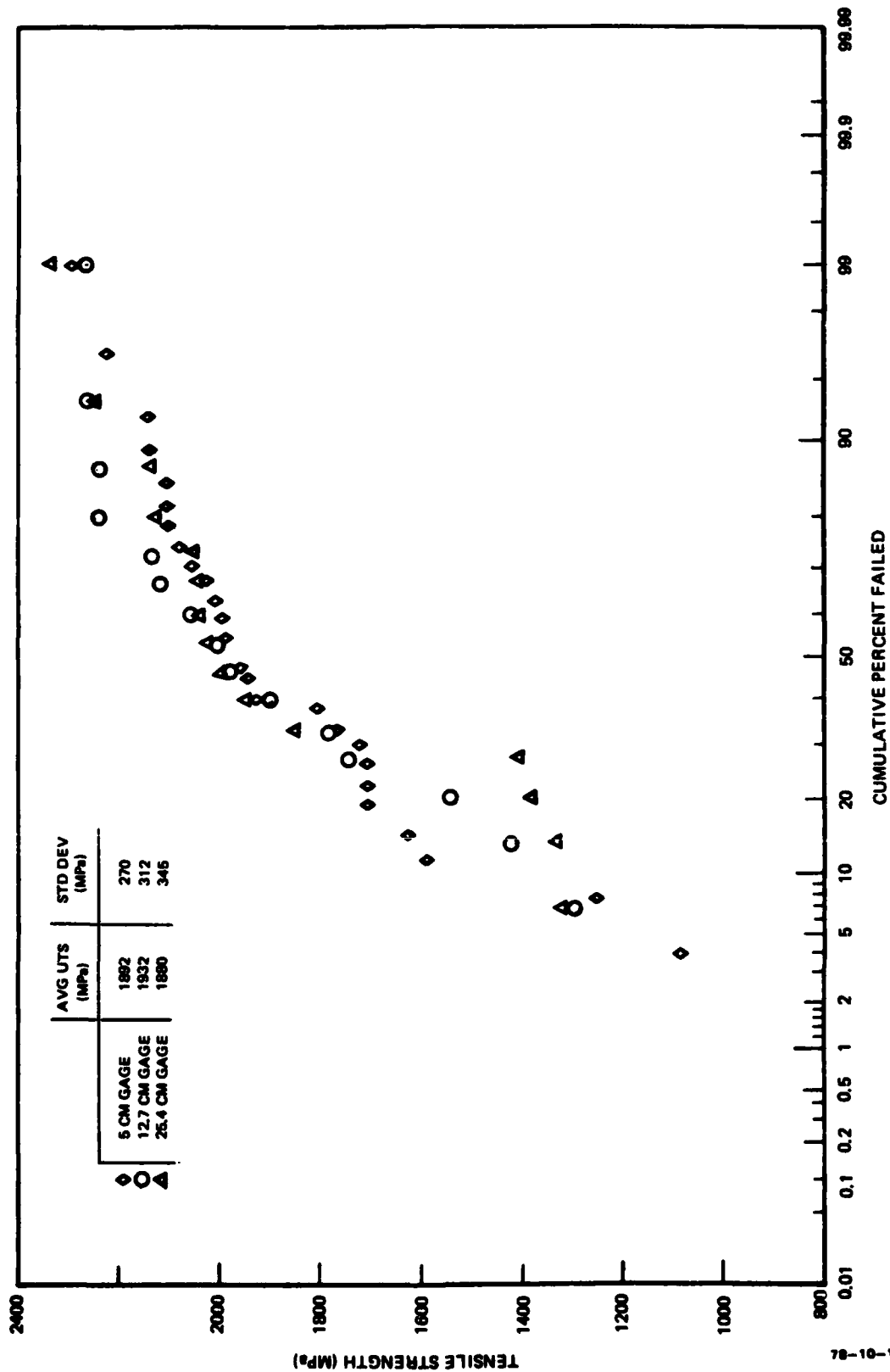


Figure 6. Effect of Gage Length on Tensile Strength



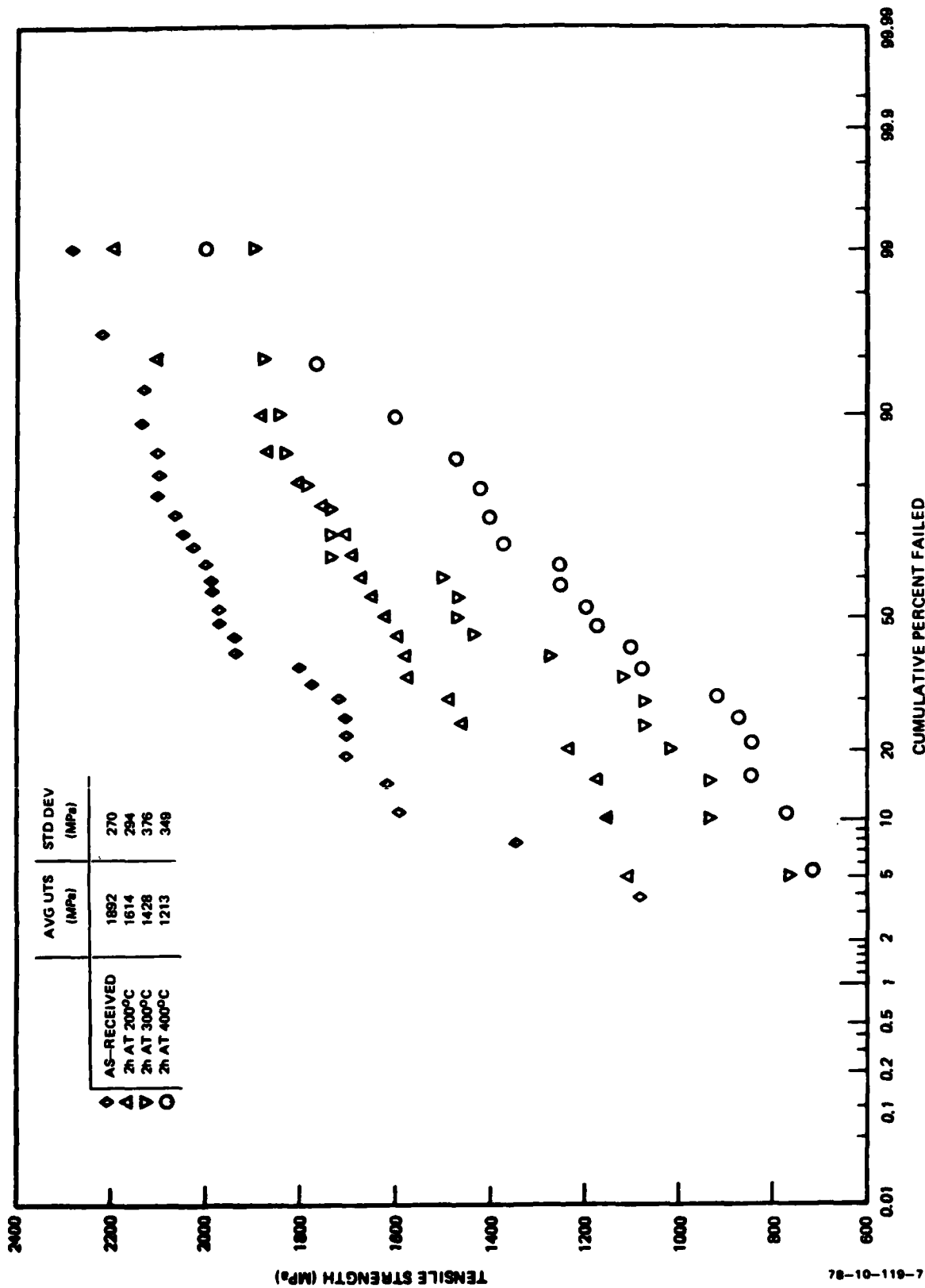


Figure 7. Effect of Elevated Temperature Exposure on Tensile Strength

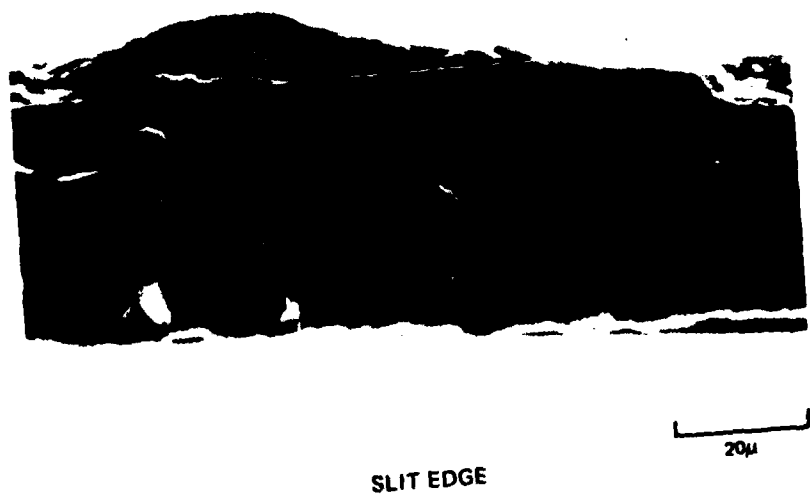
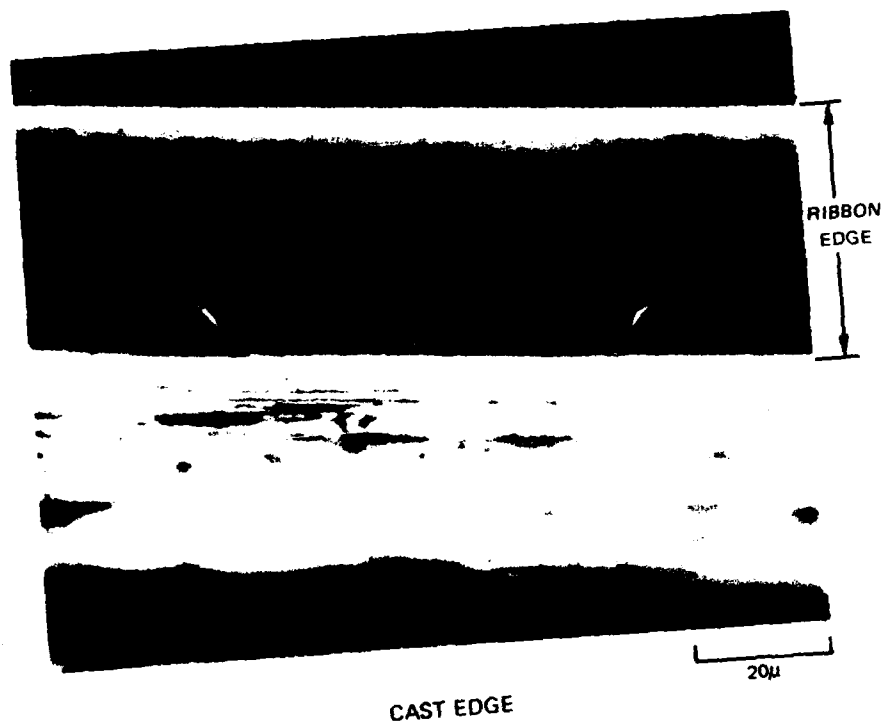
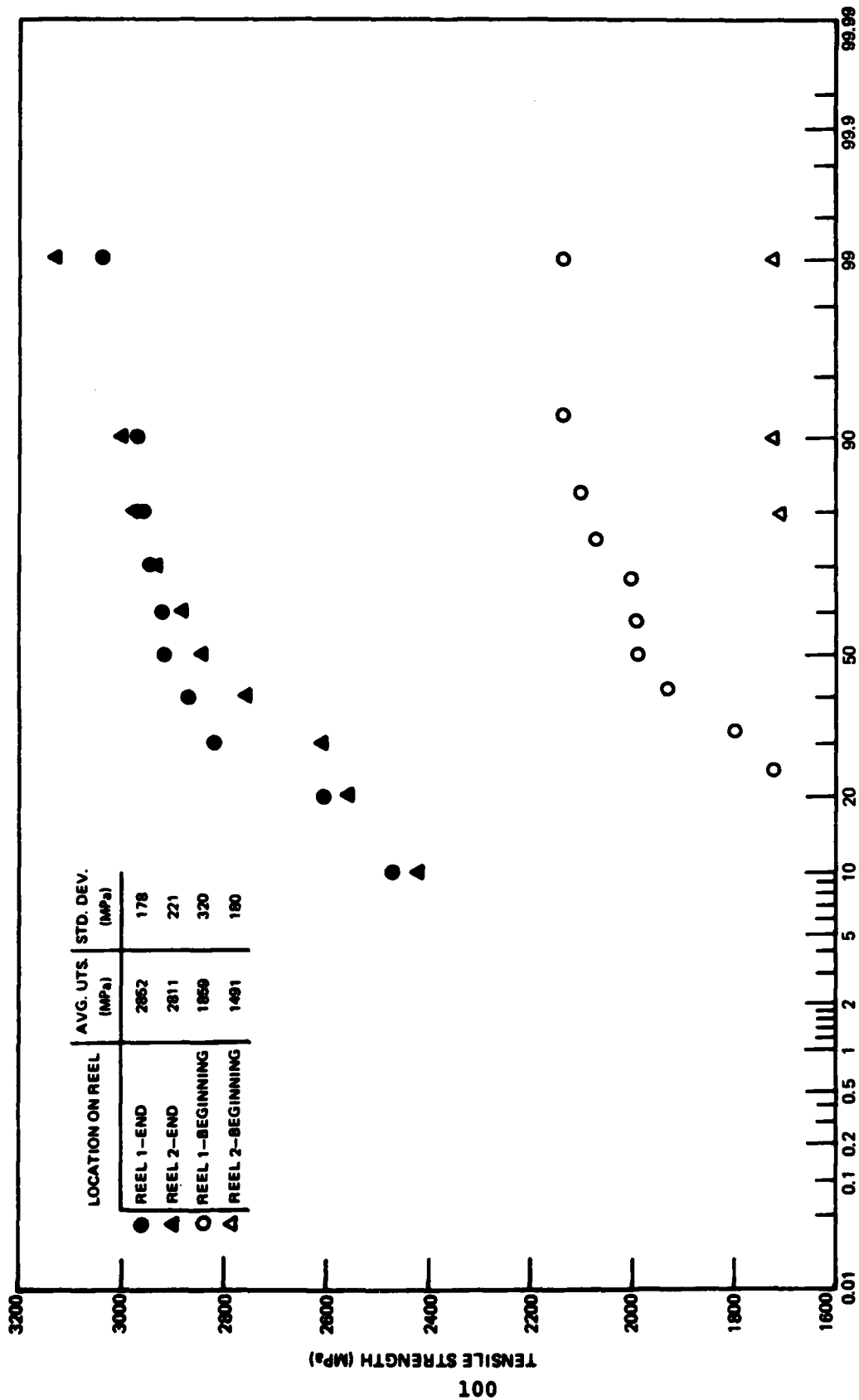


Figure 8. Scanning Electron Micrographs of Ribbon Edges

78-11-90-3



78-11-90-2

**Figure 9. Comparison of Tensile Properties of As-Received Ribbon**  
(SPECIMENS TAKEN FROM BOTH ENDS OF THE REELS)

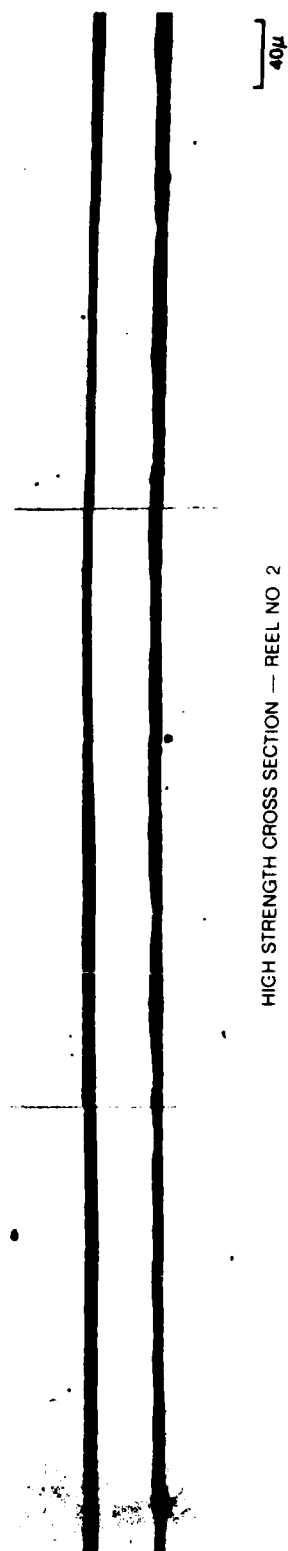
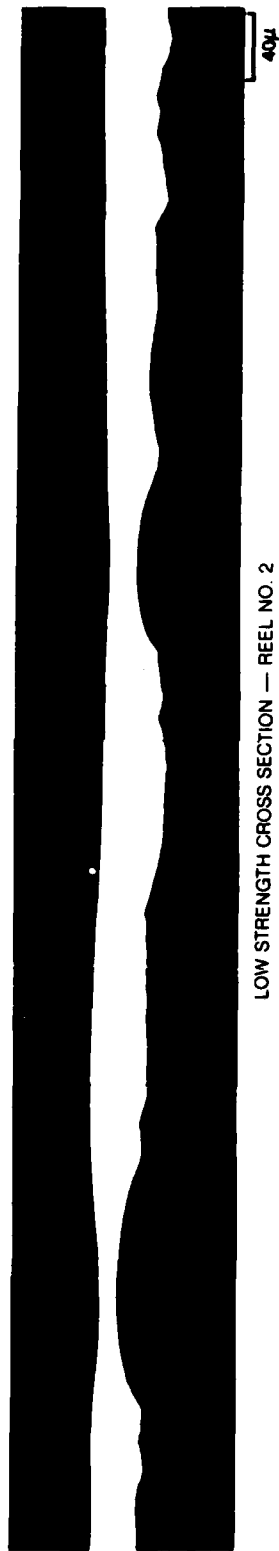


Figure 10. Optical Micrographs of Ribbon Cross Sections

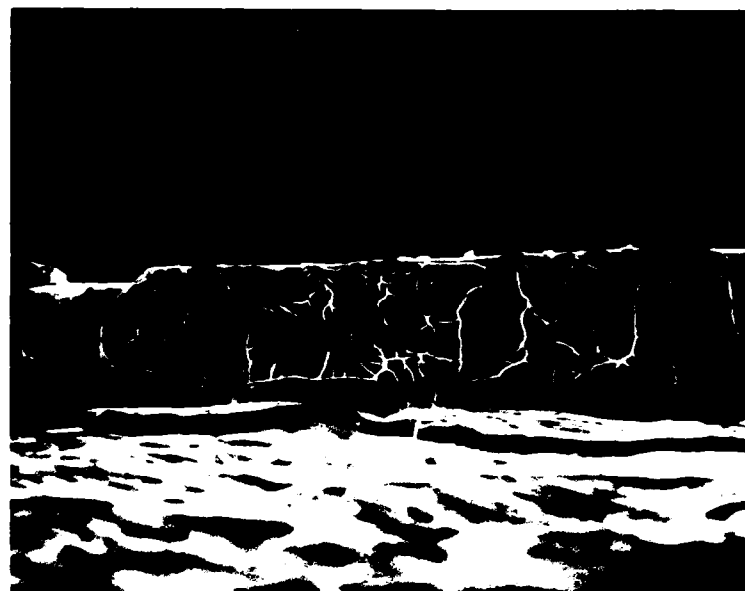


a) LOW STRENGTH SECTION — REEL NO. 2



b) HIGH STRENGTH SECTION — REEL NO. 2

Figure 11. SEM of Ribbon Surface Contacting the Wheel



40 $\mu$



20 $\mu$

**Figure 12. Scanning Electron Micrographs of Low Strength Ribbon Fracture Surfaces**

78 10 11' 4

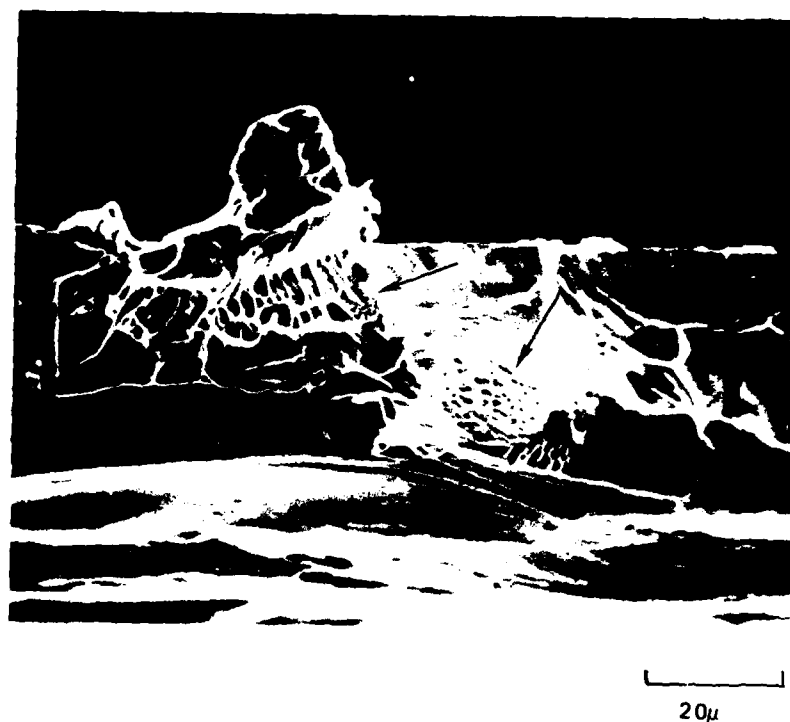


**Figure 13. Scanning Electron Micrograph of Low Strength Ribbon Fracture Surface. Arrows Indicate Areas of Plastic Deformation Characteristic of Ductile Fracture**

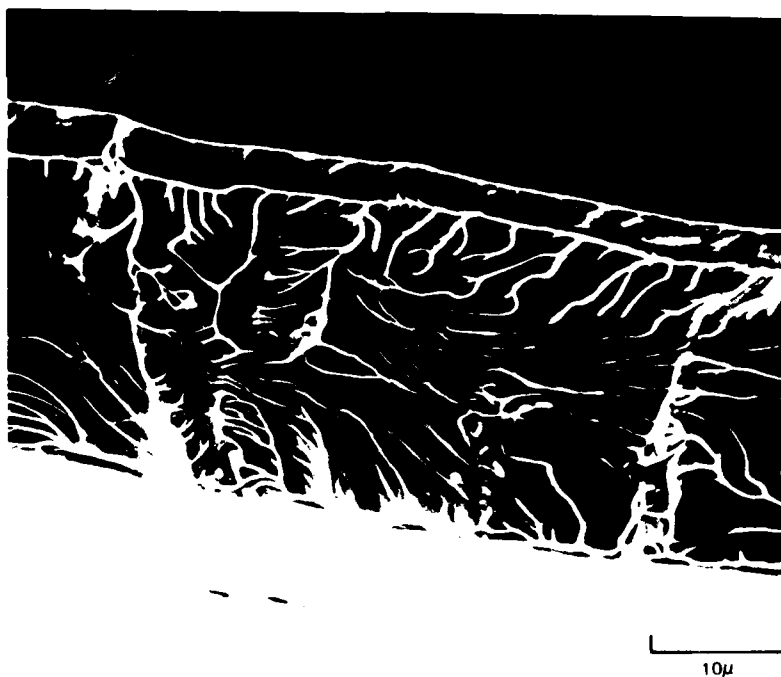
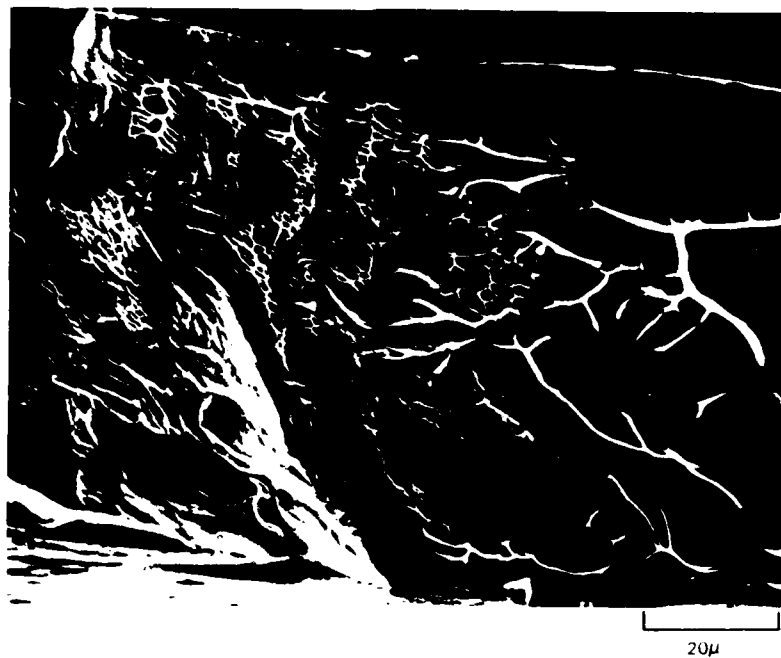


**Figure 14. Scanning Electron Micrographs of High Strength Ribbon Fracture Surfaces**



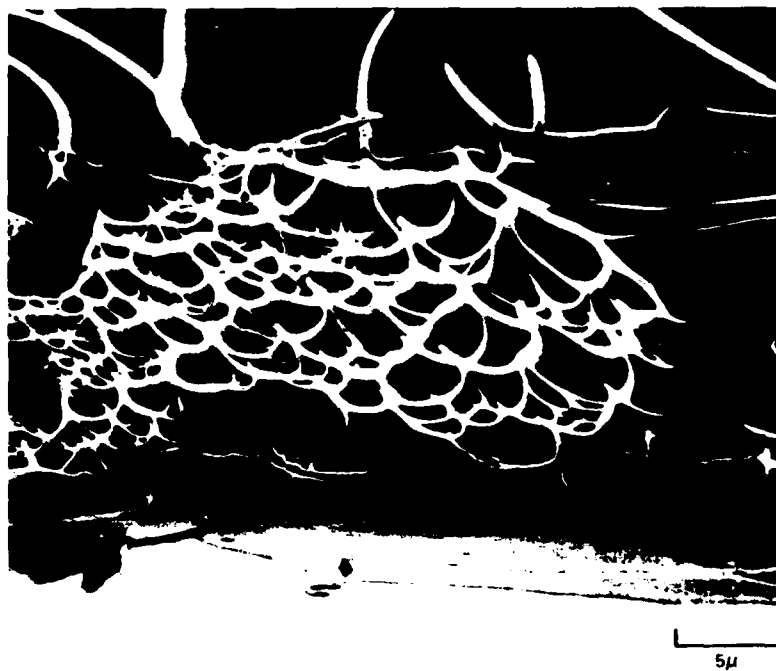


**Figure 15. Scanning Electron Micrographs of High Strength Ribbon Fracture Surface Showing Area of Extensive Plastic Deformation**

78 11 90 4

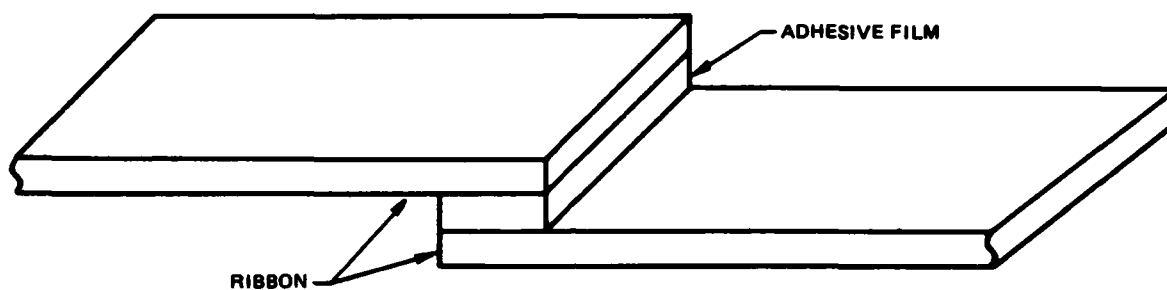
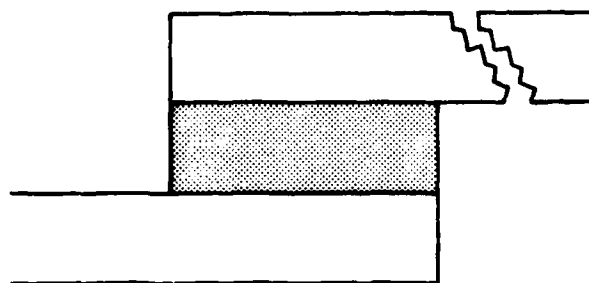
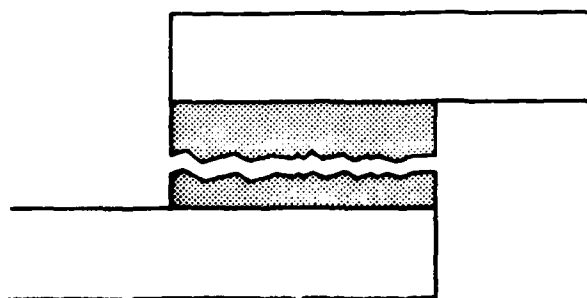


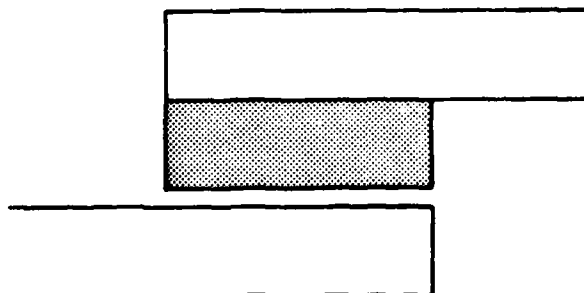
**Figure 16. Schematic of Single Lap Shear Specimen**



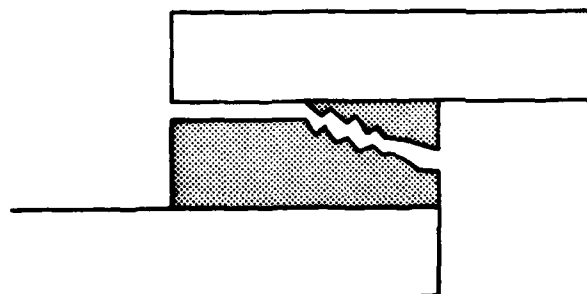
A. COHESIVE



B. COHESIVE



C. ADHESIVE



D. PARTIAL ADHESIVE, PARTIAL COHESIVE

**Figure 17. Cohesive and Adhesive Bond Failure Modes**

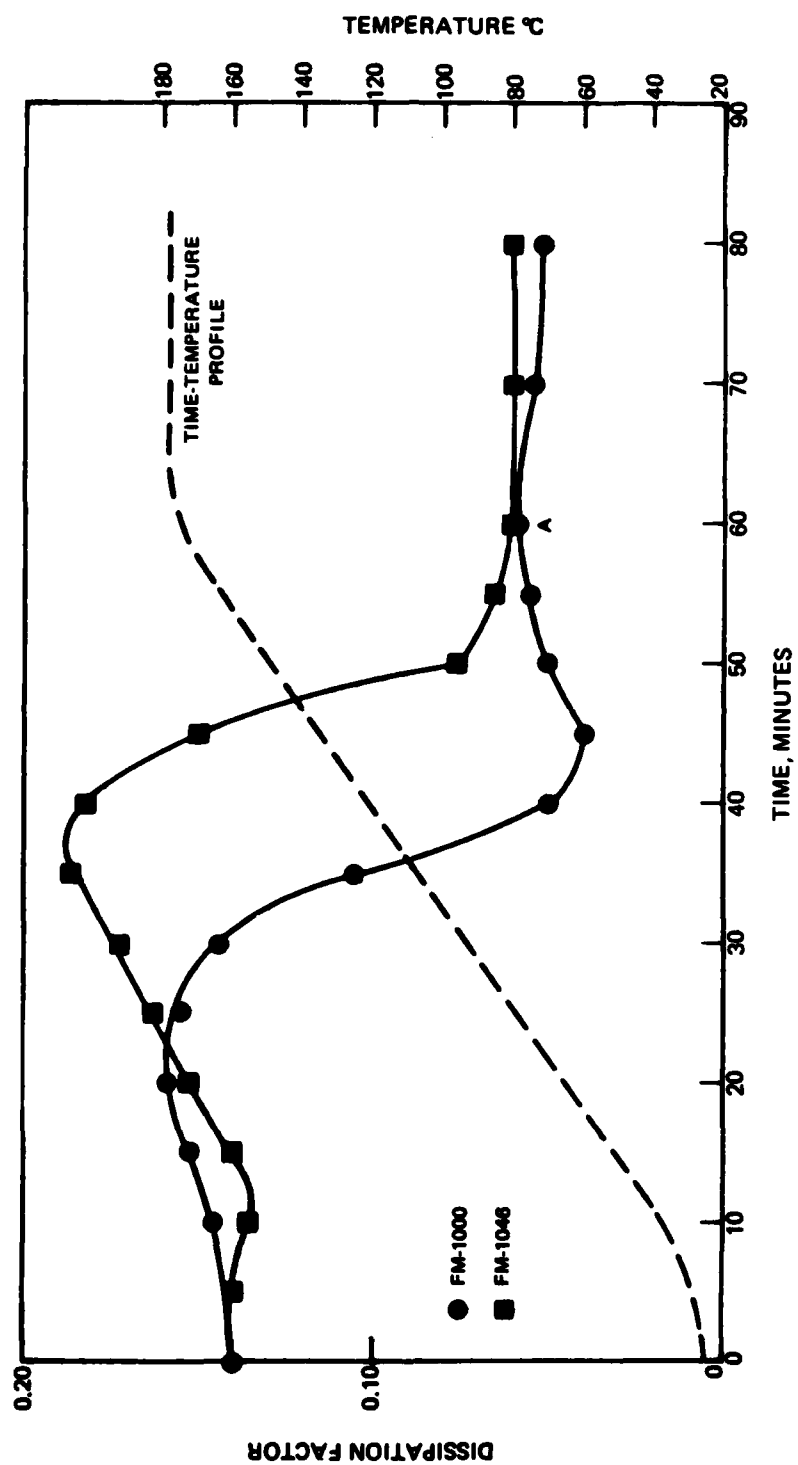


Figure 18. Curing Behavior of Epoxy-Nylon Adhesive Films

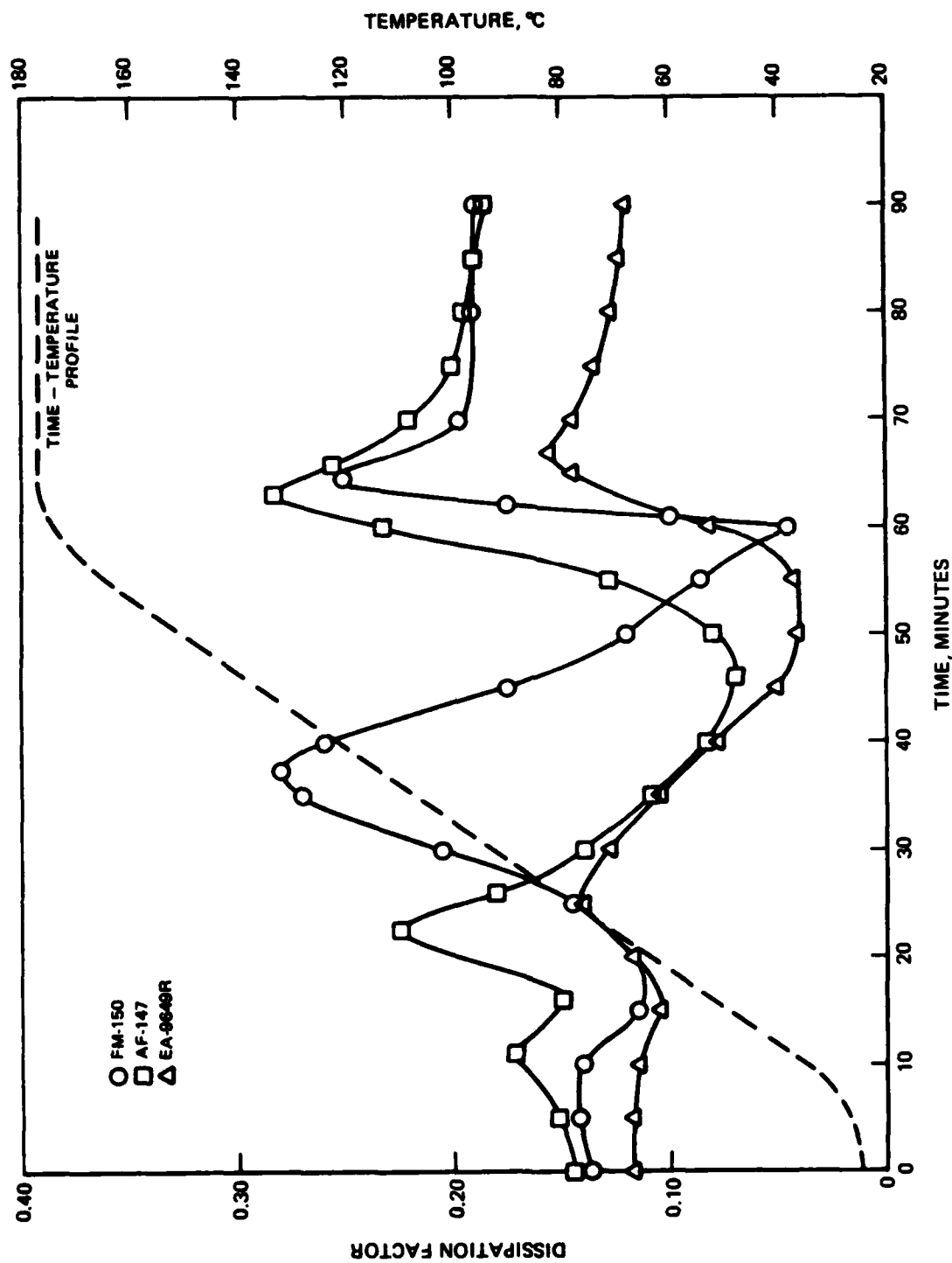


Figure 19. Curing Behavior of Epoxy Based Adhesive Films

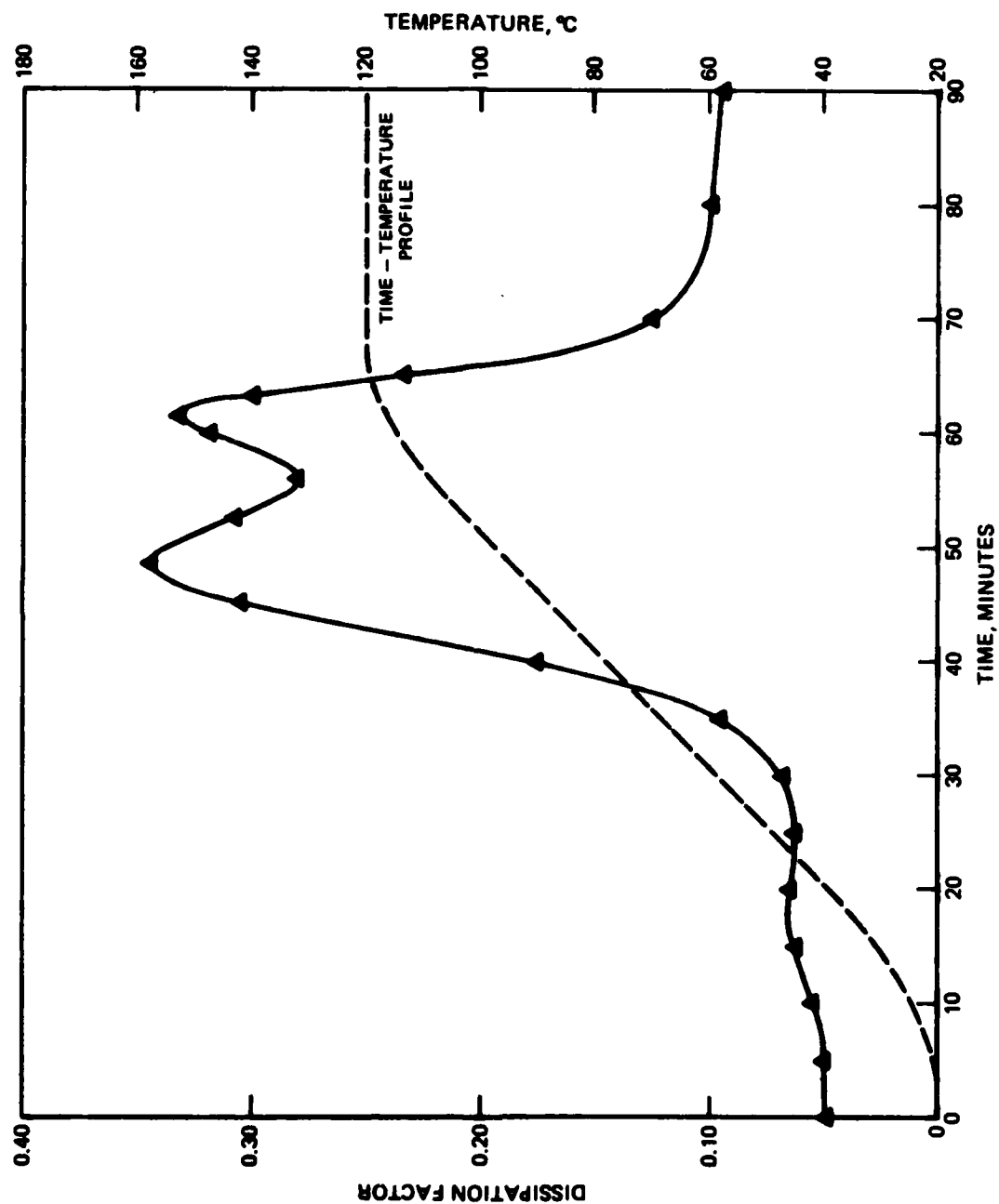


Figure 20. Curing Behavior of AF-163 Adhesive Film

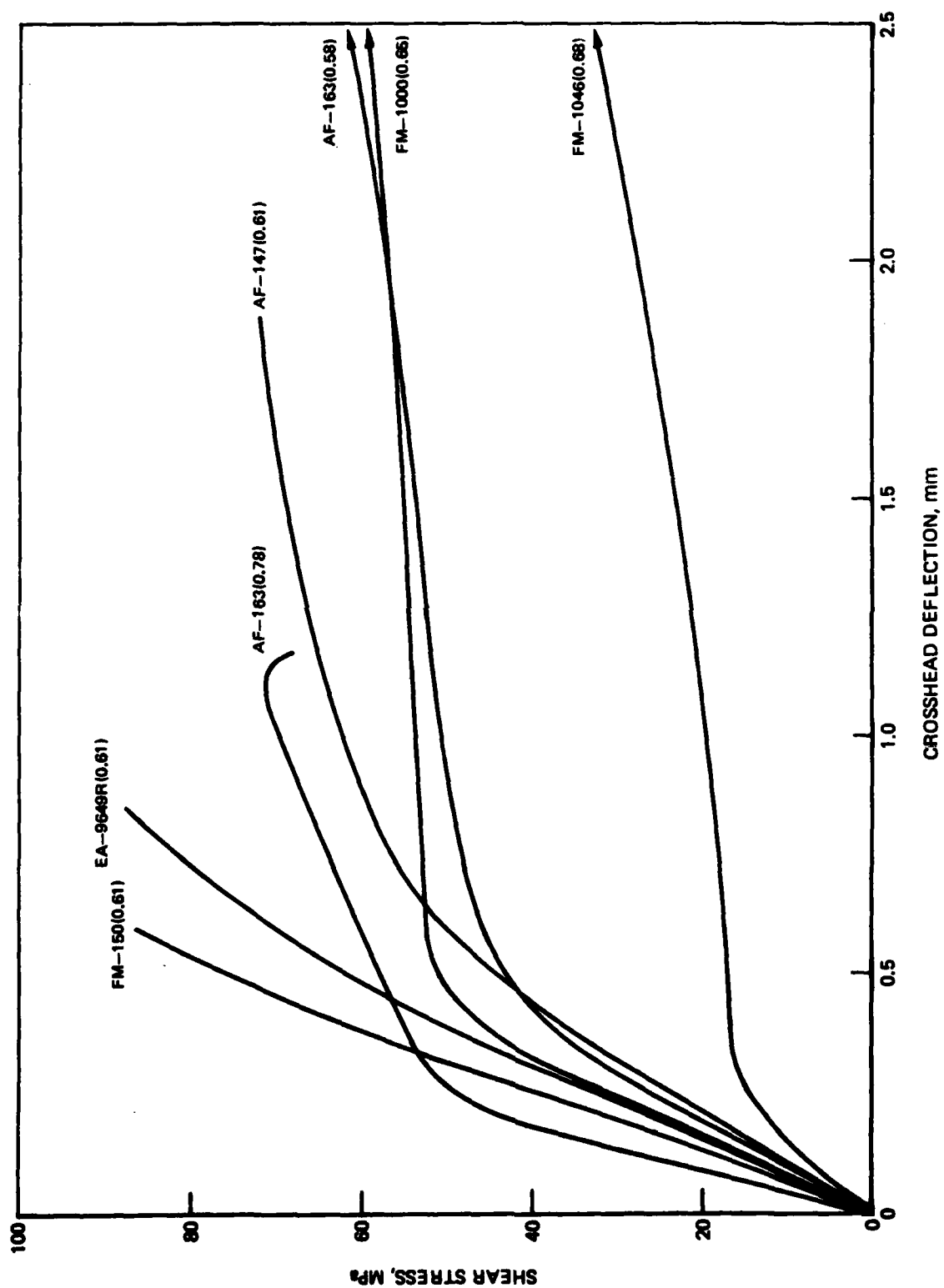


Figure 21. Shear Stress vs Crosshead Deflection for 60 Layer Laminates in 3 Point Bend at Span/Depth = 5.0

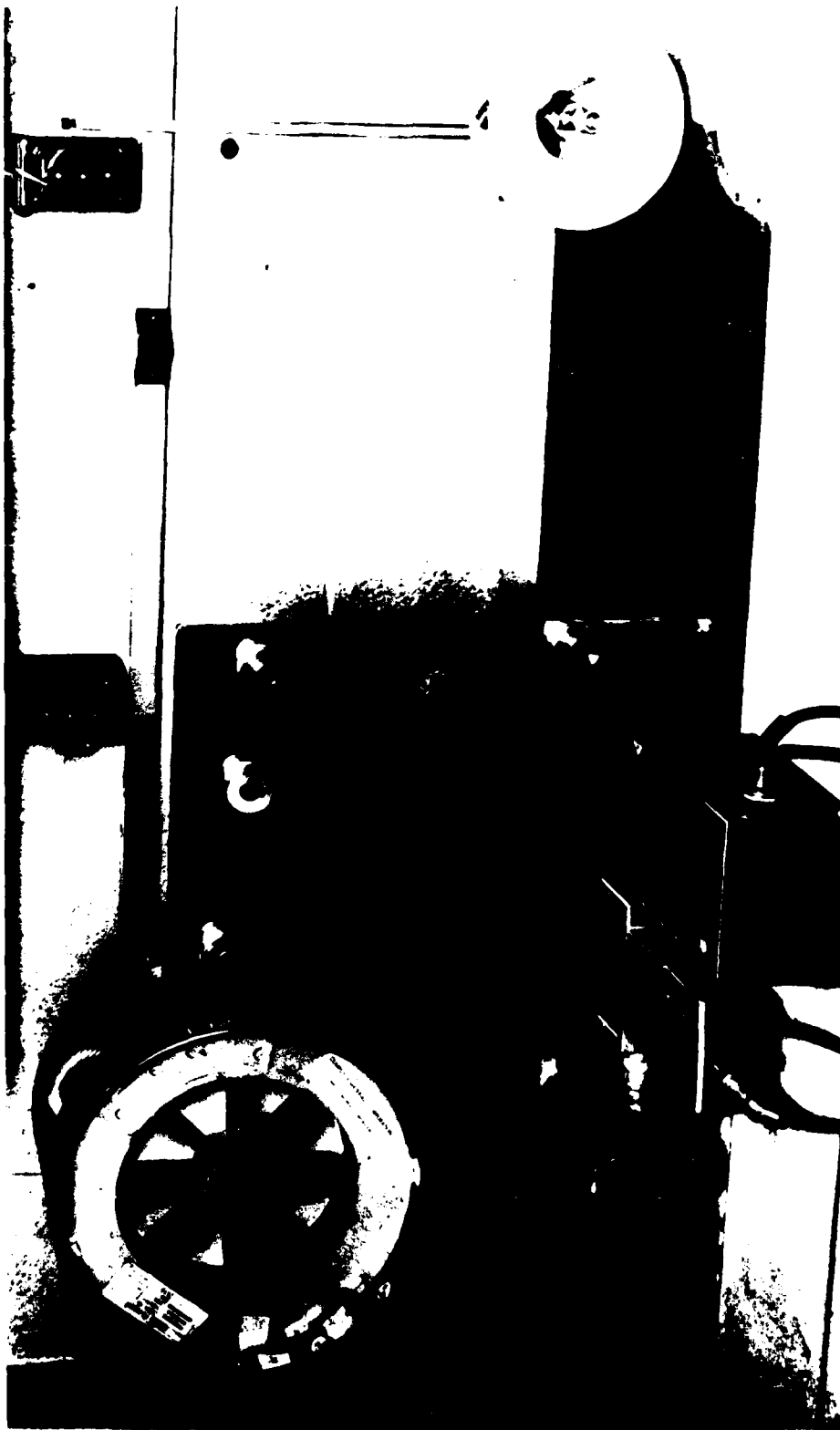


Figure 22. Low Speed Winder for Fabrication of Composite Tapes



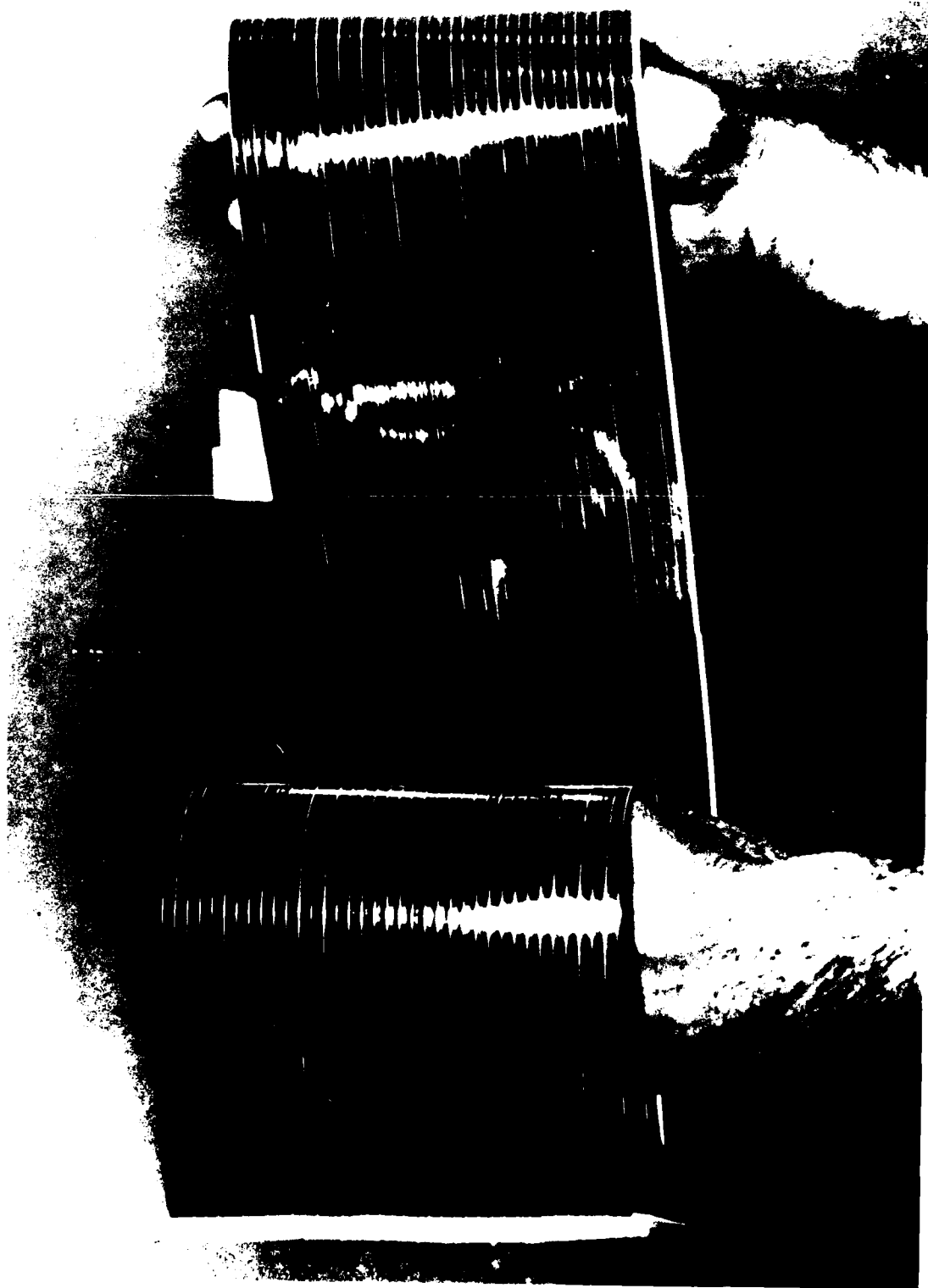
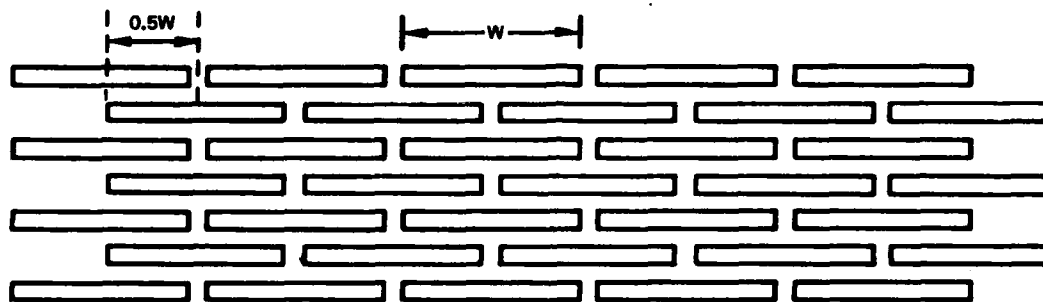
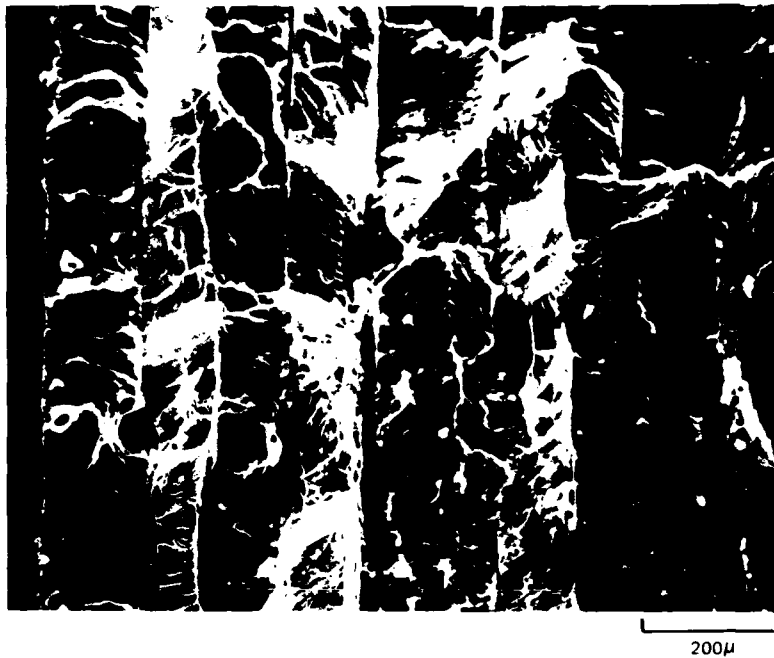


Figure 23. 2826MB/FM-1000 Tape



**Figure 24. Schematic Cross Section of Ribbon Layup Pattern Used in Composite Fabrication**



**Figure 25. Longitudinal Tensile Fracture Surfaces. 2.5 mm In-ply Ribbon Spacing.**



a) RIBBON PULLOUT

100 $\mu$



b) MIXED MODE RIBBON PULLOUT AND  
RIBBON FRACTURE

100 $\mu$

**Figure 26. Transverse Tensile Fracture Surfaces. 2.5 mm in-ply Ribbon Spacing.**

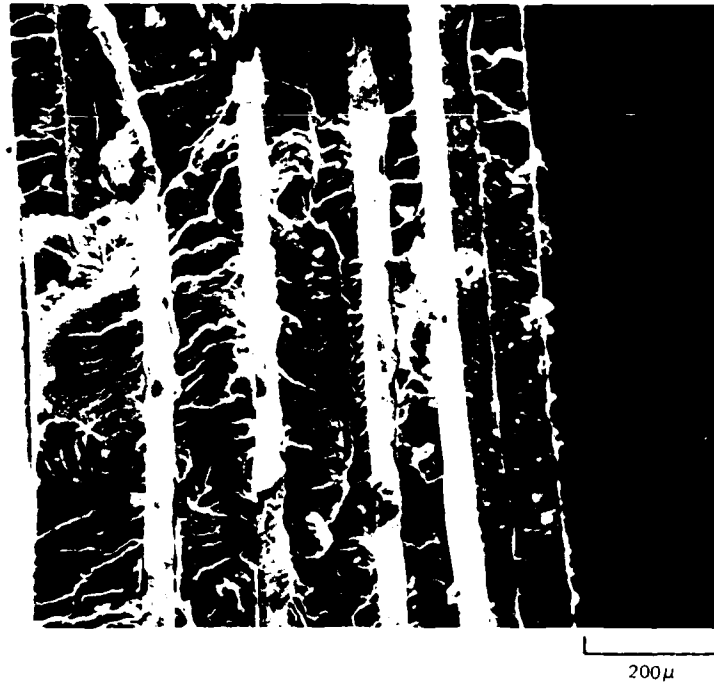


**Figure 27. Transverse Tensile Fracture Surfaces. 2.5 mm in-ply Ribbon Spacing. Ribbon Fracture Observed.**

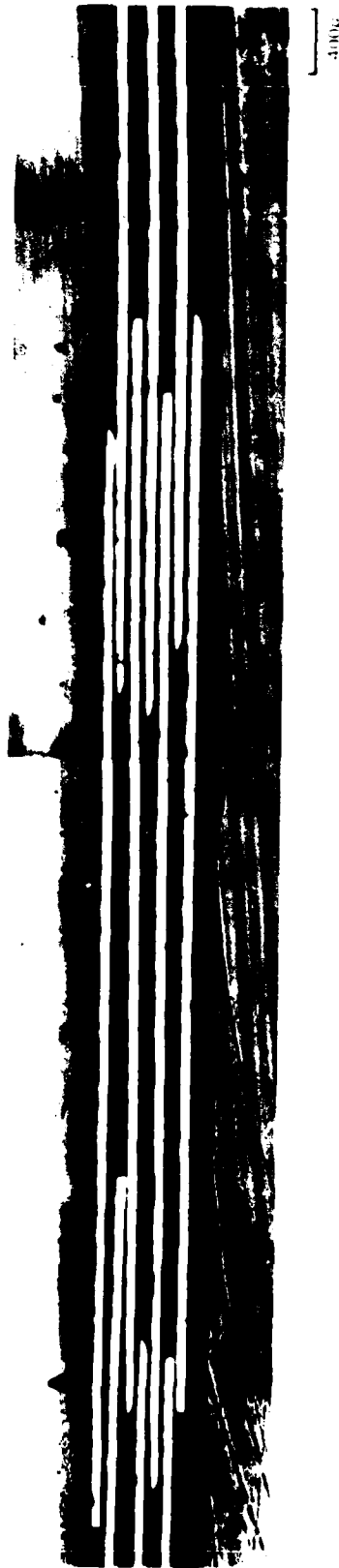


Figure 28. Transverse Composite Cross Section. 2.5 mm in-ply Ribbon Spacing. Ribbon Sliding at A.

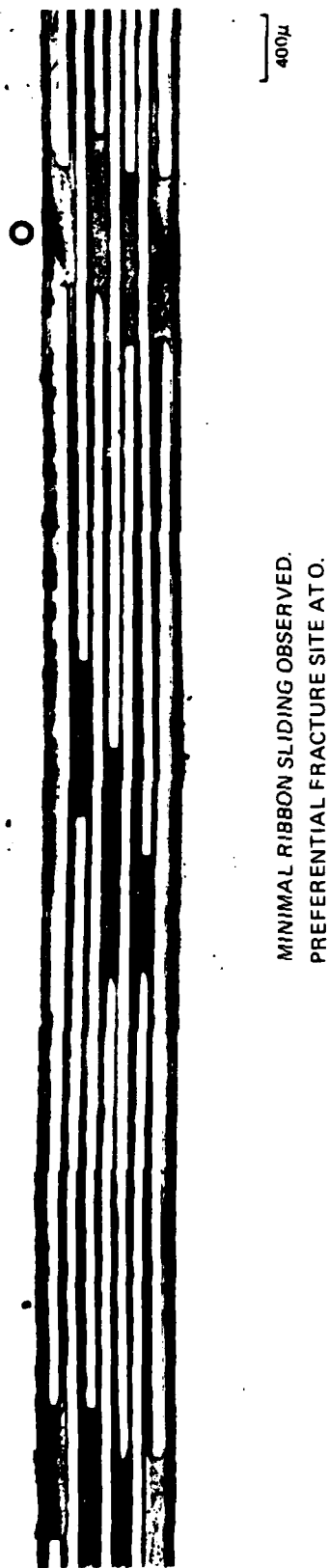


Figure 29. Transverse Composite Cross Section. 0.5 mm in-ply Ribbon Spacing.

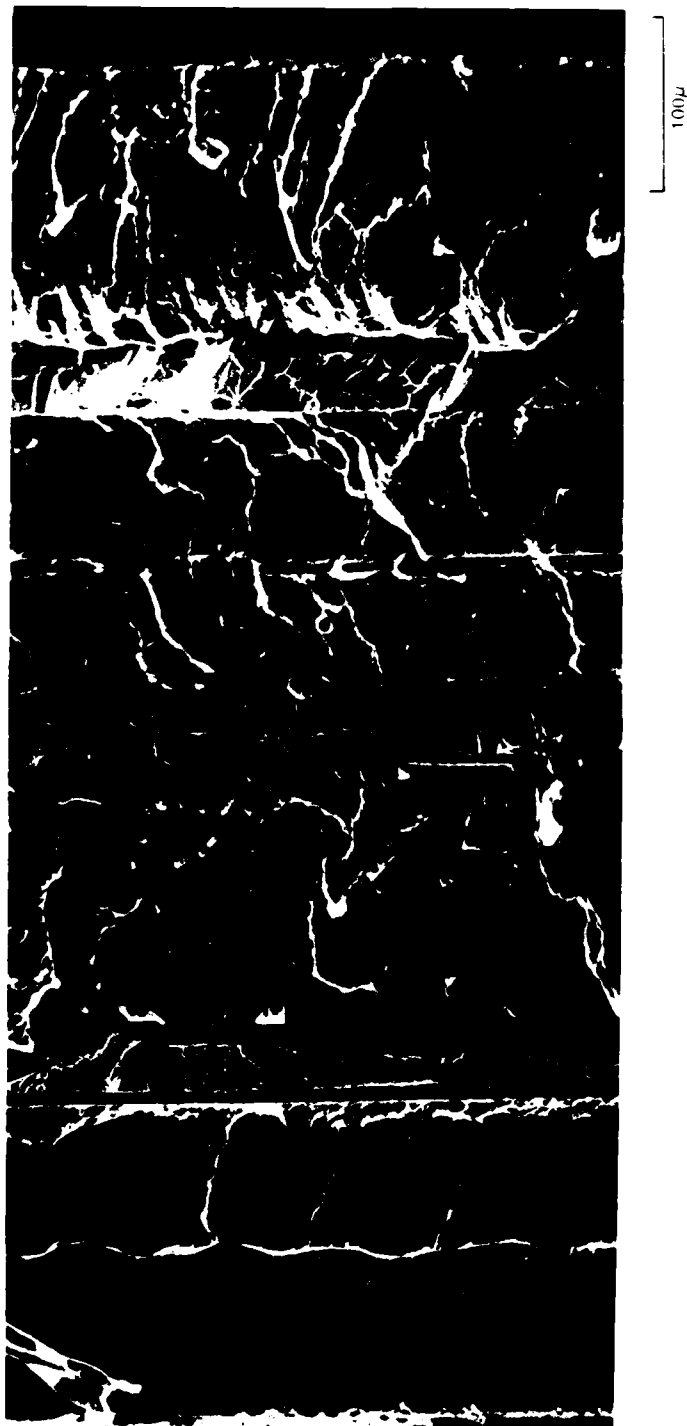


Figure 30. Transverse Tensile Fracture Surface. 0.5 mm in-ply Ribbon Spacing. Ribbon Fracture Observed.



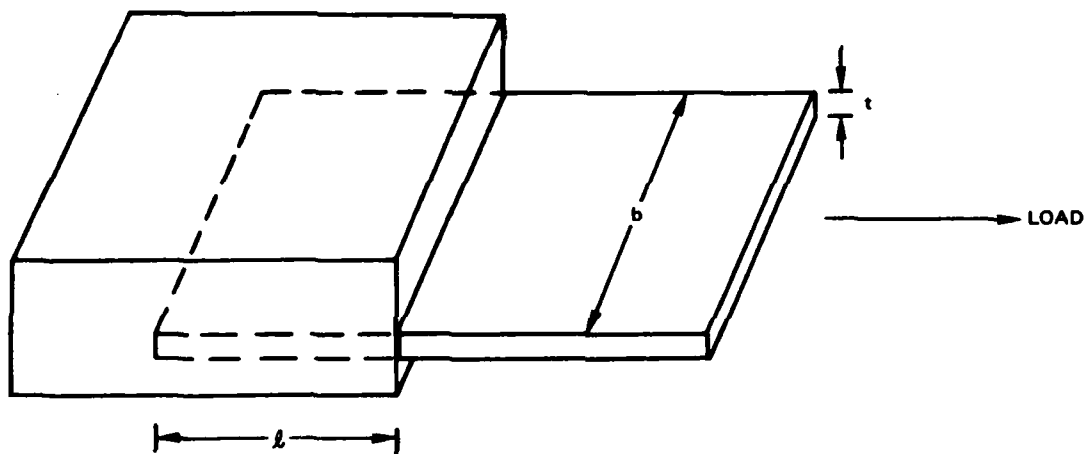


Figure 31. Ribbon Embedded in Matrix Loaded for Pullout.



Figure 32. 2826MB Ribbon in Widths of 3.18, 6.35, 13.0 mm

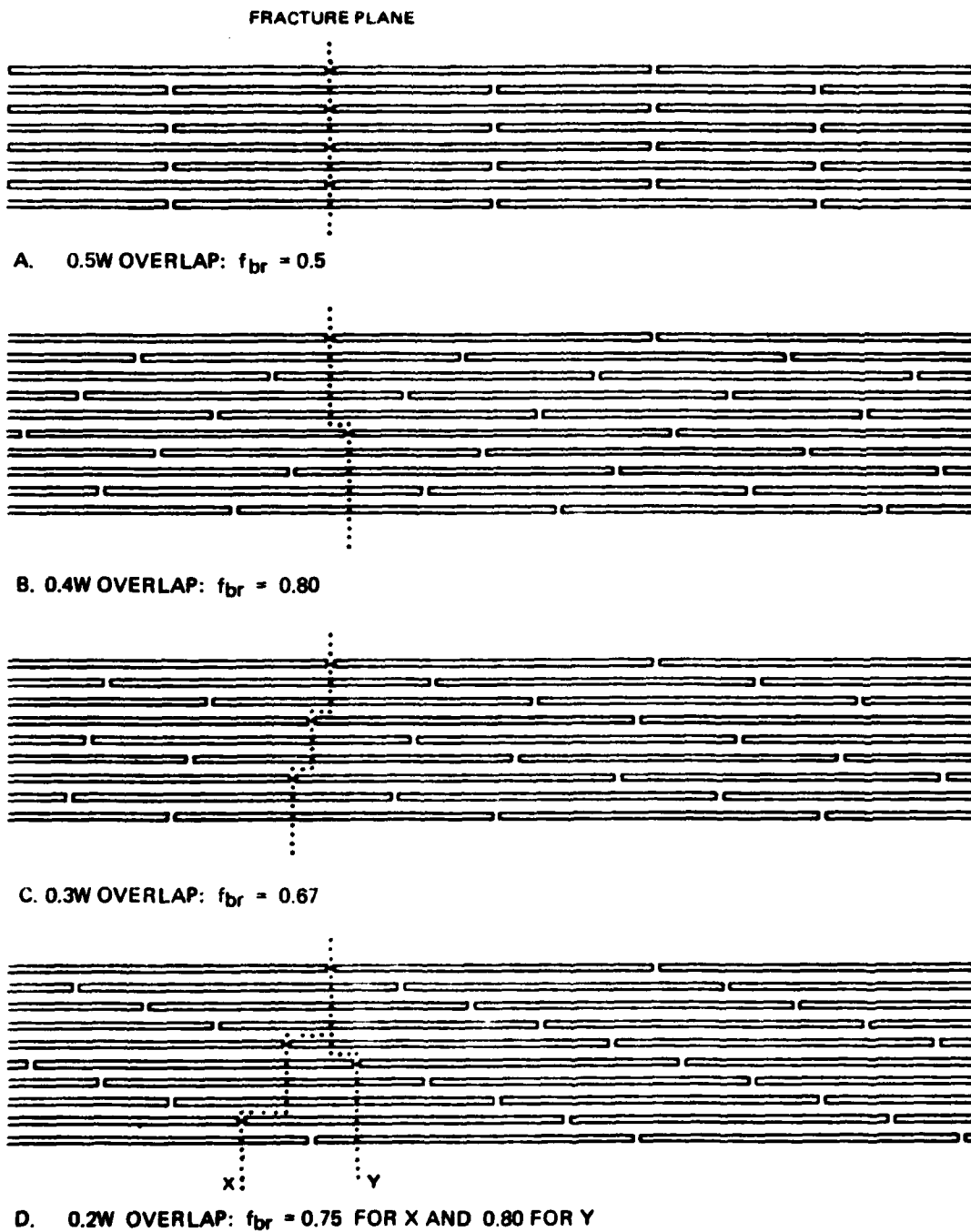
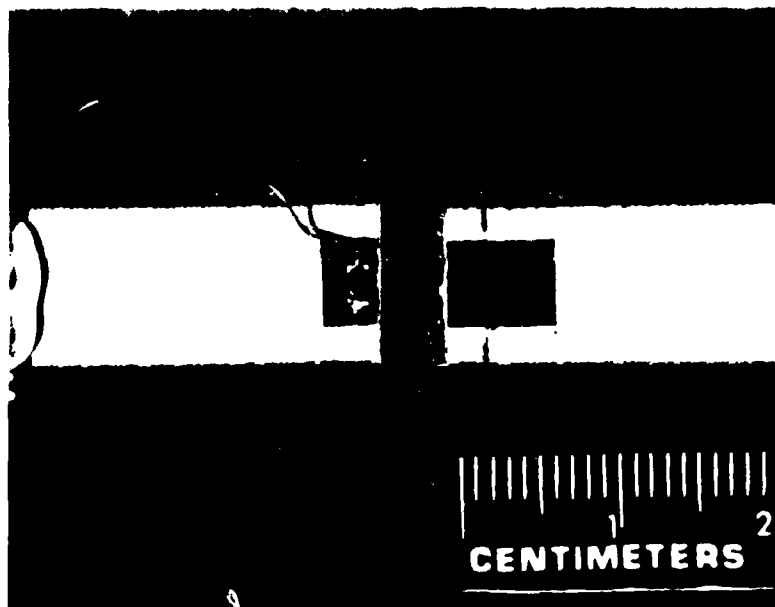
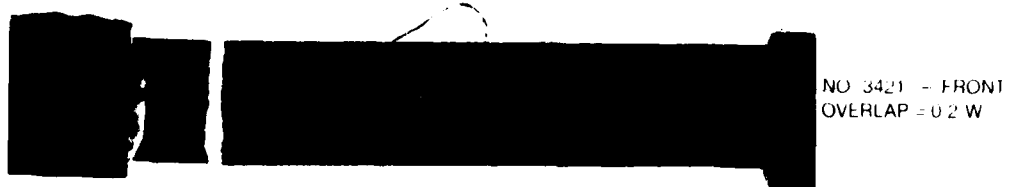


Figure 33. Schematic Transverse Composite Cross Sections with Expected Fracture Plane Indicated.

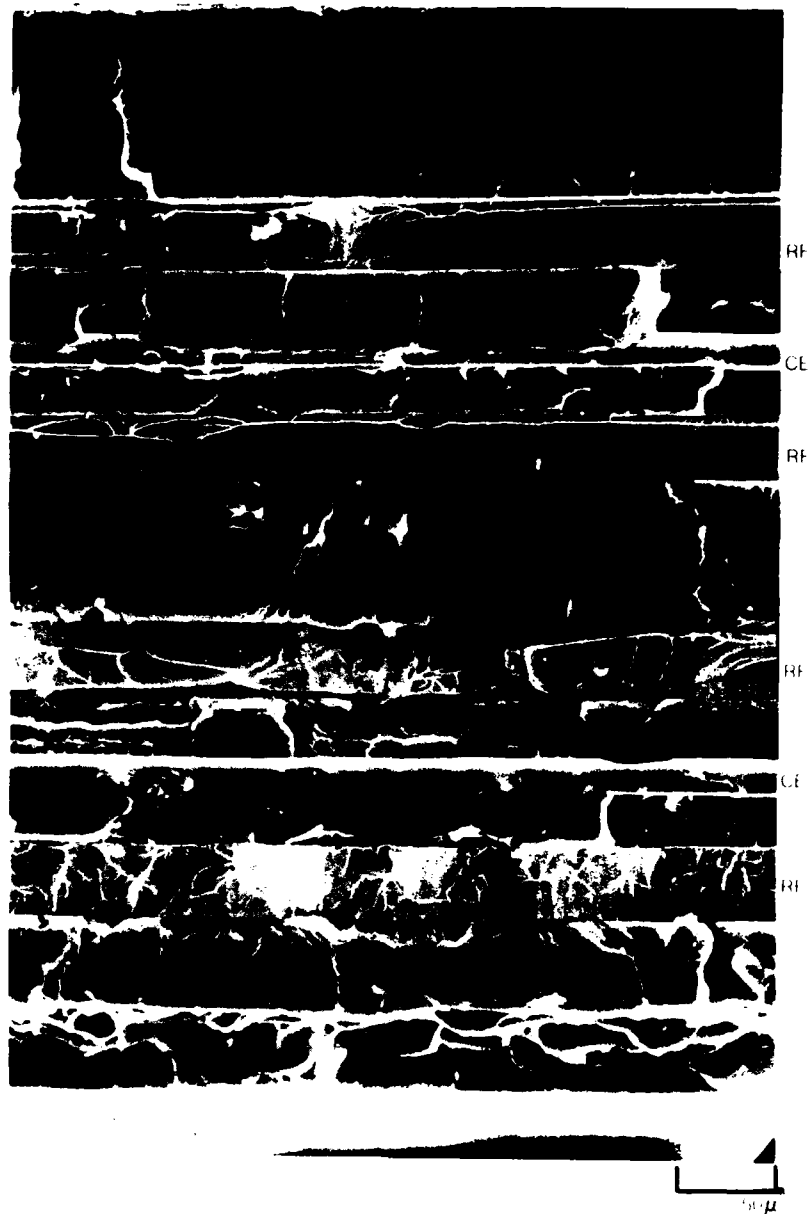


**Figure 34. Transverse Tensile Failure Showing Ribbon Pullout —  
Ribbon Width is 3.18 mm**

RO 02 138 4

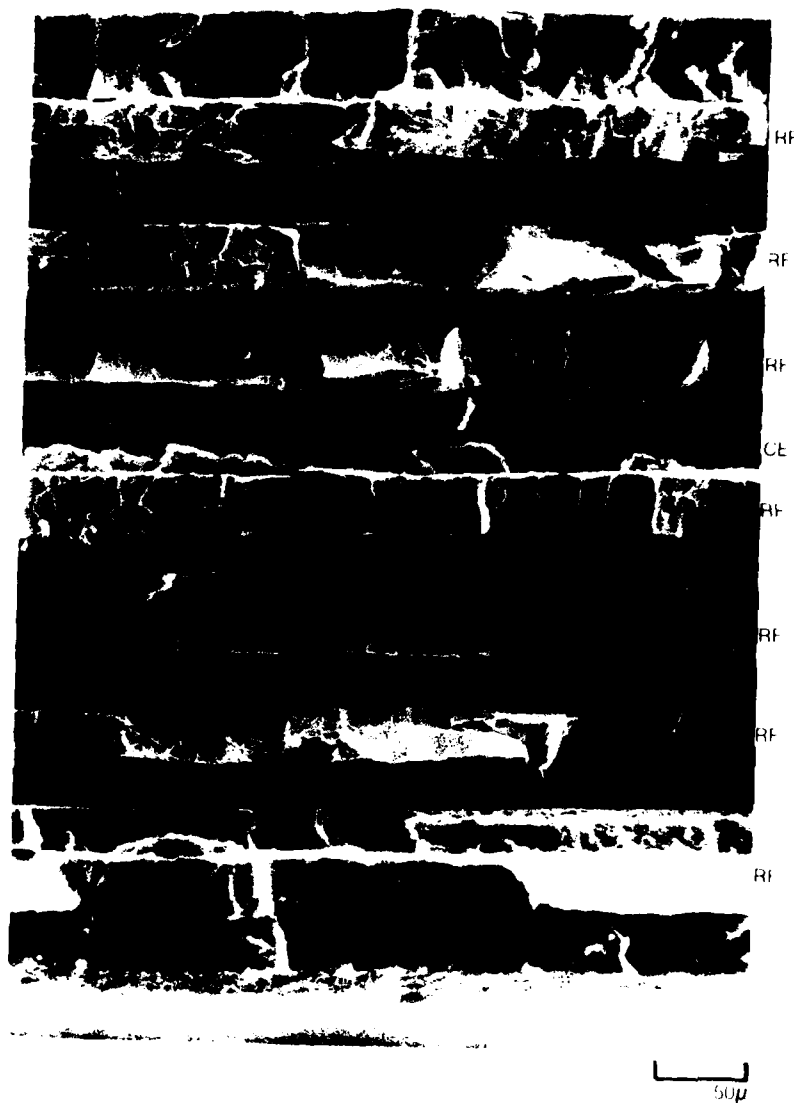


**Figure 35. Transverse Tensile Specimens Tested at Room Temperature**



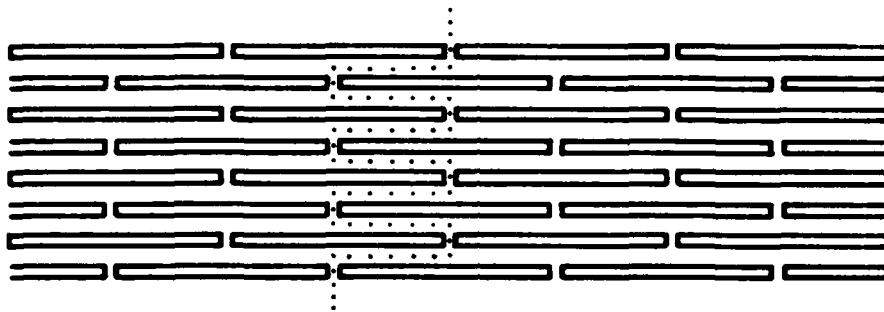
RF RIBBON FRACTURE  
CE CAST EDGE

**Figure 36. Fracture Surface of Composite Constructed with 0.5 W Ribbon Overlap**

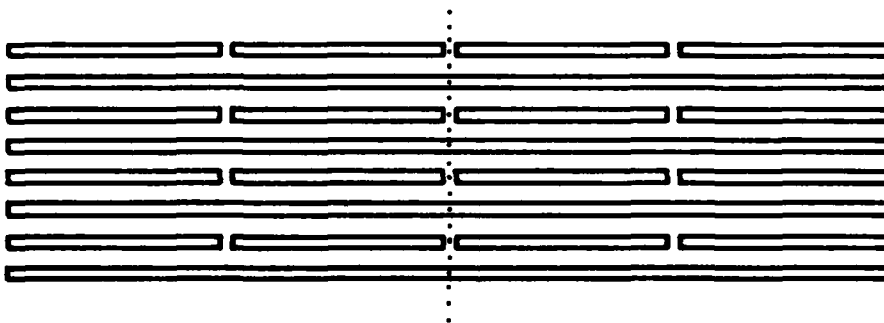


RF --- RIBBON FRACTURE  
 CE --- CAST EDGE

**Figure 37. Fracture Surface of Composite Constructed with 0.2 W Ribbon Overlap**



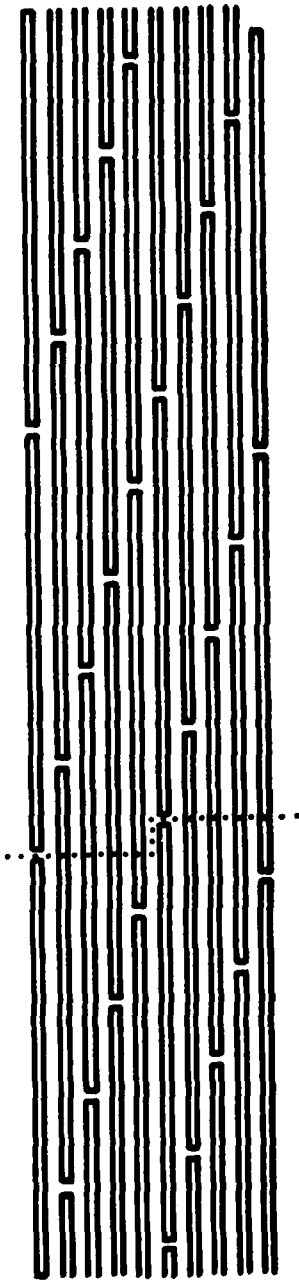
a. 0.5 W OVERLAP: PULLOUT OBSERVED



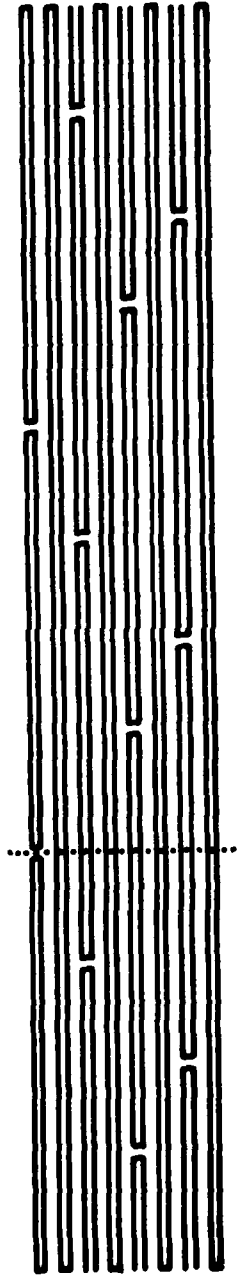
b. 0/90 LAYUP:  $f_{br} = 0.5$

**Figure 38. Schematic Transverse Composite Cross Sections With Expected Fracture Mode Utilizing 0.125 in. Wide Ribbon.**





a. 0.2W OVERLAP:  $f_{br} = 0.80$



b. 0/90 LAYUP WITH COMPLEX OVERLAP:  $f_{br} = 0.88$

Figure 39. Schematic Transverse Composite Cross Sections With Expected Fracture Mode Utilizing 0.51 in. Wide Ribbon.

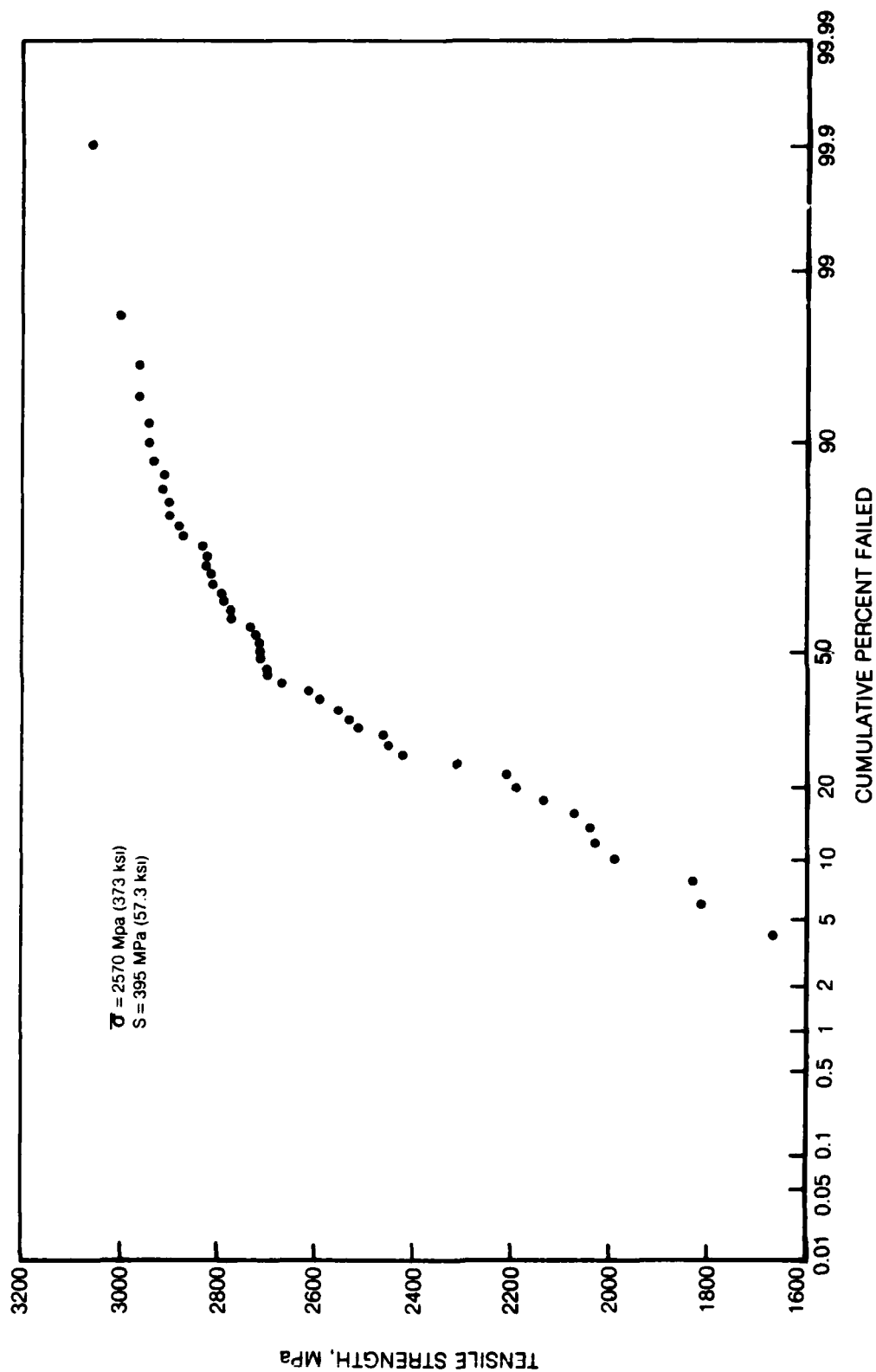


Figure 40. Tensile Properties of 13mm Ribbon — RB776-1PF4545 Spool #1

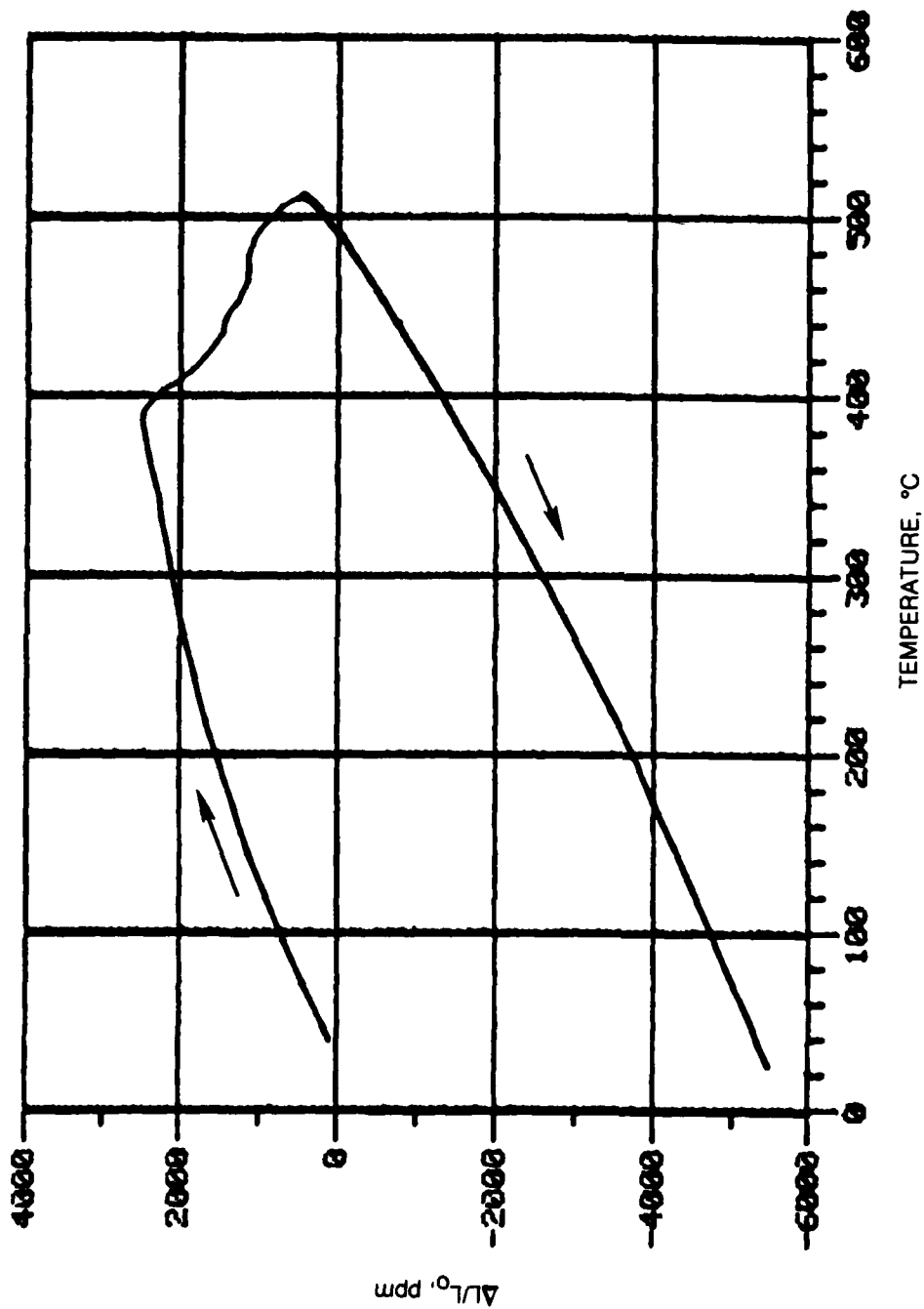


Figure 41 Thermal Expansion of 2826MB Ribbon — Longitudinal Orientation

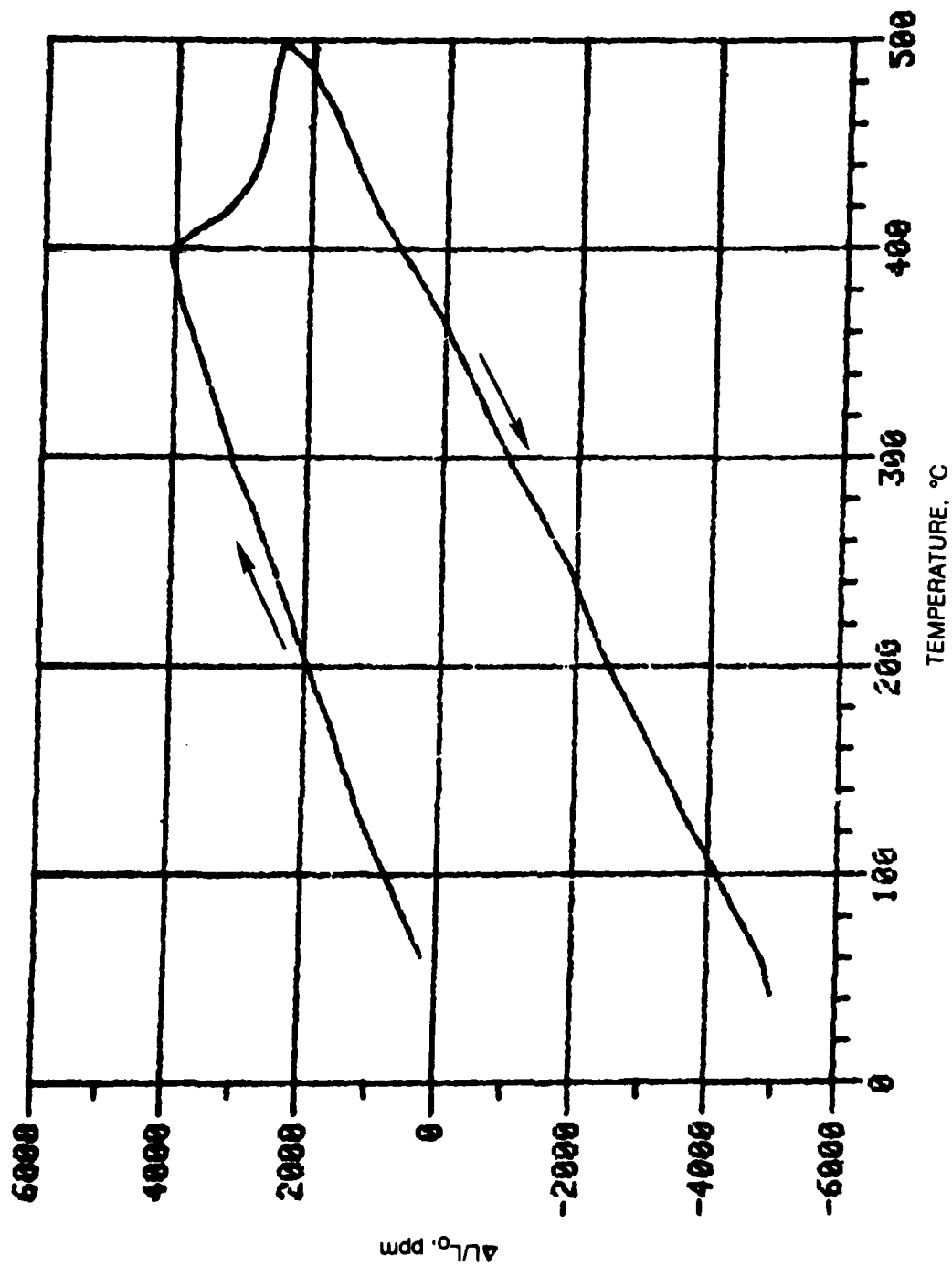


Figure 42. Thermal Expansion of 2826MB Ribbon — Transverse Orientation

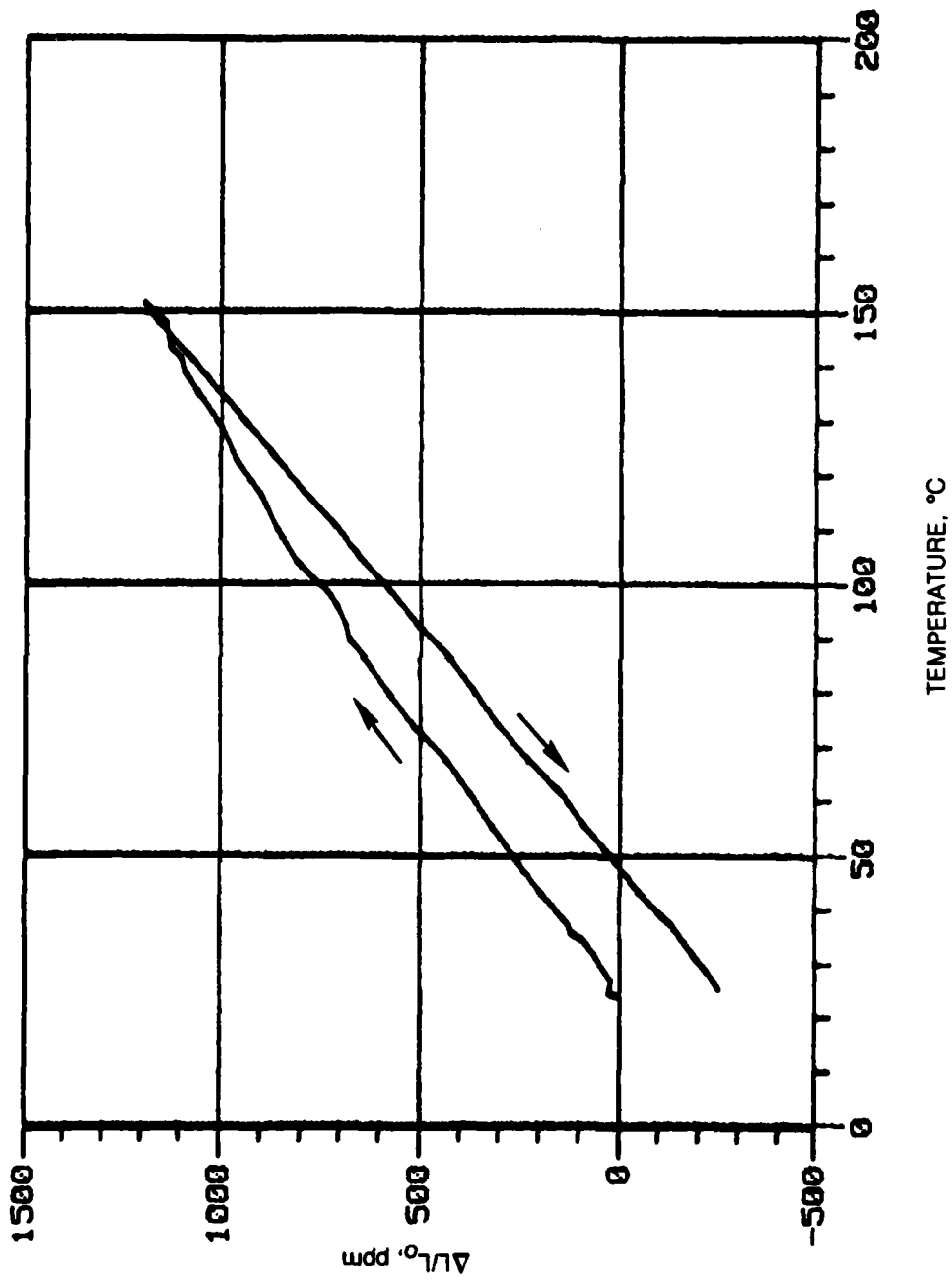


Figure 43 Thermal Expansion of 2826MB Ribbon — Longitudinal Orientation

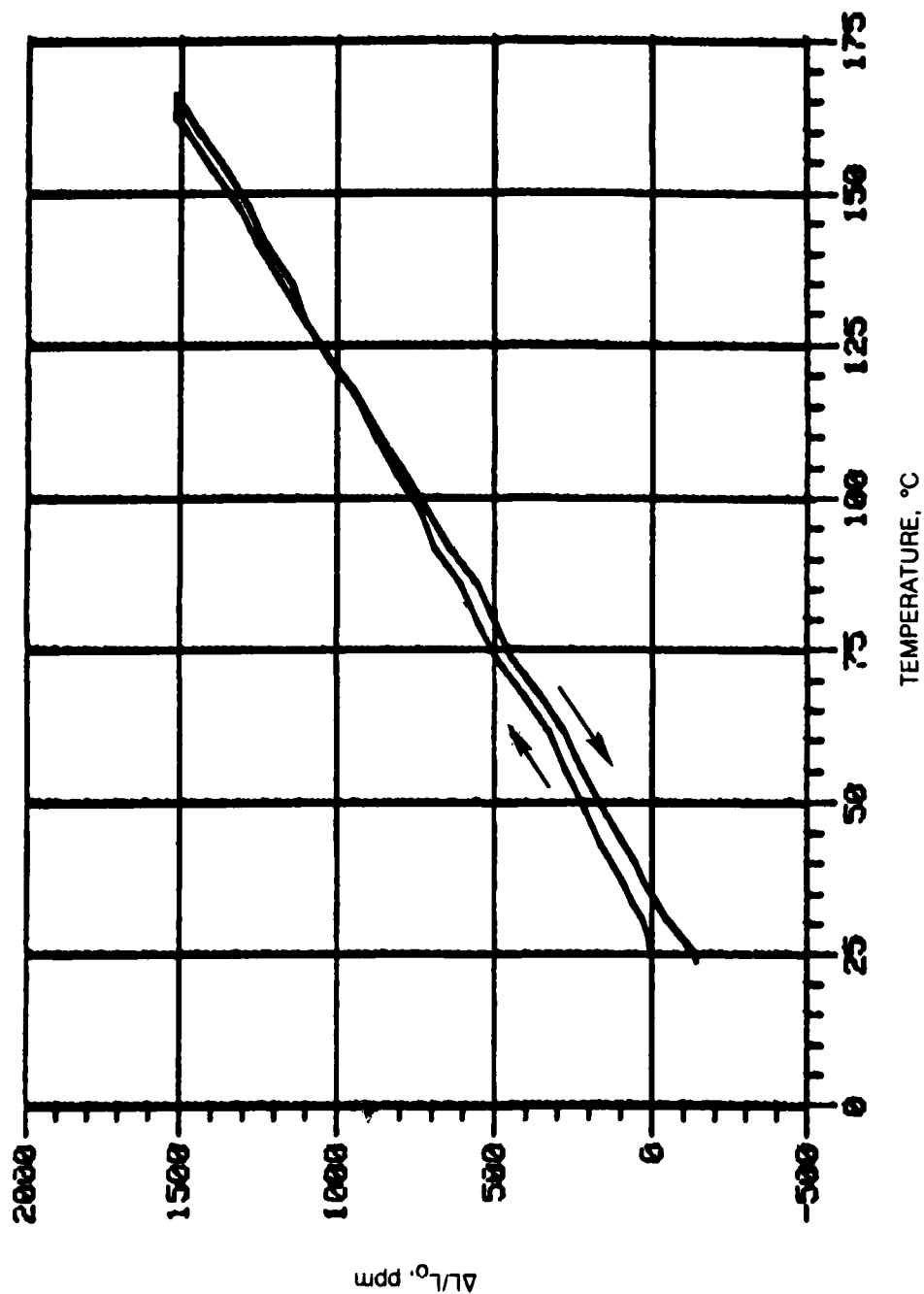


Figure 44. Thermal Expansion of 2826MB Ribbon — Transverse Orientation

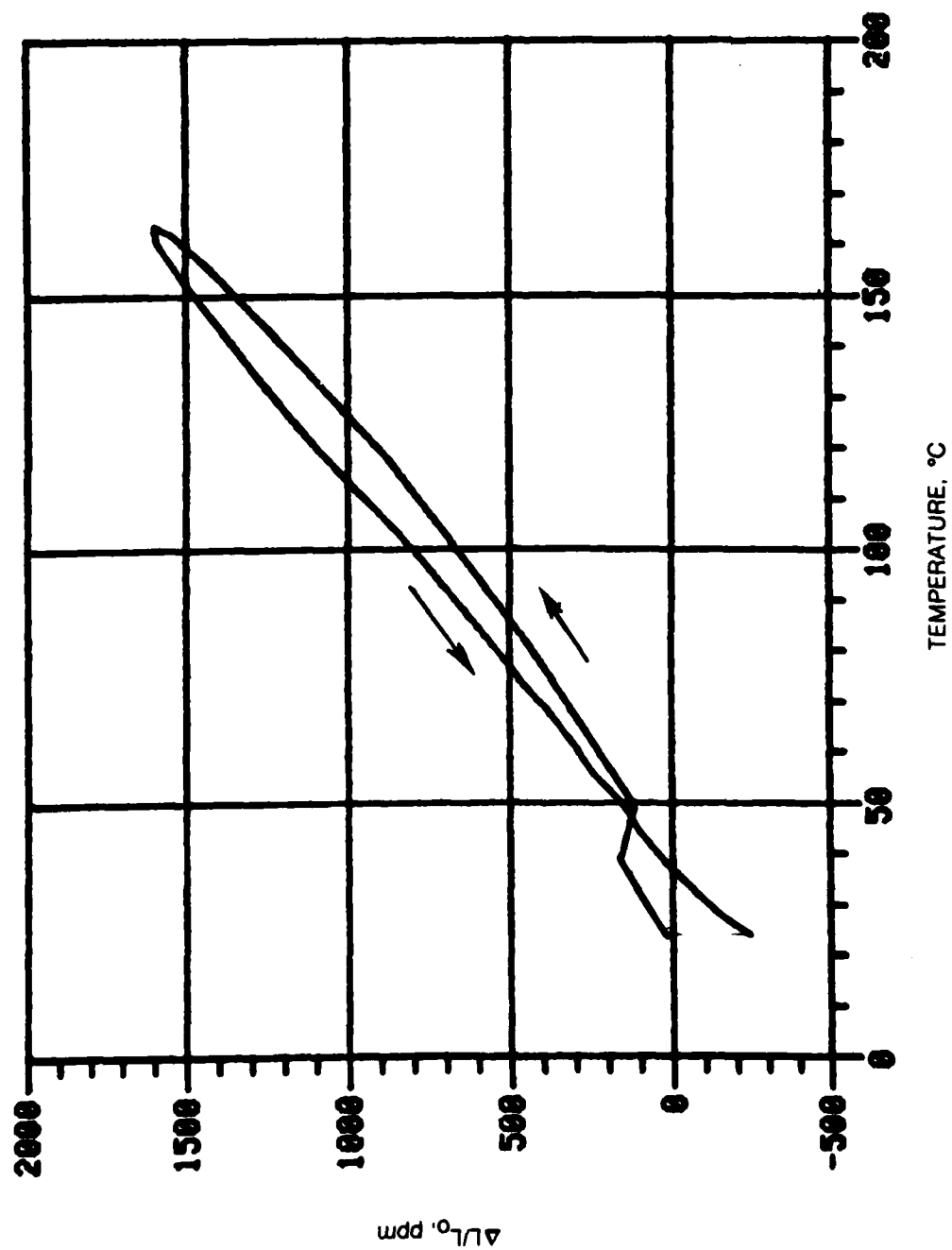


Figure 45 Composite Thermal Expansion Behavior — 0° Ribbon Orientation

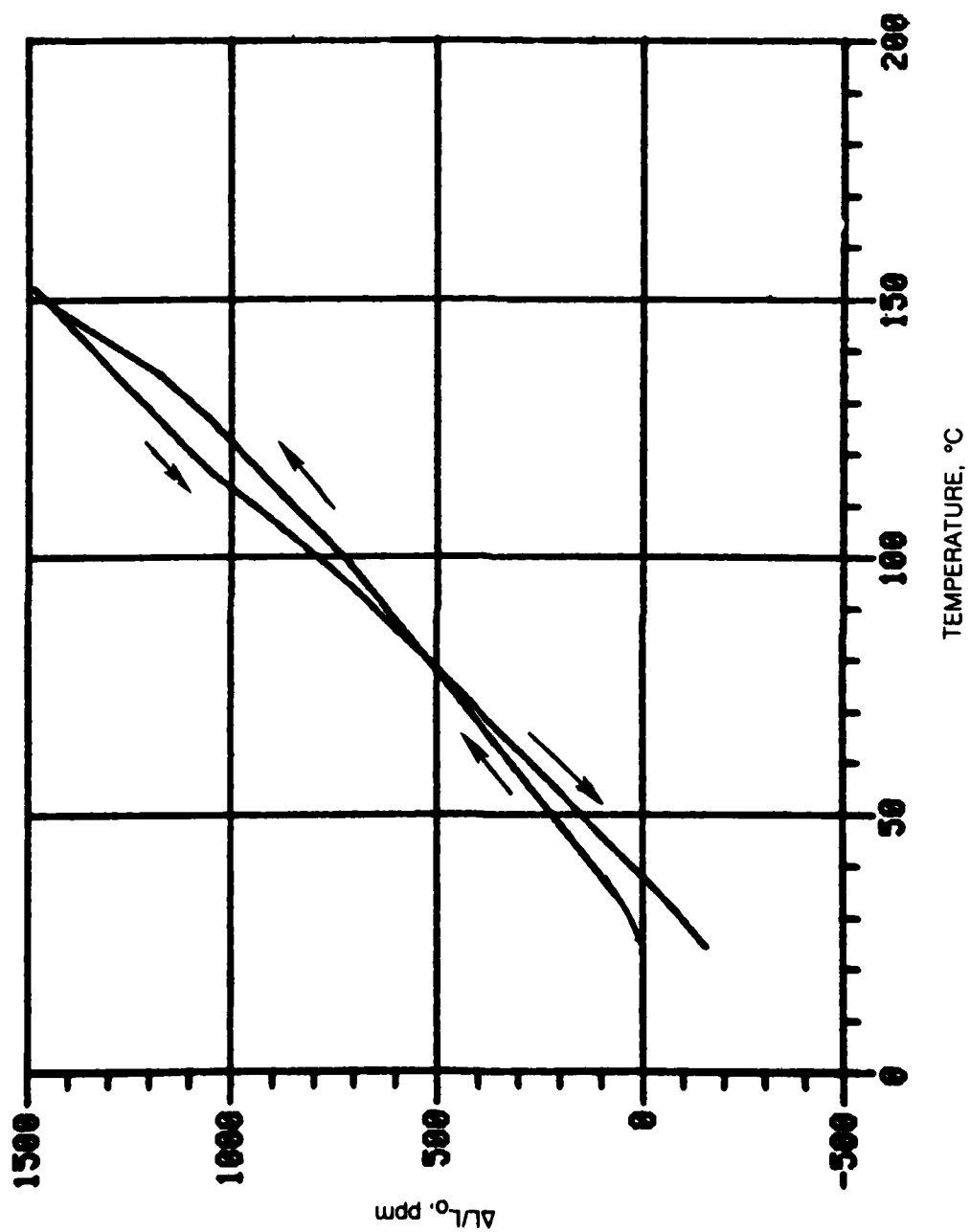


Figure 46. Composite Thermal Expansion Behavior — 45° Ribbon Orientation



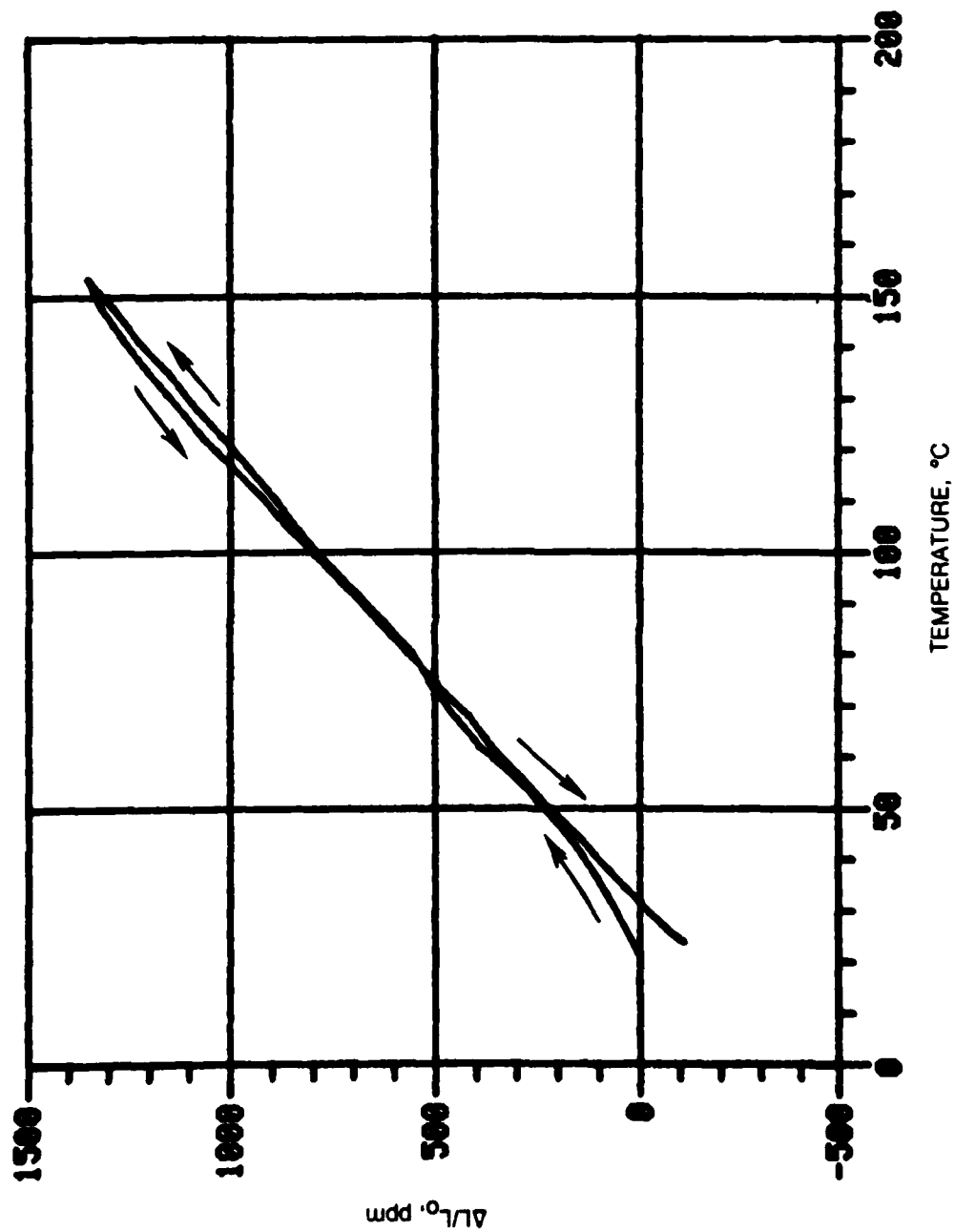
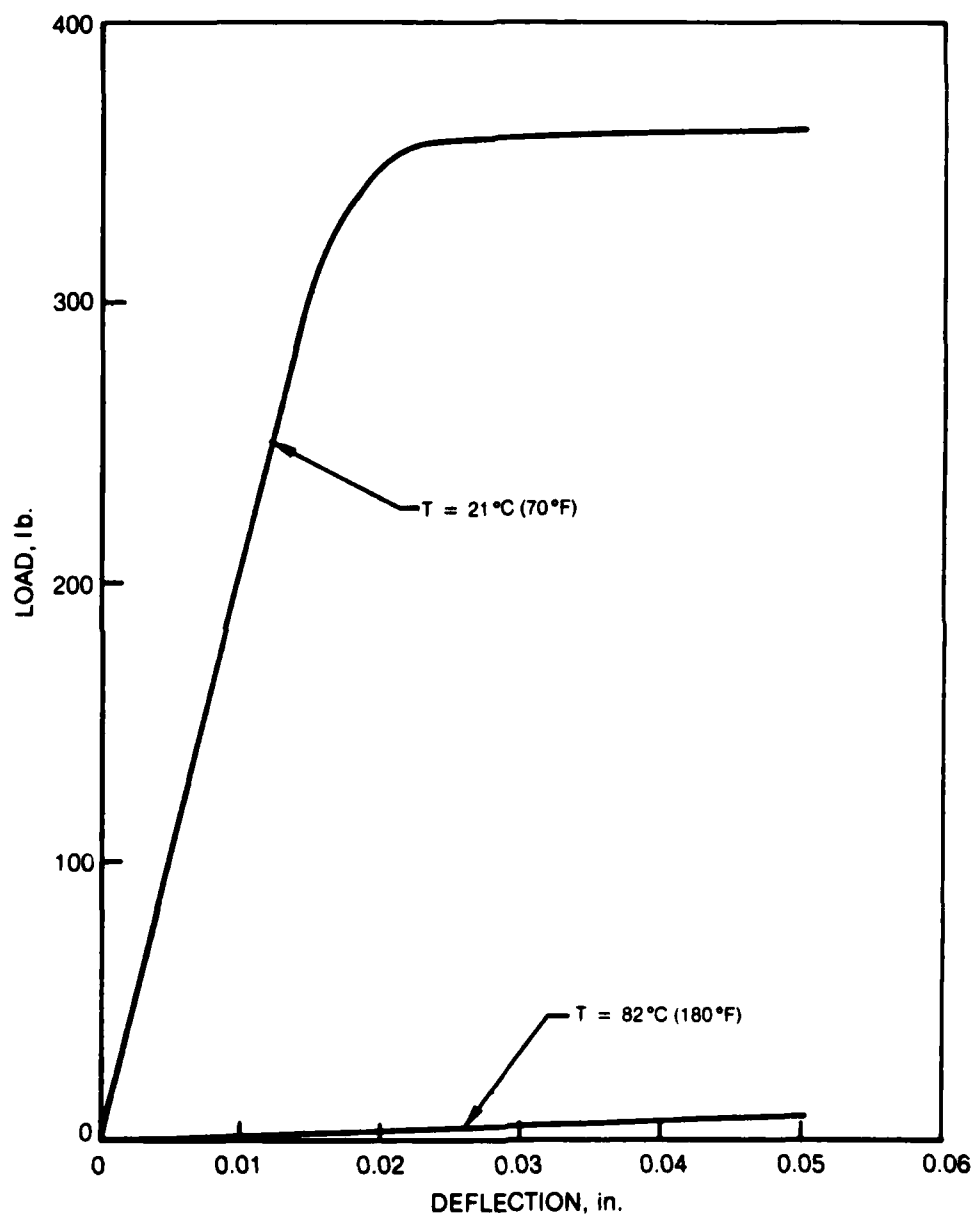


Figure 47 Composite Thermal Expansion Behavior — 90° Ribbon Orientation



**Figure 48. Load-Deflection Curves for 2826MB/FM1000 Composites  
Tested in 3 Point Bend at  $S/h = 5$**

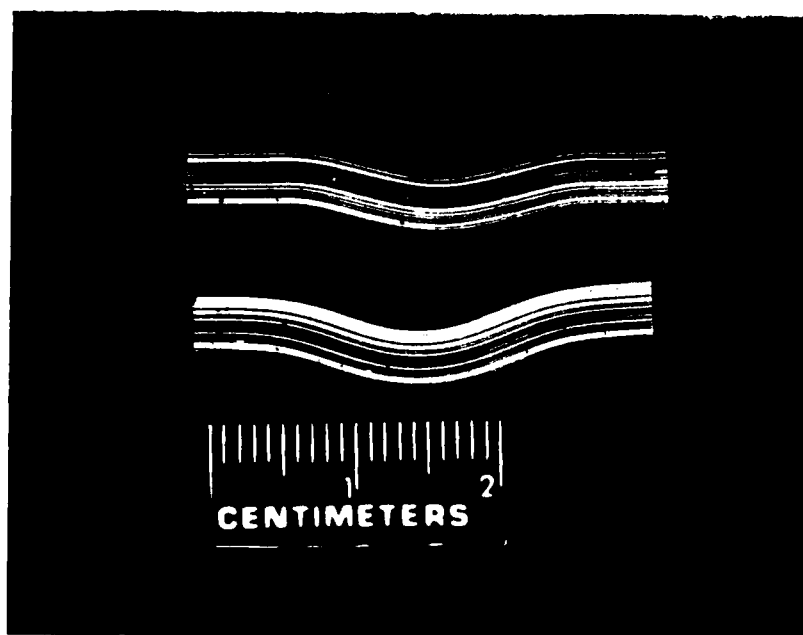
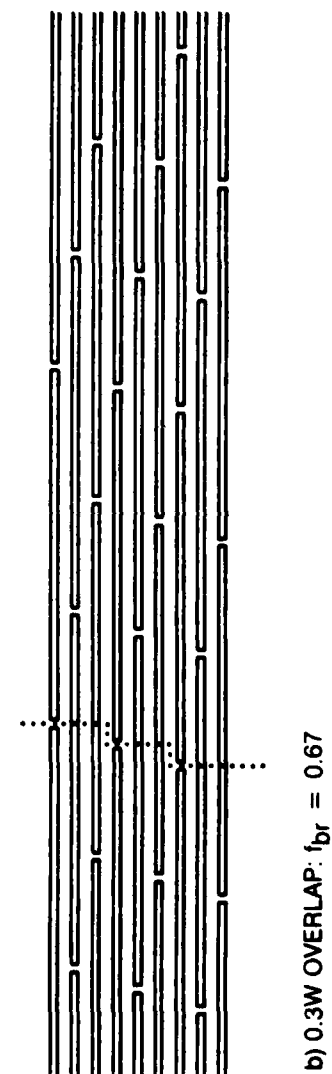
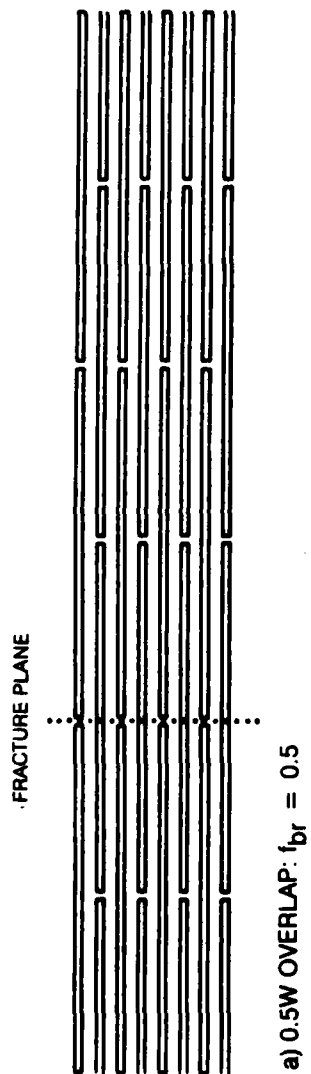


Figure 49. Laminates Tested in Three Point Bend at  $S/h = 5$



**Figure 50 Schematic Transverse Composite Cross Sections with Expected Fracture Plane Indicated**

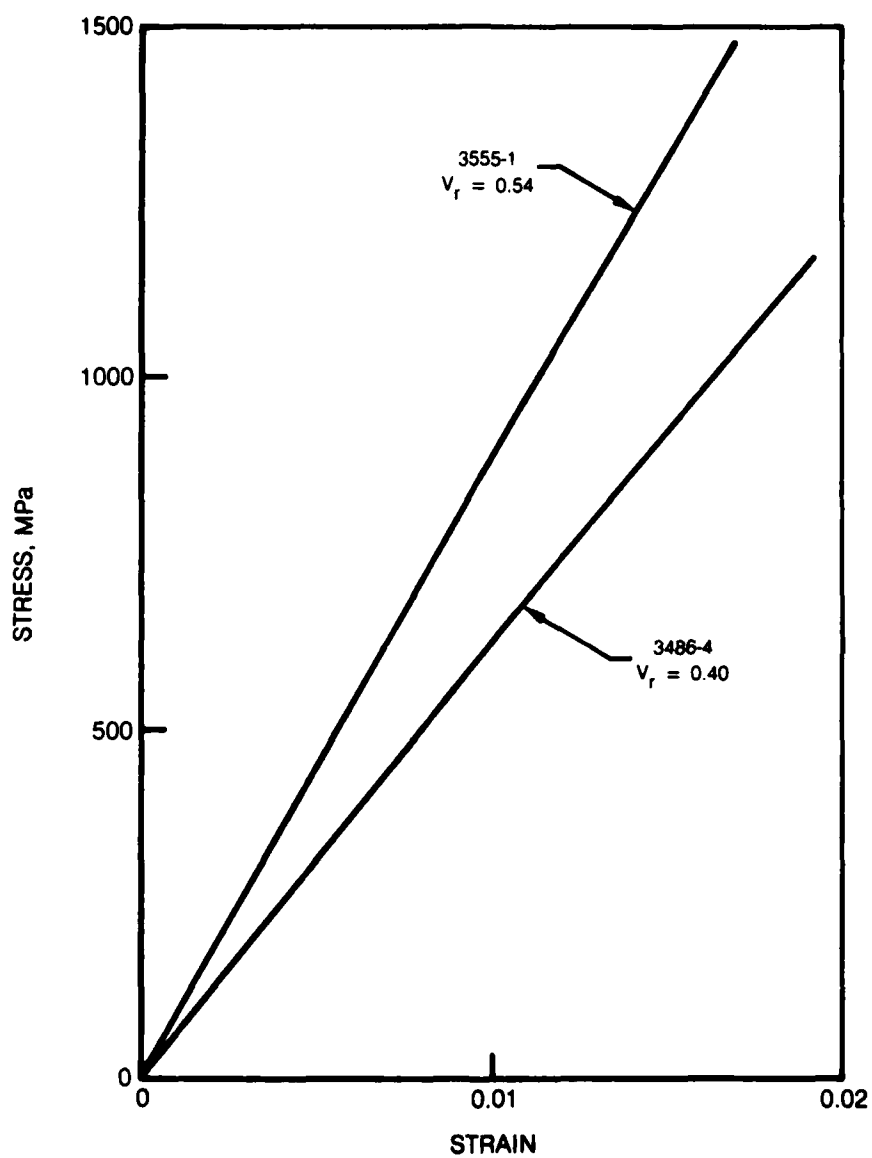
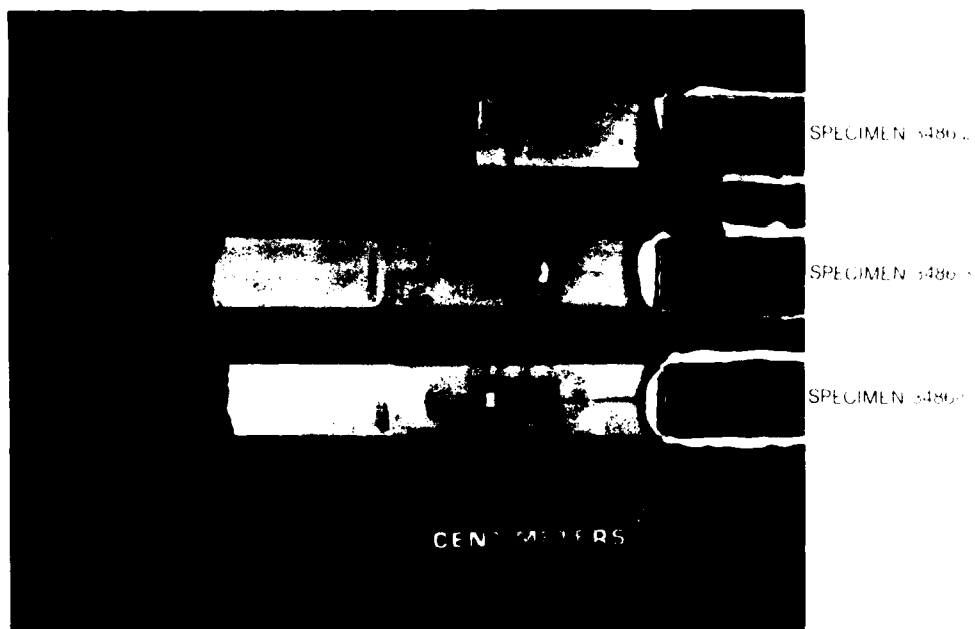


Figure 51. Longitudinal Stress-Strain Behavior at Room Temperature



**Figure 52. Longitudinal Tensile Fractures — Testing at Room Temperature**

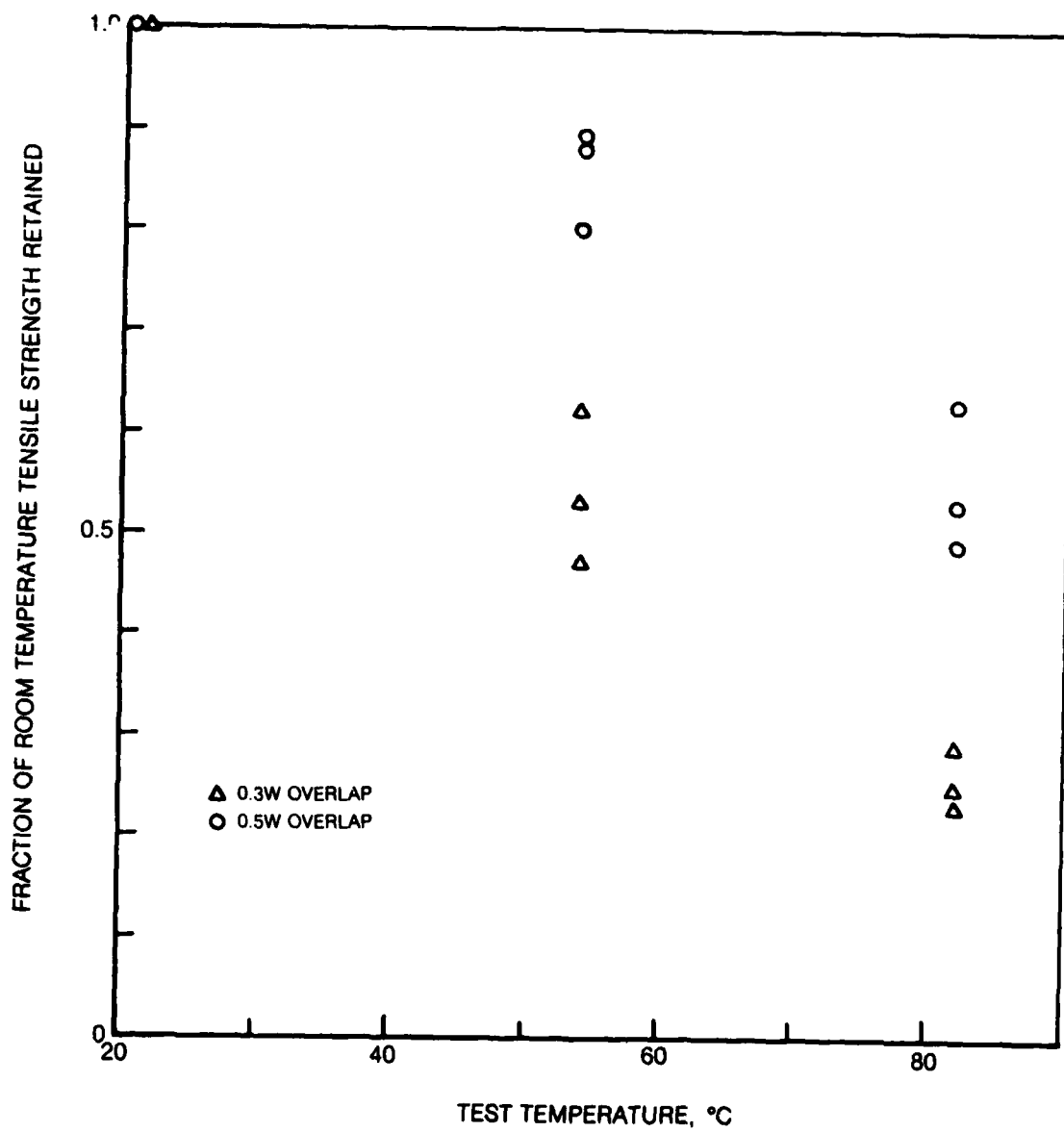
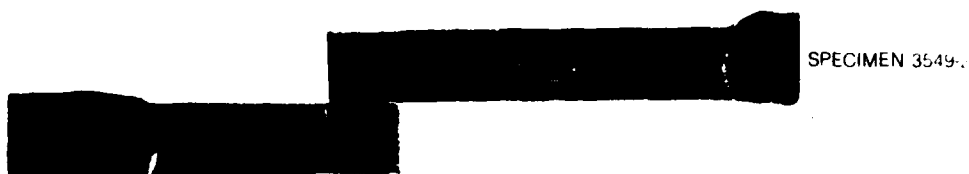
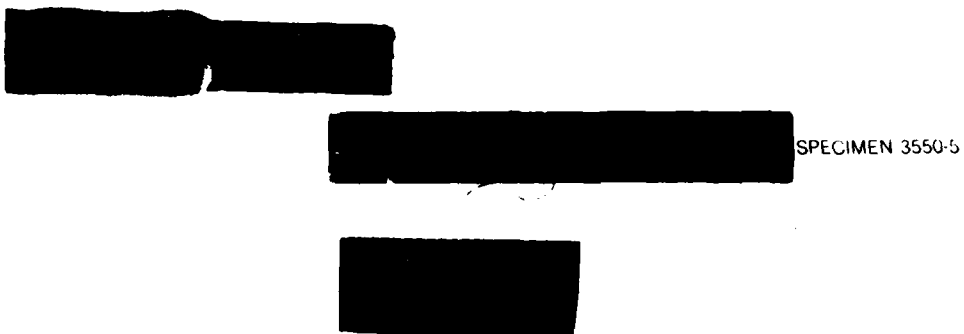


Figure 53 Effect of Test Temperature on Transverse Tensile Properties

a) TEST TEMPERATURE = 54 °C (130 °F)



b) TEST TEMPERATURE = 82 °C (180 °F)



**Figure 54. Transverse Tensile Fracture — Ribbon Overlap was 0.5 W**



a) TEST TEMPERATURE = 54 °C (130 °F)



SPECIMEN 3503-4



SPECIMEN 3509-5



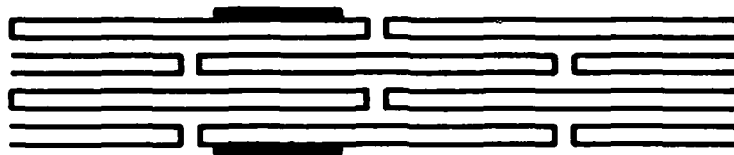
b) TEST TEMPERATURE = 82 °C (180 °F)



SPECIMEN 3503-3



**Figure 55. Transverse Tensile Fractures — Ribbon Overlap was 0.3 W**



a) STRAIN GAGES DO NOT OVERLAY A RIBBON GAP



b) ONE STRAIN GAGE OVERLAYS A RIBBON GAP

**Figure 56. Schematic Diagrams of Strain Gage Pair Locations for Transverse Tensile Test**

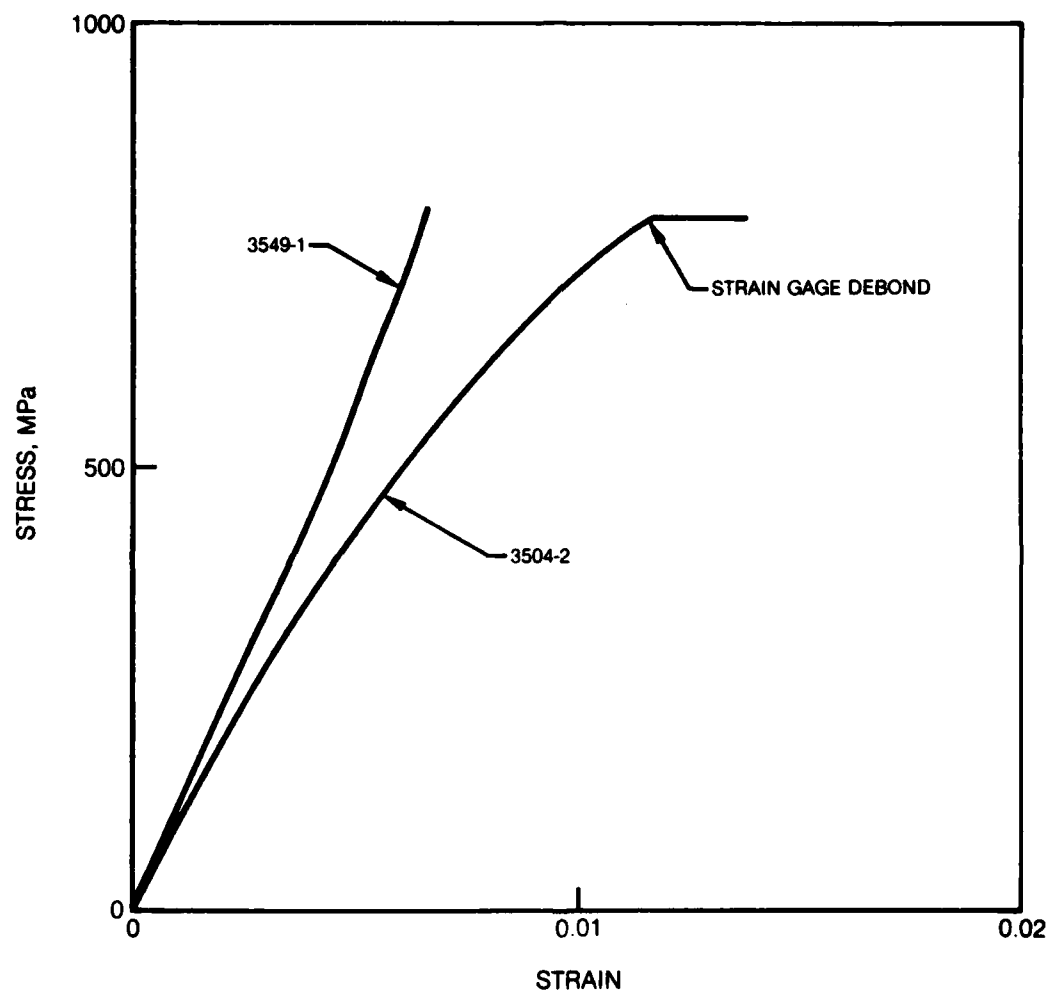


**Figure 57 Transverse Stress-Strain Behavior at Room Temperature**

a) RIBBON OVERLAP = 0.5 W



b) RIBBON OVERLAP = 0.3 W



**Figure 58. Tensile Fractures at Room Temperature — Ribbons Oriented at 45° to the Tensile Axis**

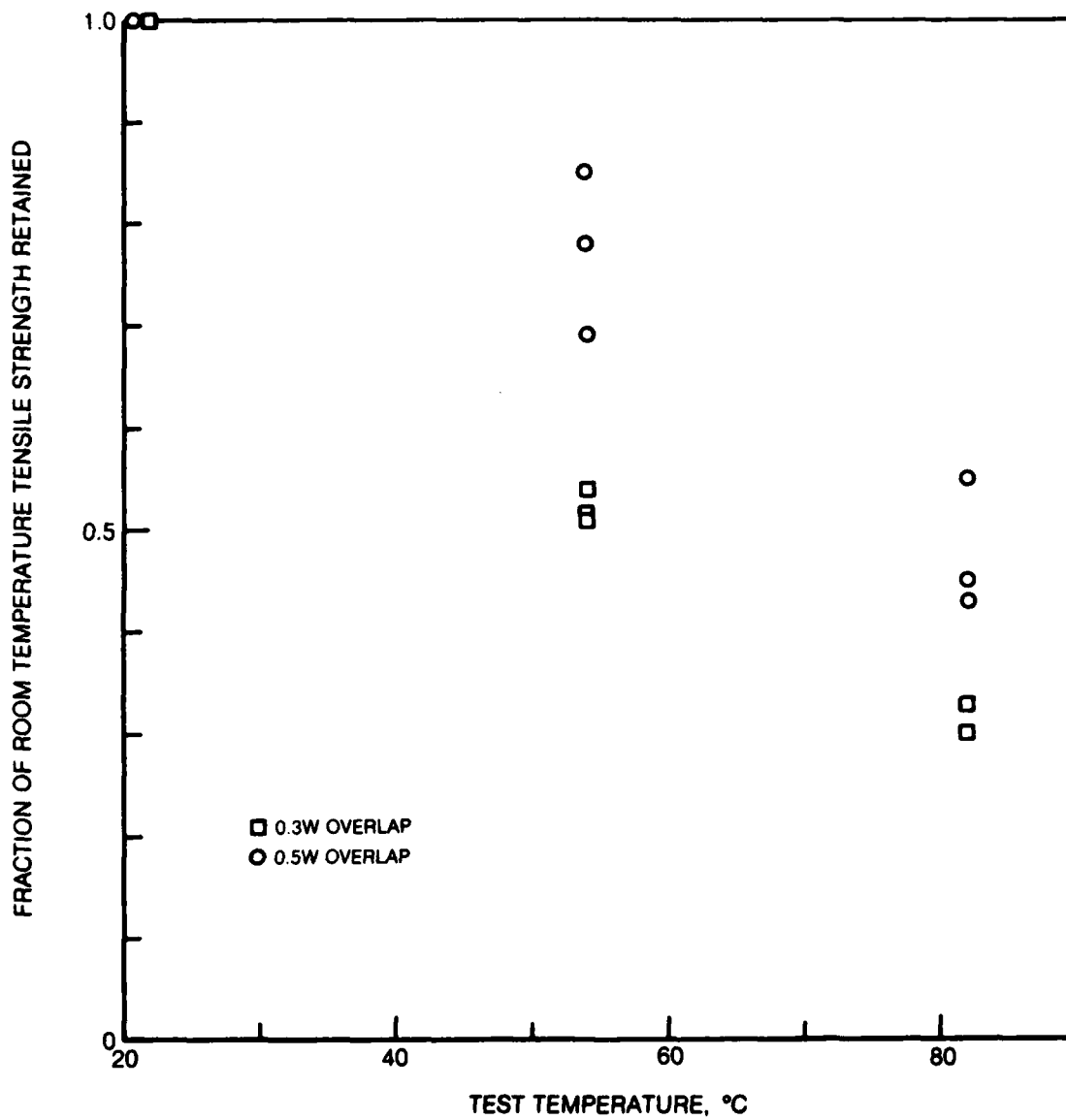
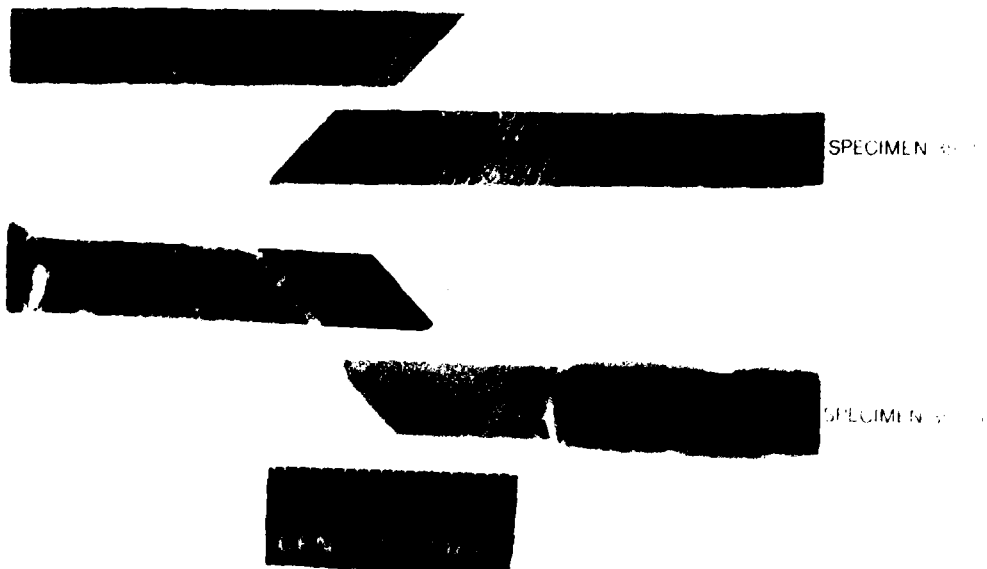


**Figure 59. Effect of Test Temperature on Tensile Properties with Ribbons Oriented at 45° to the Tensile Axis**

a) TEST TEMPERATURE = 54°C (130°F)

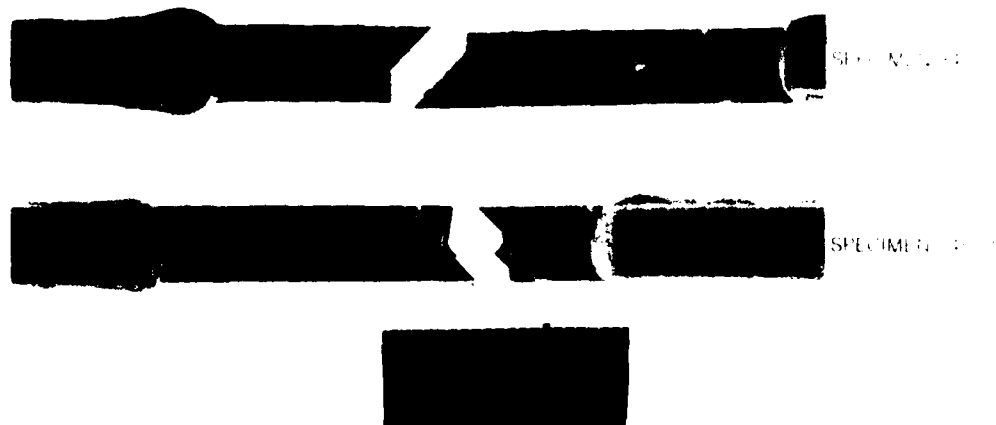


b) TEST TEMPERATURE = 82°C (180°F)



**Figure 60. Tensile Fractures for 45° Ribbon Orientation — Ribbon Overlap Was 0.5 W**

a) TEST TEMPERATURE = 54°C (130°F)



b) TEST TEMPERATURE = 82°C (180°F)

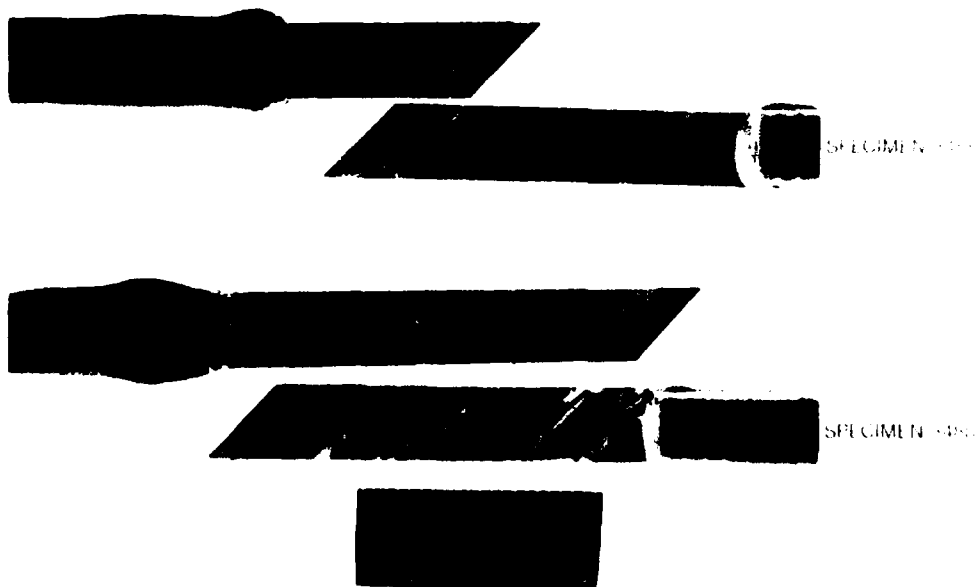


**Figure 61. Tensile Fractures for 45° Ribbon Orientation — Ribbon Overlap was 0.3 W**

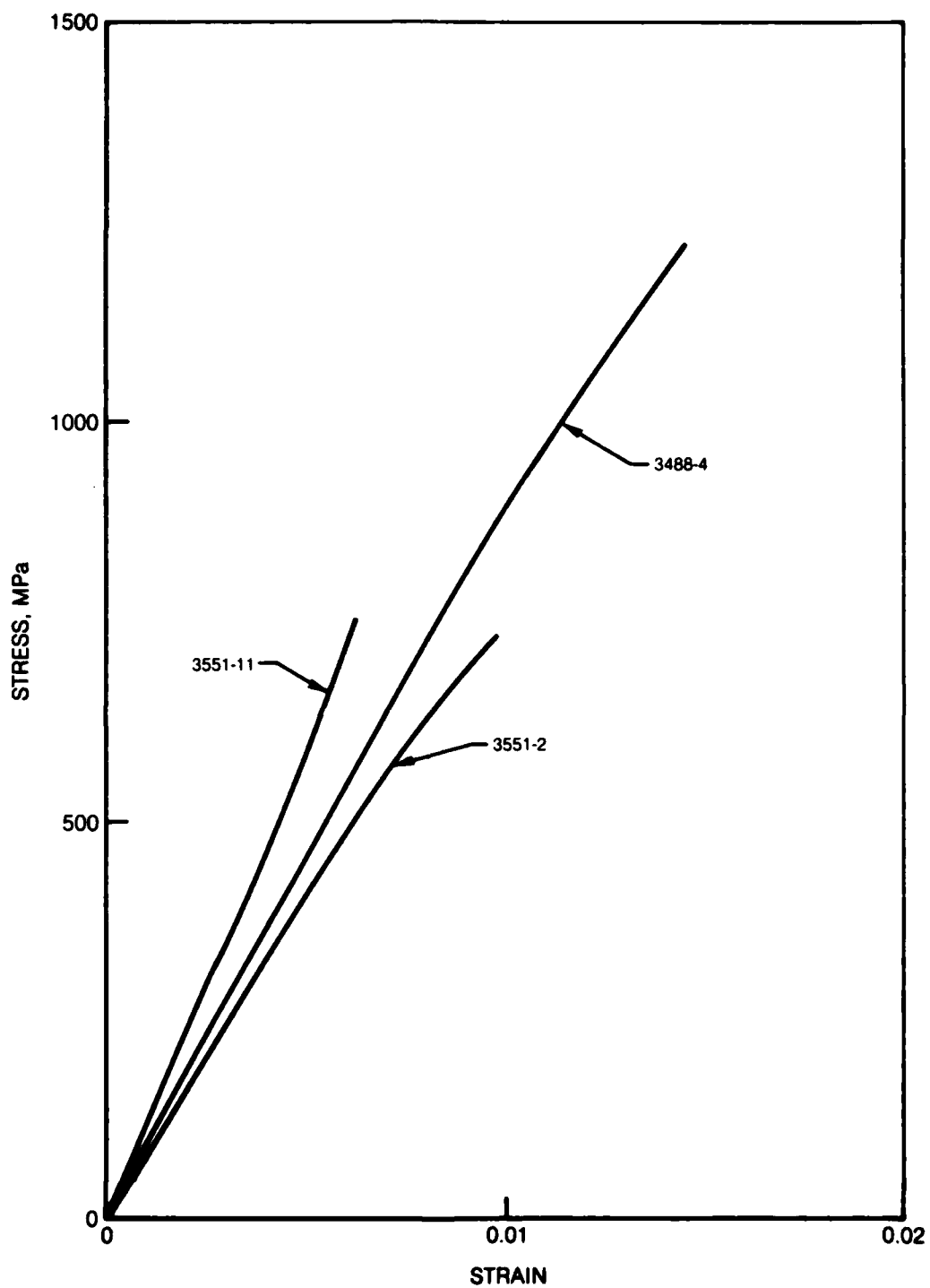


**Figure 62 Stress-Strain Behavior at Room Temperature with Ribbons Oriented at 45° to the Tensile Axis**



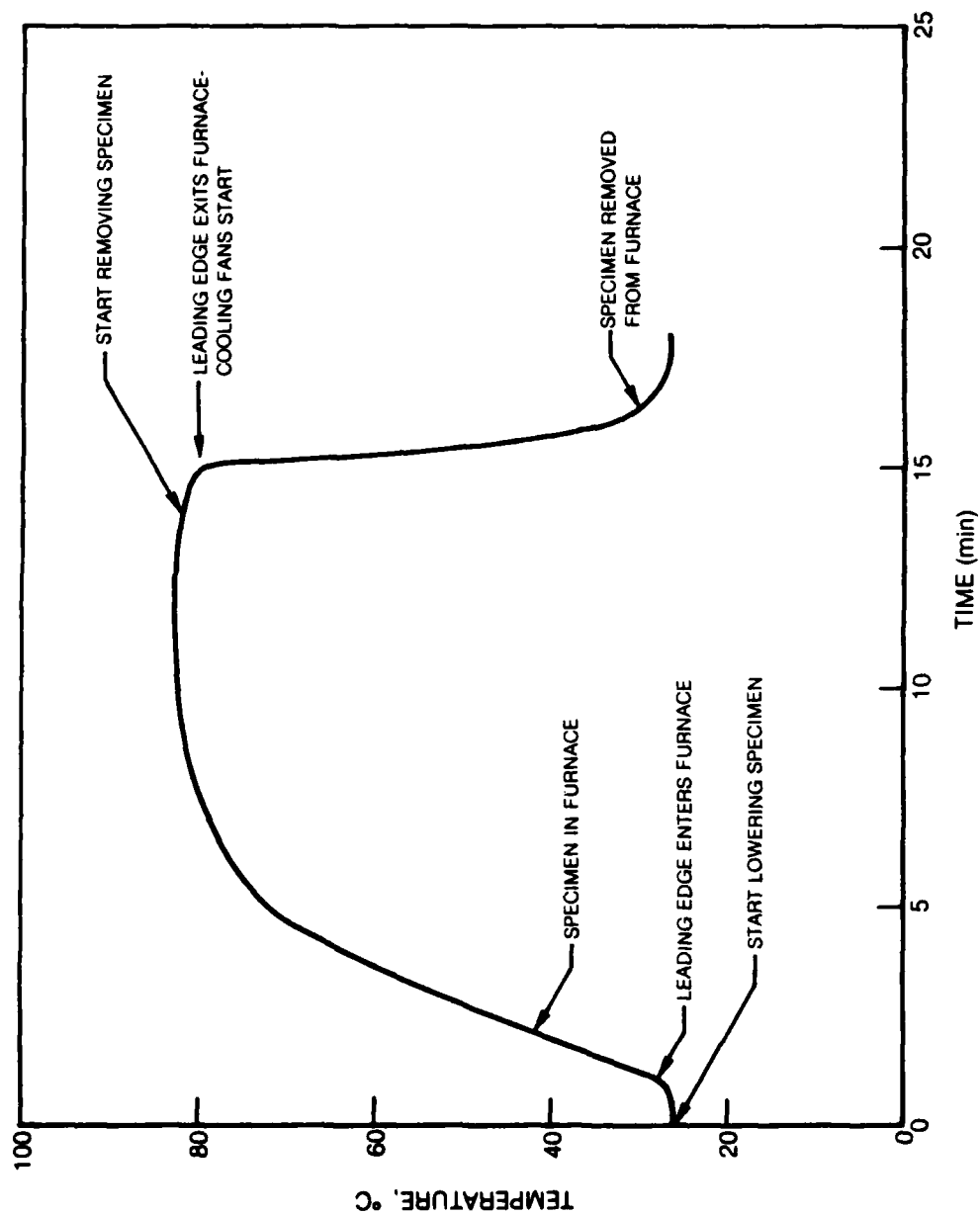
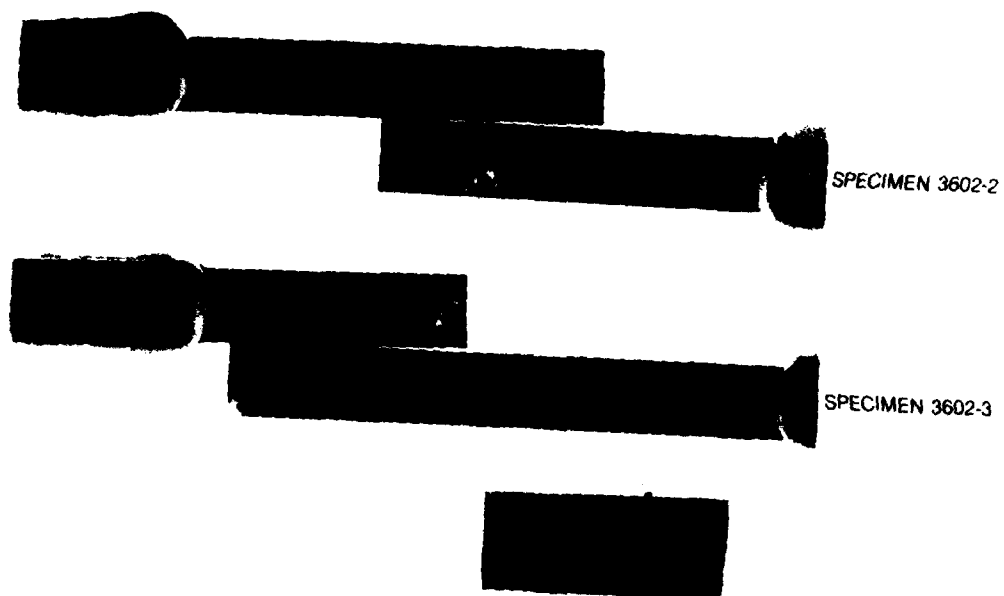
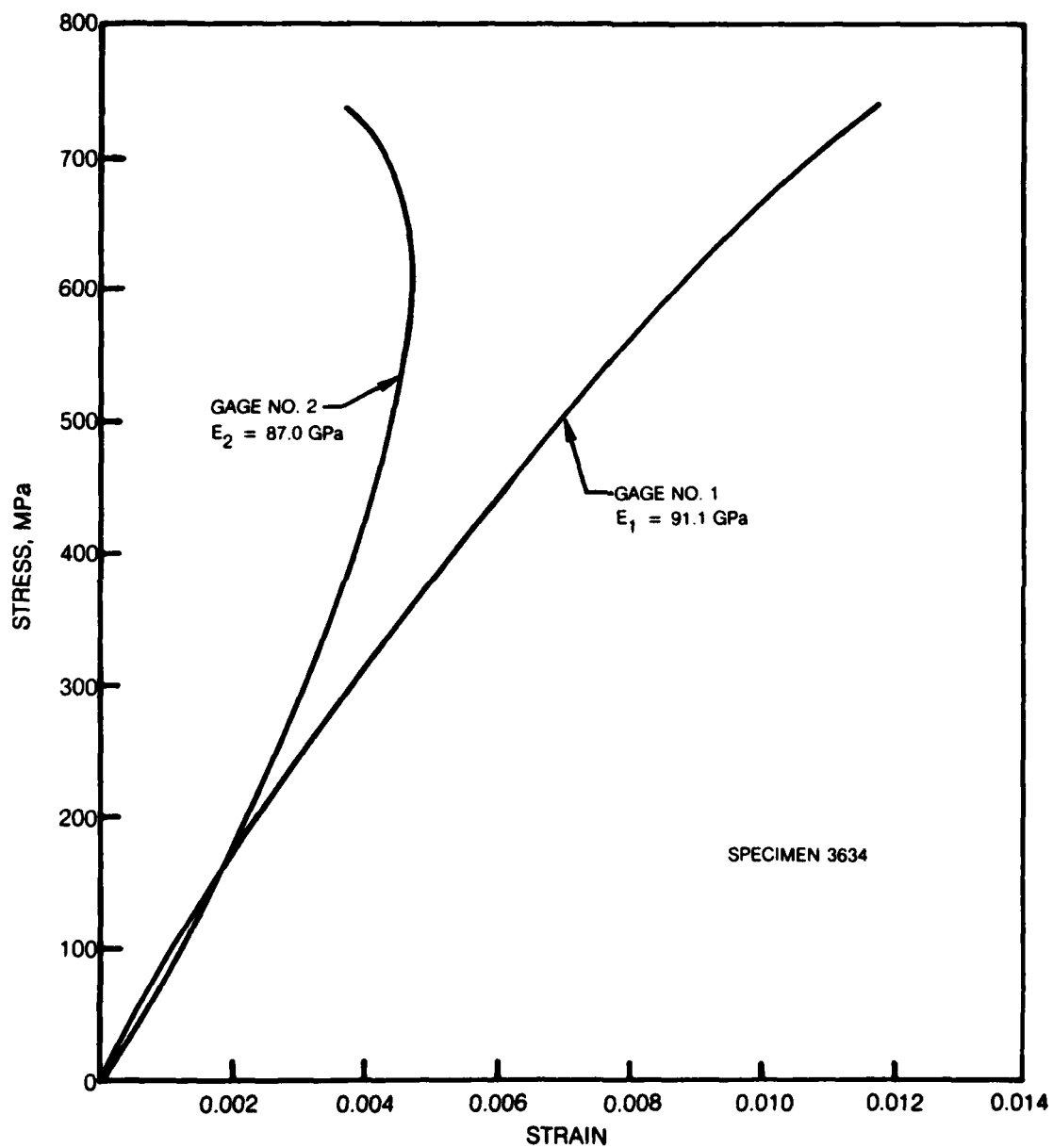


Figure 63 Thermal Cycle Utilized for Thermal Fatigue Test



**Figure 64. Transverse Tensile Specimens Exposed to Moist Environment**



**Figure 65 Compression Stress-Strain Curve for 0° Ribbon Orientation**

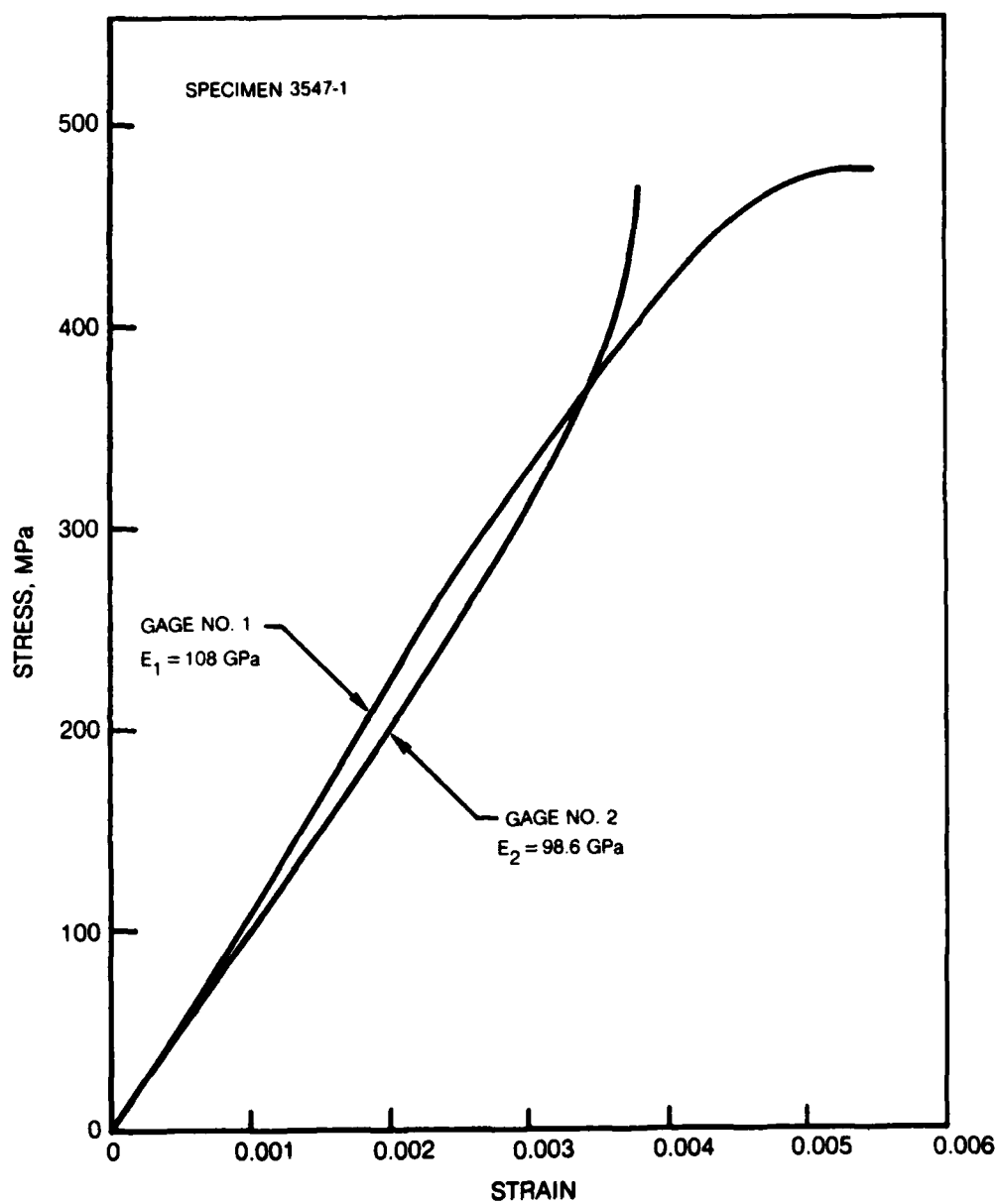


Figure 66. Compression Stress-Strain Curve for 90° Ribbon Orientation



158



SPECIMEN 3594-5  
0° RIBBON ORIENTATION



SPECIMEN 3556-1  
90° RIBBON ORIENTATION



SPECIMEN 3588-L  
LONGITUDINAL LAMINATE



SPECIMEN 3622-L  
LONGITUDINAL LAMINATE



**Figure 68. Tension-Tension Fatigue Failures**

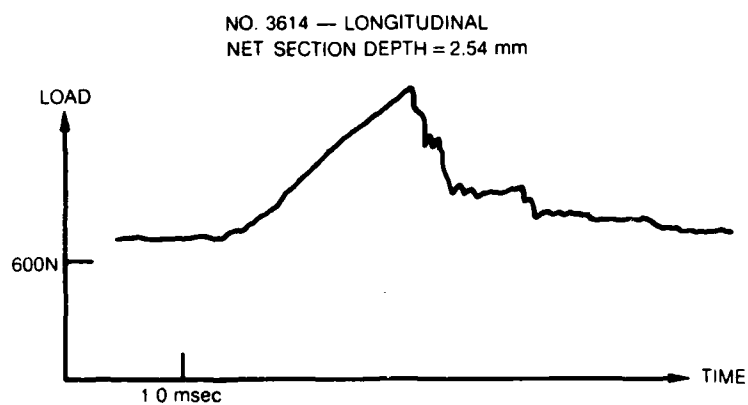
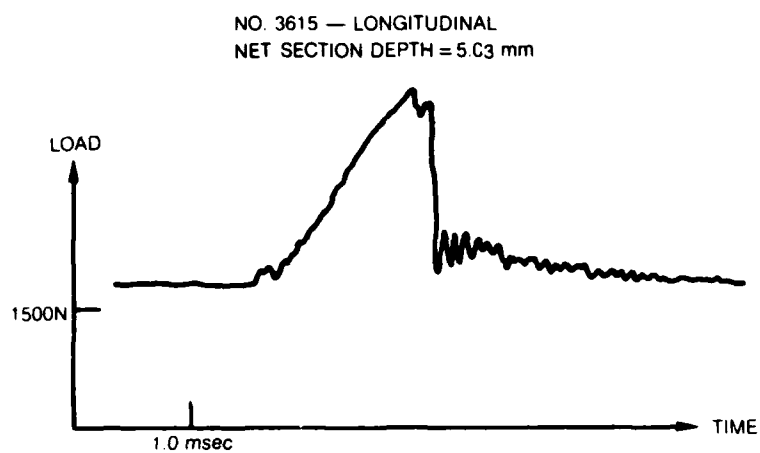
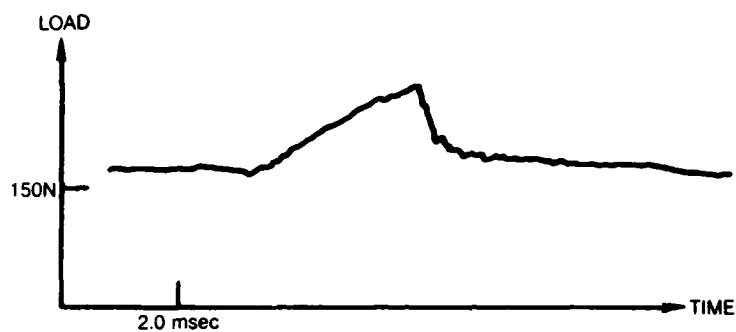


**Figure 69. Instrumented Impact Tests**

NO. 3612 — LONGITUDINAL  
NET SECTION DEPTH = 1.27 mm



NO. 3547-5 — TRANSVERSE  
NET SECTION DEPTH = 1.27 mm



**Figure 70 Instrumented Impact Traces**





**Figure 71. Impact Specimens — Longitudinal Laminates**

80 02 138 1P

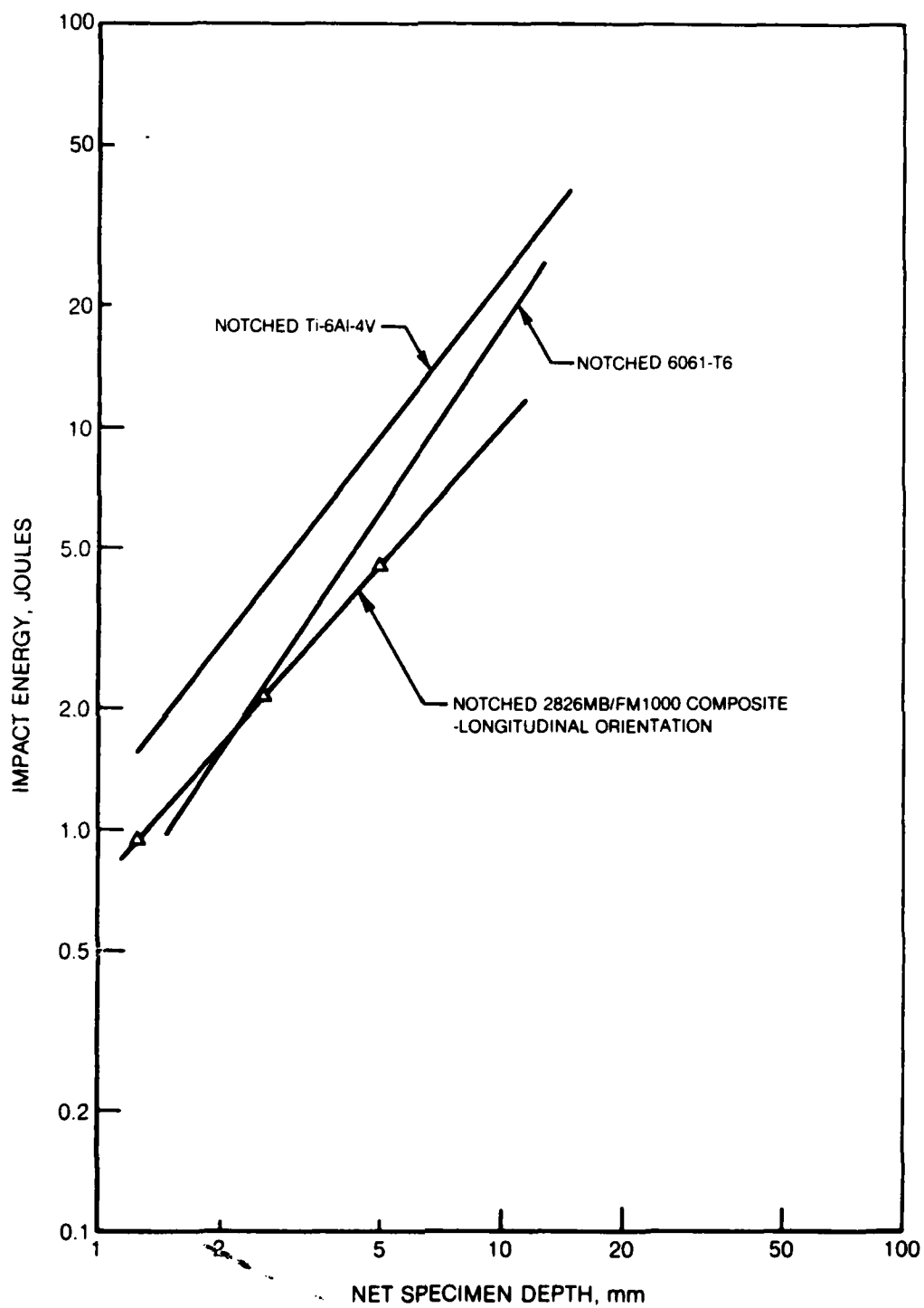
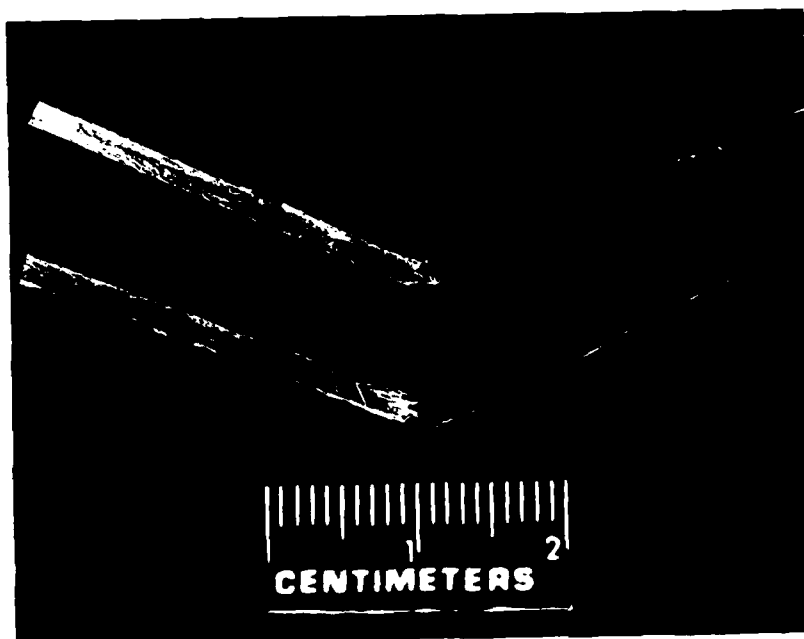


Figure 72. Energy Dissipated as a Function of Specimen Geometry



SPECIMEN #1

SPECIMEN #2

**Figure 73. Impact Specimens — Transverse Ribbon Orientation**

80 02 138 19

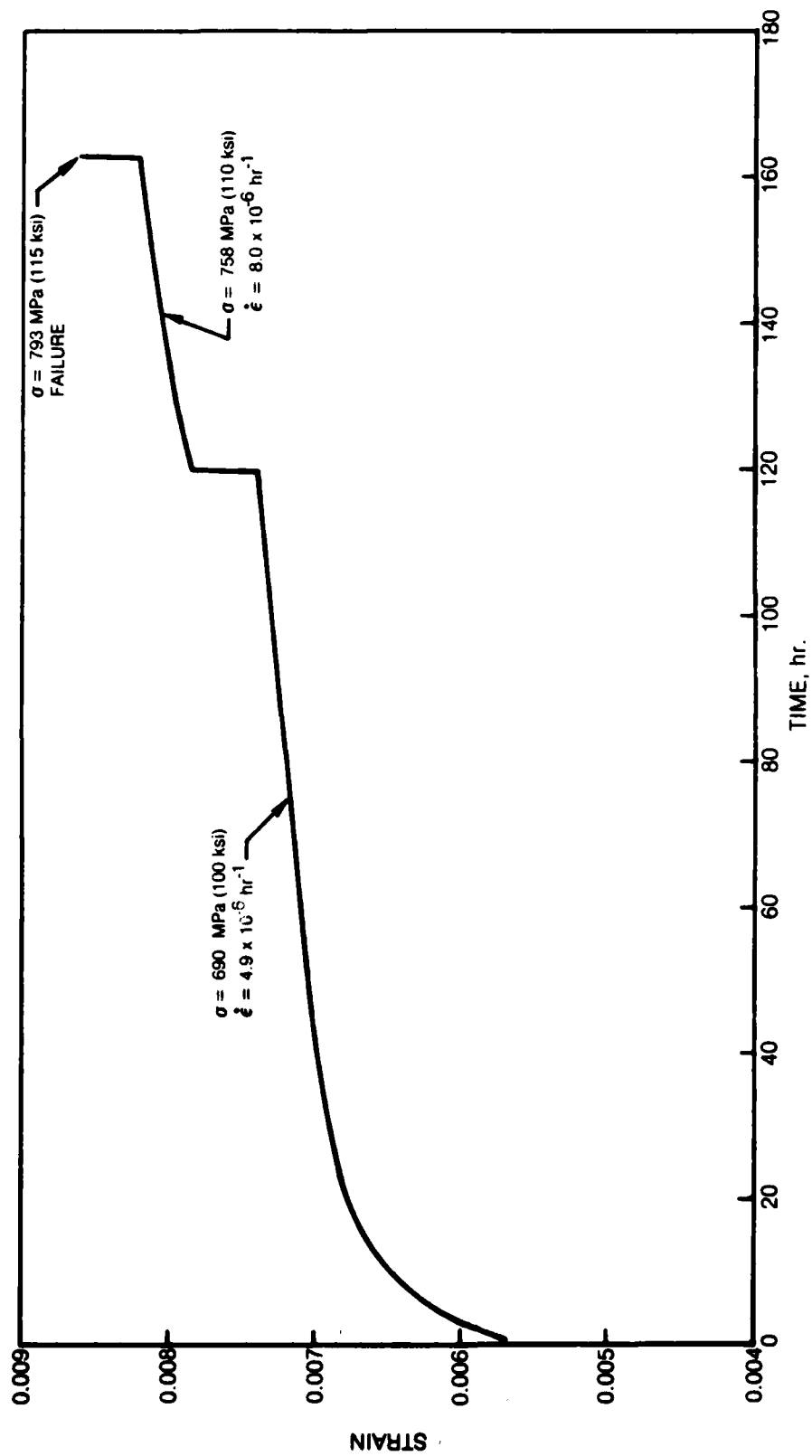


Figure 74 Room Temperature Creep Behavior — Transverse Ribbon Orientation

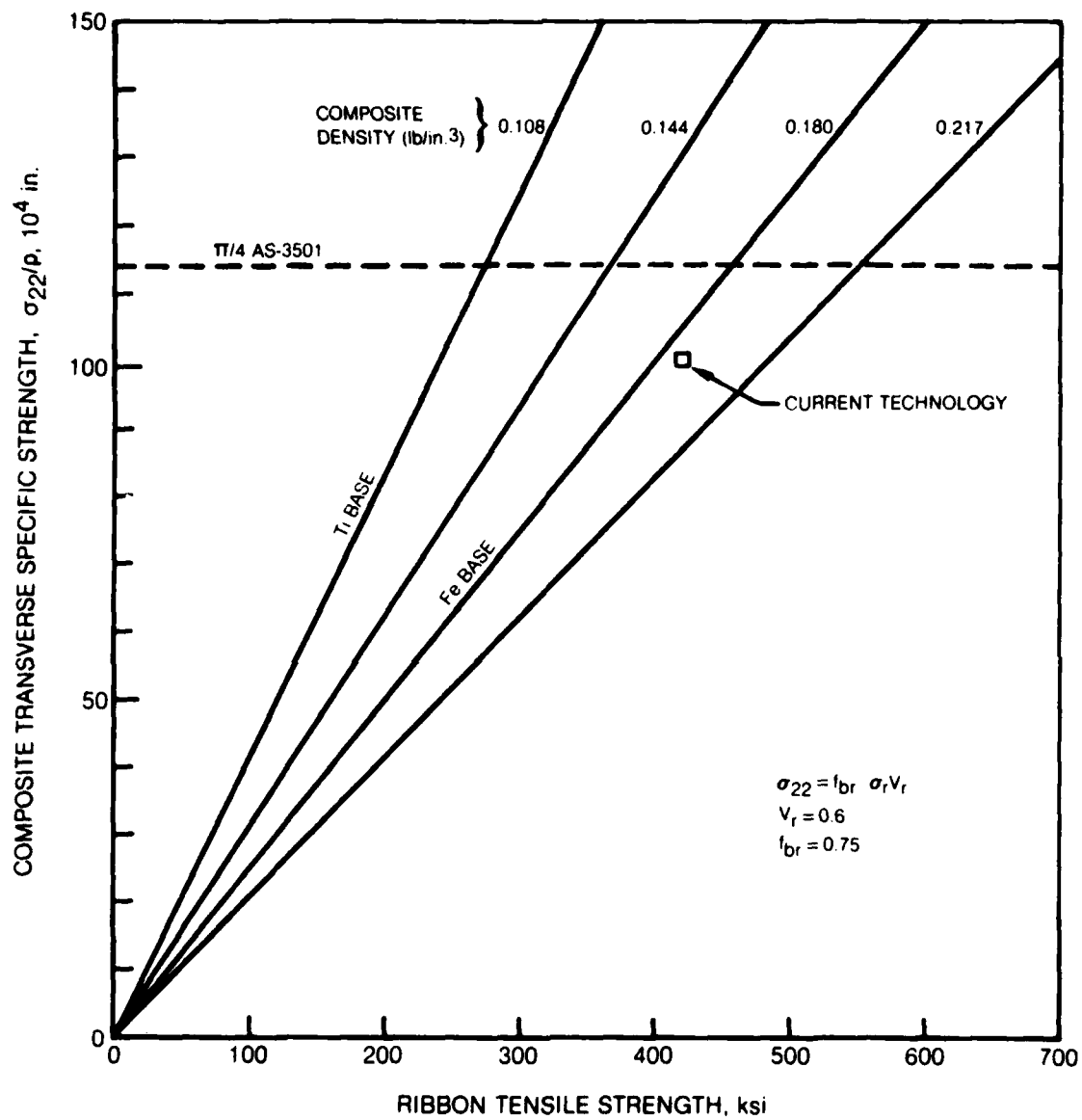
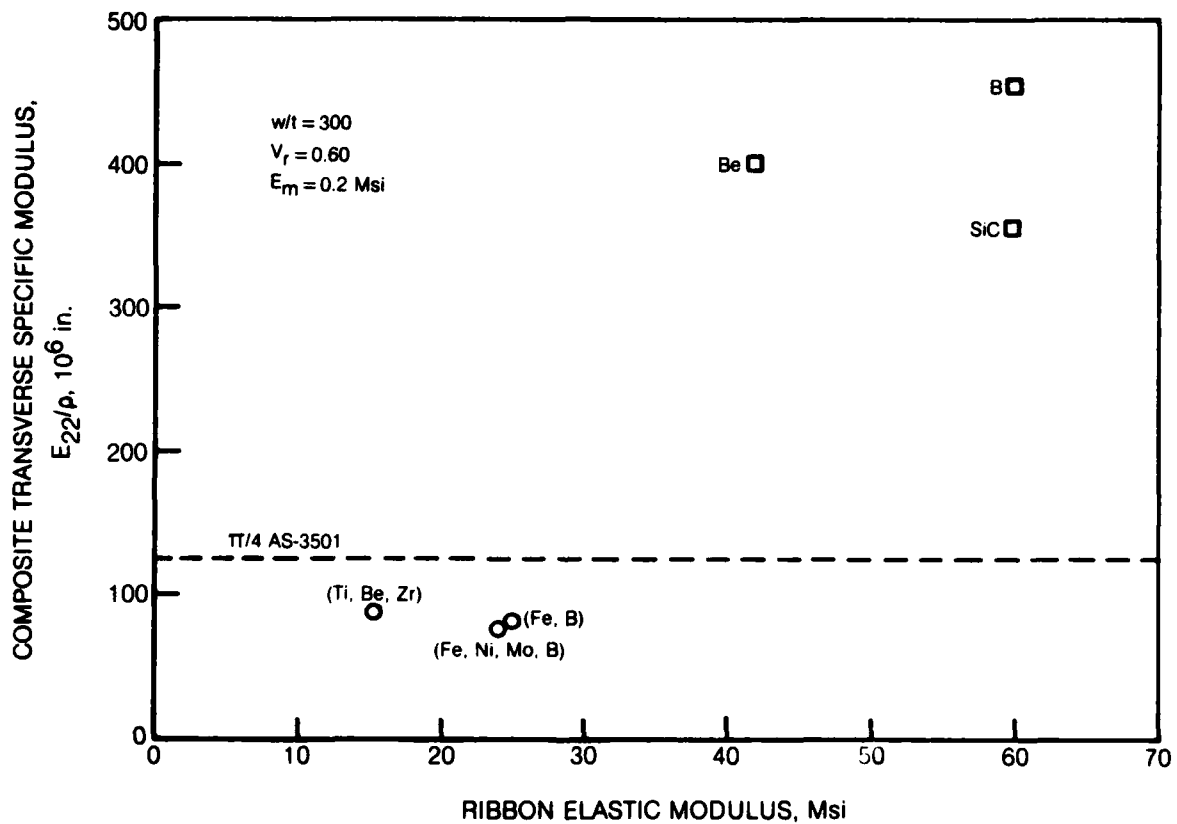


Figure 75 Assessment of Composite Transverse Specific Strength



**Figure 76 Assessment of Composite Transverse Specific Modulus**